ULTRAFAST REDISTRIBUTION OF VIBRATIONAL ENERGY IN LIQUIDS

M.A.F.H. VAN DEN BROEK

ULTRAFAST REDISTRIBUTION OF VIBRATIONAL ENERGY IN LIQUIDS

ULTRAFAST REDISTRIBUTION OF VIBRATIONAL ENERGY IN LIQUIDS

Academisch Proefschrift

ter verkrijging van de graad van doctor aan de Universiteit van Amsterdam
op gezag van de Rector Magnificus Prof. Mr P.F. van der Heijden
ten overstaan van een door het college voor promoties ingestelde commissie,
in het openbaar te verdedigen in de Aula der Universiteit
op dinsdag 25 juni 2002, te 12.00 uur

door

Marie Adriaan Frederik Hendrik van den Broek
geboren te Utrecht

Promotor: Prof. Dr H.J. Bakker

Faculteit der Natuurwetenschappen, Wiskunde en Informatica

ISBN 90-9015895-2

NUGI 813

The work described in this thesis was performed at the FOM Institute for Atomic and Molecular Physiscs (AMOLF), Kruislaan 407, 1098 SJ Amsterdam, The Netherlands. This work is part of the research programme of the *Stichting Fundamenteel Onderzoek der Materie* (FOM), which is financially supported by the *Nederlandse Organisatie voor Wetenschappelijk Onderzoek* (NWO).

Contents

Publications covered in this thesis

M. A. F. H. van den Broek and H. J. Bakker. Observation of a bottleneck in the vibrational relaxation of liquid bromoform. *Chem. Phys.* **253**(1), 157–164 (2000).

I. A. M. E. Giebels, M. A. F. H. van den Broek, M. F. Kropman, and H. J. Bakker. Vibrational dynamics of hydrogen-bonded HCl-diethyl ether complexes. *J. Chem. Phys.* **112**(11), 5127–5132 (2000).

M. A. F. H. van den Broek, H.-K. Nienhuys, and H. J. Bakker. Vibrational dynamics of the C–O stretch vibration in alcohols. *J. Chem. Phys.* **114**(7), 3182–3186 (2001).

M. A. F. H. van den Broek, M. F. Kropman, and H. J. Bakker. Ultrafast pump-probe spectroscopy of strongly hydrogen-bonded hydrogen fluoride-pyridine complexes. *Chem. Phys. Lett.* **357**(1–2), 8–14 (2002).

Other publications

G. M. Kapteijn, M. J. Verhoef, M. A. F. H. van den Broek, D. M. Grove, and G. van Koten. Carbonylation of diamino-ligated methylpalladium(II) methoxide complexes. *J. Organomet. Chem.* **503**(1), C26–C28 (1995).

G. M. Kapteijn, A. Dervisi, M. J. Verhoef, M. A. F. H. van den Broek, D. M. Grove, and G. van Koten. Chemistry of diamino-ligated methylpalladium(II) alkoxides and aryloxides. 2. Methoxide formation and carbonylation reactions. *J. Organomet. Chem.* **517**(1–2), 123–131 (1996).

1 Introduction

1.1 Brief history of optics

The adage "in the country of the blind, the one-eyed man is King" is a good illustration of the great appreciation there has always been for light and the sense of vision. For a long time, sources of light like the sun, fire or lightning were only encountered with religious reverence. The perspective changed when scientific reasoning took hold and systematic observations were made and theories were formulated in the field of optics. The notion that light can be thought of as rays was already conceived in antiquity by Euclides of Alexandria (325 – 265 BC). In his work *Optica*, he noted that light travels in straight lines and he described the concept of perspective. Euclides followed the Platonic tradition that vision is caused by rays that emanate from the eye. This theory of vision was also propagated a few centuries later by Heron of Alexandria (around 10 – 75) who derived the law of reflection by a geometrical method in his *Catoptrica*. This work was previously attributed to Claudius Ptolemaeus (85 – 165). Ptolemaeus did author a work devoted to optical phenomena, *Optica*. The last book of this five-volume edition includes a study on refraction, especially the refraction suffered by light from celestial bodies travelling through air.

The first correct explanation of vision was given by the Arabian scholar Abu Ali al-Hasan ibn al-Hasan ibn al-Haytham (965 – 1040), also known as Alhazen or al-Hazen. He noted that light is the same, irrespective of the source, and that light is reflected from an object into the eye. Al-Haytham formulated his findings and theories on optics after extensive experimental work, where he used spherical and parabolic mirrors and investigated the refraction of light. He also was the first to mention the use of a *camera obscura*. With his seven-volume work *Kitab al-Manazir* (translated in Latin as *Opticae thesaurus Alhazeni*[2] in 1270), he is often considered the father of modern optics.

The field of optics was greatly advanced by the many discoveries from the 17th century onwards, starting when Johannes Kepler (1571 – 1630) discovered the concept of total internal reflection. The discovery and formulation of the law of refraction by Willebrord Snell (1580 – 1626) and the formulation of a wave theory of light by Christiaan Huygens (1629 – 1695) in his book *Traité de la lumière*,[123] are probably the most significant achievements of that era, providing the basis for many discoveries and advances in the centuries to follow. One other name from the 17th century which should be mentioned is of course Isaac Newton (1643 – 1727), who observed the dispersion of sunlight and who, in contrast to Huygens, proposed a corpuscular nature of light in his work *Opticks*.[159]

In the centuries to follow many discoveries and theories were put forward by people like Young, Fraunhofer, Brewster, Fresnel, and Faraday, to name but a few. The conclusion that light is an electromagnetic wave and the mathematical formulation by James Clerk Maxwell (1831 – 1871) was another significant step forward in the field of optics and the description of light and its interaction with matter. Another significant advance was however made

by Albert Einstein (1879 – 1955) with the notion that light is quantised.[66,67] Einstein also proposed that stimulated emission should occur in addition to spontaneous emission and absorption.[69] Elements from the field of quantum mechanics in the first decades of the 20th century strengthened the notion that light is quantised and that it can be viewed both as particles and as electromagnetic waves.

In 1954 an experimental device was described that produced coherent electromagnetic radiation in the microwave-regime.[84] This apparatus was later dubbed MASER, an acronym for Microwave Amplification by Stimulated Emission of Radiation. This source of radiation with a very narrowly defined frequency was first greeted with disbelief, as for example Von Neumann was said to have declared: "That can't be right".[203] Four years later Townes and Schawlow proposed to extend this principle to optical frequencies,[184] giving rise to the LASER, which was an acronym for Light Amplification by Stimulated Emission of Radiation. The first laser was described in 1960, producing coherent visible light from a set-up based on a rod of ruby as the active medium.[152] The high intensities and coherence of the electromagnetic radiation gave rise to a new area of in the field of optics: non-linear optics, of which some aspects are described in the following section. For a comprehensive overview of different types of lasers, that have been developed over the years, see e.g. References 199, 212, and 213.

1.2 Non-linear optics

The first non-linear optical experiment was the second harmonic generation experiment, reported in 1961 by Franken *et al.*[74] They passed a red ruby laser beam with a wavelength of 6943 Å through a quartz crystal and observed ultraviolet radiation from the crystal at 3471 Å, which is twice the frequency or half the wavelength of the original laser beam. The dielectric response of a medium is generally described by the dielectric polarisation **P**, which is a function of the electric field **E**. Second harmonic generation is one of the processes that can occur when the dielectric response of a medium is no longer predominantly linear in terms of **E**, meaning that higher-order terms become non-negligible. These higher-order terms only become non-negligible at high field strengths. At optical frequencies, the high intensities corresponding to these high field strengths are only practically attainable with the use of a laser. With the ongoing development of the laser, many experiments were carried out involving optical phenomena connected with the lowest order non-linear term. These phenomena include second-harmonic generation (SHG), sum-frequency generation (SFG), difference-frequency generation (DFG), and optical parametric generation (OPG) and optical parametric amplification (OPA).

These so-called three-wave mixing processes were and still are a useful way to generate coherent radiation at other frequencies than the different types of lasers can provide and many areas of spectroscopy have benefited from these techniques. For example, very few lasers are available that emit in the mid-infrared (wavelengths in the region 1–10 μm), but DFG and OPG/OPA provided coherent and tunable sources for spectroscopy in this wavelength region. The development of pulsed lasers with short pulses was another great achievement which opened up new areas of spectroscopy. With shorter and shorter pulse durations, from nanosecond, through picosecond to the femtosecond† titanium-sapphire

† 1 ns = 10^{-9} s, 1 ps = 10^{-12} s, 1 fs = 10^{-15} s.

lasers of today, peak powers and time-resolutions in experiments have become higher and higher.[29,103,199,212] Recently, even pulses with sub-femtosecond ("attosecond") duration have been reported.[172] One area of spectroscopy which has greatly benefited from developments in non-linear optics is time-resolved vibrational spectroscopy, which is the experimental technique used in Chapters 3, 4, 5, and 6, and which is introduced in Section 2.2.

In the linear case, the dielectric polarisation $\mathbf{P}(\mathbf{r}, t)$ at a time t, which describes the dielectric response of a medium, can be written as[190]

$$\mathbf{P}(\mathbf{r}, t) = \int_{-\infty}^{\infty}\int_{-\infty}^{\infty} \chi^{(1)}(\mathbf{r} - \mathbf{r}_1, t - t_1) \cdot \mathbf{E}(\mathbf{r}_1, t_1) d\mathbf{r}_1 dt_1, \tag{1.1}$$

where $\chi^{(1)}$ is the linear susceptibility and $\mathbf{E}(\mathbf{r}, t)$ the electric field at position $\mathbf{r}$ and time t. Let $\mathbf{E}$ be a monochromatic plane wave with

$$\mathbf{E}(\mathbf{r}, t) = \tilde{\mathbf{E}}(\mathbf{k}, \omega) = \iint \mathbf{E}(\mathbf{k}, \omega) e^{i(\mathbf{k}\cdot\mathbf{r} - \omega t)} d\mathbf{k}\, d\omega, \tag{1.2}$$

where $\mathbf{k}$ is the wave vector, $k = n(\omega)\omega/c$, with $n(\omega)$ the refractive index at frequency ω and c the velocity of light. The Fourier transform of Equation (1.1) then yields the relation

$$\mathbf{P}(\mathbf{r}, t) = \tilde{\mathbf{P}}(\mathbf{k}, \omega) = \chi^{(1)}(\mathbf{k}, \omega) \cdot \tilde{\mathbf{E}}(\mathbf{k}, \omega), \tag{1.3}$$

with

$$\chi^{(1)}(\mathbf{k}, \omega) = \int_{-\infty}^{\infty}\int_{-\infty}^{\infty} \chi^{(1)}(\mathbf{r}, t) e^{-i(\mathbf{k}\cdot\mathbf{r} - \omega t)} d\mathbf{r} dt. \tag{1.4}$$

The linear dielectric constant $\varepsilon(\mathbf{k}, \omega)$ is related to $\chi^{(1)}(\mathbf{k}, \omega)$, in Gaussian units, by

$$\varepsilon(\mathbf{k}, \omega) = 1 + 4\pi\chi^{(1)}(\mathbf{k}, \omega). \tag{1.5}$$

In the electric-dipole approximation, when the magnetic dipole and higher-order multipoles can be neglected, $\chi^{(1)}(\mathbf{r}, t)$ is independent of $\mathbf{r}$ and hence, both $\varepsilon(\mathbf{k}, \omega)$ and $\chi^{(1)}(\mathbf{k}, \omega)$ are independent of $\mathbf{k}$.

In the non-linear case, the polarisation $\mathbf{P}$ can be expanded into a power series of $\mathbf{E}$:

$$\begin{aligned} \mathbf{P}(\mathbf{r}, t) \quad = \quad & \int_{-\infty}^{\infty}\int_{-\infty}^{\infty} \chi^{(1)}(\mathbf{r} - \mathbf{r}_1, t - t_1) \cdot \mathbf{E}(\mathbf{r}, t_1) d\mathbf{r}_1 dt \\ & + \int_{-\infty}^{\infty}\int_{-\infty}^{\infty}\int_{-\infty}^{\infty}\int_{-\infty}^{\infty} \boldsymbol{\chi}^{(2)}(\mathbf{r} - \mathbf{r}_1, t - t_1; \mathbf{r} - \mathbf{r}_2, t - t_2) \\ & : \mathbf{E}(\mathbf{r}_1, t_1)\mathbf{E}(\mathbf{r}_2, t_2) d\mathbf{r}_1 dt_1 d\mathbf{r}_2 dt_2 + \cdots \end{aligned} \tag{1.6}$$

where the tensors $\boldsymbol{\chi}^{(n)}$ are the n^{th} order susceptibilities of the medium. If $\mathbf{E}$ can be expressed as a group of monochromatic plane waves

$$\mathbf{E}(\mathbf{r}, t) = \sum_i \tilde{\mathbf{E}}(\mathbf{k}_i, \omega_i), \tag{1.7}$$

then the Fourier transform of Equation (1.6) gives

$$\mathbf{P}(\mathbf{k}, \omega) = \sum_{n \geq 1} \mathbf{P}^{(n)}(\mathbf{k}, \omega) \tag{1.8}$$

with

$$\begin{aligned}\mathbf{P}^{(1)}(\mathbf{k},\omega) &= \chi^{(1)}(\mathbf{k},\omega)\cdot\mathbf{E}(\mathbf{k},\omega),\\ \mathbf{P}^{(2)}(\mathbf{k},\omega) &= \boldsymbol{\chi}^{(2)}(\mathbf{k}_i+\mathbf{k}_j,\omega_i+\omega_j):\mathbf{E}(\mathbf{k}_i,\omega_i)\mathbf{E}(\mathbf{k}_j,\omega_j),\end{aligned} \tag{1.9}$$

and

$$\begin{aligned}&\boldsymbol{\chi}^{(n)}(\mathbf{k}_1+\mathbf{k}_2+\cdots+\mathbf{k}_n,\omega_1+\omega 2+\cdots+\omega_n)\\ &\quad= \int_{-\infty}^{\infty}\int_{-\infty}^{\infty}\cdots\int_{-\infty}^{\infty}\int_{-\infty}^{\infty}\boldsymbol{\chi}^{(n)}(\mathbf{r}-\mathbf{r}_1,t-t_1;\cdots;\mathbf{r}-\mathbf{r}_n,t-t_n)\\ &\qquad\times e^{-i[\mathbf{k}_1(\mathbf{r}-\mathbf{r}_1)-\omega_1(t-t_1)+\cdots+\mathbf{k}_n(\mathbf{r}-\mathbf{r}_n)-\omega_n(t-t_n)]}d\mathbf{r}_1dt_1\cdots d\mathbf{r}_ndt_n.\end{aligned} \tag{1.10}$$

Three-wave mixing processes involve the second order term in this expansion and can therefore only occur in non-centrosymmetric media, which have a $\boldsymbol{\chi}^{(2)}$ which is non-zero.[190] Consider an electrical field $\mathbf{E}$ consisting of two pulses with central frequencies ω_1 and ω_2

$$\mathbf{E}(\mathbf{r},t)=\mathbf{E}_1(\mathbf{r},t)e^{-i(\omega_1t-\mathbf{k}_1\cdot\mathbf{r})}+\mathbf{E}_2(\mathbf{r},t)e^{-i(\omega_2t-\mathbf{k}_2\cdot\mathbf{r})}+\text{c.c.}, \tag{1.11}$$

where c.c. stands for complex conjugate. When using short laser pulses in three-wave mixing processes at frequencies away from any resonances, the dispersion of $\boldsymbol{\chi}^{(2)}$ can be neglected and the second-order term in Equation (1.6) can be written as

$$\mathbf{P}^{(2)}(\mathbf{r},t)=\boldsymbol{\chi}^{(2)}:\mathbf{E}(\mathbf{r},t)\mathbf{E}^*(\mathbf{r},t), \tag{1.12}$$

indicating an instantaneous dielectric response to the incoming short pulses. Using Equation (1.11), we can write Equation (1.12) as[38]

$$\begin{aligned}P^{(2)}(\mathbf{r},t) &= \chi^{(2)}[E_1^2(\mathbf{r}e^{-2i(\omega_1t-\mathbf{k}_1\cdot\mathbf{r})}+E_2^2e^{-2i(\omega_2t-\mathbf{k}_2\cdot\mathbf{r})}+2E_1E_2e^{-i((\omega_1+\omega_2)t-(\mathbf{k}_1+\mathbf{k}_2)\cdot\mathbf{r})}\\ &\quad+2E_1E_2^*e^{-i((\omega_1-\omega_2))t-(\mathbf{k}_1-\mathbf{k}_2)\cdot\mathbf{r})}+\text{c.c.}]+2\chi^{(2)}[E_1E_1^*+E_2E_2^*].\end{aligned} \tag{1.13}$$

The terms in this expression correspond to the second harmonic of the field at ω_1, the second harmonic of the field at ω_2, the sum-frequency generation at frequency $(\omega_1+\omega_2)$, the difference frequency generation at $(\omega_1-\omega_2)$ and the optically rectified signal, respectively. For a more comprehensive overview of the subject of three-wave mixing see References 28, 38, 45, 64, 185, 190, 212, and 213.

For the field generated at the sum frequency $\omega_3=\omega_1+\omega_2$ with wave vector $\mathbf{k}_3$, the component of the second-order polarisation will have the form

$$P^{(2)}(\mathbf{r},t)_{\omega_3=\omega_1+\omega_2}\propto 2E_1E_2e^{-i(\omega_3t-(\mathbf{k}_1+\mathbf{k}_2)\cdot\mathbf{r})}. \tag{1.14}$$

A high intensity at frequency ω_3 will only occur if the *phase matching condition*

$$\mathbf{k}_3=\mathbf{k}_1+\mathbf{k}_2 \tag{1.15}$$

is satisfied. DFG involves two fields with comparable magnitude, when two relatively intense laser pulses with frequencies ω_3 and ω_2 (ω_1) are used to generate a third pulse at frequency ω_1 (ω_2). OPA can be considered a special case of DFG where one of the incident pulses is much lower in intensity than the other. The intense pulse is normally called the pump

pulse. The other two fields are called signal and idler, where generally the idler is the one lowest in frequency. In the remainder of this chapter and in the next chapter, the pump frequency will be denoted by ω_3, the signal frequency by ω_2 and the idler frequency by ω_1.

For collinearly propagating beams the phase matching condition can be written as

$$n_3(\omega_3)\omega_3 = n_1(\omega_1)\omega_1 + n_2(\omega_2)\omega_2. \tag{1.16}$$

Condition (1.16), in combination with energy conservation $\omega_3 = \omega_1 + \omega_2$, can normally only be satisfied in birefringent materials, as in normal materials $n(\omega)$ usually increases monotonically with ω. However, in birefringent materials, the refractive index differs for different directions of the polarisation. Hence, if one of the three linearly polarised waves has a polarisation perpendicular to the others, condition (1.16) can be satisfied. Three different polarisation geometries can be identified: in type I phase matching the pump polarisation is perpendicular to signal and idler; in type II the signal polarisation is perpendicular to pump and idler; and in type III the idler polarisation is perpendicular to pump and signal.

Light polarised perpendicular to the plane containing the propagation vector $\mathbf{k}$ and the optical axis of a uni-axial birefringent material is said to have the ordinary polarisation and experiences a refractive index n^o. Light polarised parallel to the plane containing the propagation vector $\mathbf{k}$ and the optical axis of the material is said to have the extraordinary polarisation and experiences a refractive index n^e. For extraordinary polarisation, the refractive index will depend on the angle θ between the direction of propagation and the optical axis, according to the relation

$$\frac{1}{(n^e)^2(\theta)} = \frac{\sin^2\theta}{(\bar{n}^e)^2} + \frac{\cos^2\theta}{(n^o)^2}, \tag{1.17}$$

where $\bar{n}^e$ is the principal value for n^e at $\theta = 90°$.

For the case of type I phase matching with collinear propagating beams Equation (1.16) has the form

$$n_3^e(\omega_3, \theta)\omega_3 = n_1^o(\omega_1)\omega_1 + n_2^o(\omega_2)\omega_2, \tag{1.18}$$

where the superscripts o and e stand for ordinary and extraordinary, respectively. Combining Equations (1.17) and (1.18), one can calculate phase-match angles for the type I process for different combinations of ω_1 and ω_2 using the Sellmeier dispersion relations for the refractive indices. It is clear that by rotating the crystal, one can tune the frequencies of signal and idler, as at each angle the phase-matching condition for a different pair of signal and idler frequencies is fulfilled. This method of frequency tuning is generally known as *angle tuning*. For some crystals, like for example lithium niobate ($LiNbO_3$), the birefringence is also strongly dependent on temperature. This offers the possibility of tuning the frequency of signal and idler by *temperature tuning*.

1.3 Molecular vibrations and vibrational dynamics

The atoms of molecules vibrate around their equilibrium positions. Let us first consider the vibration of the simplest molecule, a diatomic molecule, like hydrogen chloride (HCl) or carbon monoxide (CO). In these diatomic molecules there is one vibrational mode, the

stretch mode, in which the relative distance of the atoms changes periodically with the period of oscillation. To determine the energy levels of this vibration, we first assume that the atoms are driven back by a restoring force, which is proportional to the displacement from the equilibrium distance r_e. The potential $V(r)$ can be described in terms of a harmonic oscillator with a force constant k along the line connecting the two atoms and has the form:

$$V(r) = \frac{k}{2}(r - r_e)^2, \tag{1.19}$$

where r is the internuclear distance and r_e the equilibrium distance. The eigenfrequency of this harmonic oscillator is given by

$$\omega = \sqrt{\frac{k}{\mu}}, \tag{1.20}$$

with μ the reduced mass of the system. Solving the time-independent Schrödinger equation with the potential of Equation (1.19) leads to the following energy levels

$$E_v = \hbar\omega\left(v + \frac{1}{2}\right), \quad v = 0, 1, 2, \ldots \tag{1.21}$$

In this equation, ω is the oscillator frequency, $\hbar = h/2\pi$, with h Planck's constant and v the vibrational quantum number. The lowest energy is the zero-point energy $E_{v=0} = \hbar\omega/2$. The energy levels associated with this parabolic potential have an equal spacing of $\hbar\omega$.

In reality, the potential curve of a diatomic molecule is not parabolic. In fact, it is easy to see that the potential must be asymmetric with respect to the equilibrium distance r_e. For distances $r < r_e$, a reduction of the distance r will lead to an increase in repulsion, as at short range a repulsive potential is superposed on the parabolic potential, which prevents the two nuclei from penetrating each other. On the other hand, increasing the distance from r_e will eventually lead to dissociation, as the chemical bond is weakened. So for $r > r_e$ the potential will become flatter. An often used potential which agrees well with experimental evidence is the so-called Morse potential:[97]

$$V(r) = E_d\left(1 - e^{-\zeta(r-r_e)}\right)^2. \tag{1.22}$$

Here, E_d is the depth of the potential well and ζ is a quantity, characteristic for the molecule under consideration:

$$\zeta = \omega_h\sqrt{\frac{\mu}{2E_d}}, \tag{1.23}$$

where ω_h is the harmonic oscillator frequency. Solving the Schrödinger equation for the anharmonic oscillator with Equation (1.22) as the potential energy, yields the energy levels, which are given by:

$$E_v = \hbar\omega_h\left(v + \frac{1}{2}\right) - x\hbar\omega_h\left(v + \frac{1}{2}\right)^2, \tag{1.24}$$

where the terms with higher powers of $\left(v + \frac{1}{2}\right)$ have been neglected, as their contributions are very small for small values of v. The number of bound levels is finite.[12] The constant x is the anharmonicity constant, which is defined as

$$x = \frac{\hbar\omega_h}{4E_d} = \frac{\zeta^2\hbar}{2\mu\omega_h}, \tag{1.25}$$

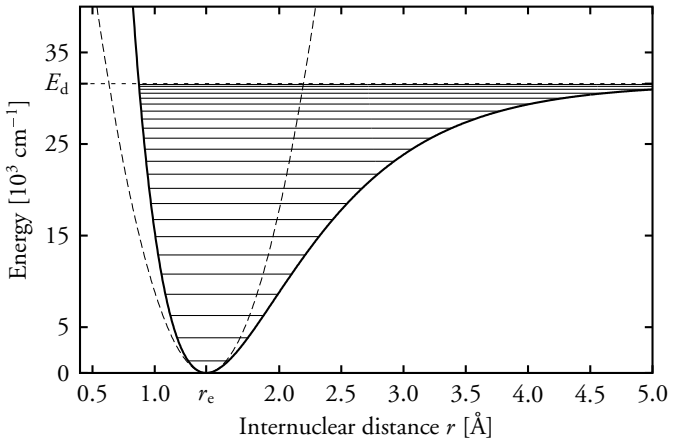

FIGURE 1.1. Morse potential (solid line) and its energy levels and the corresponding harmonic potential (dashed line). These curves were calculated using the following parameters, which give a good description for the vibrational states of hydrogen bromide (HBr):[108] E_d = 31590 cm^{-1}, k = 103600 cm^{-1} Å^{-2}, r_e = 1.414 Å, and $\hbar\omega_h$ = 3649.67 cm^{-1}.

and is usually of order 0.01.

If we rewrite Equation (1.24) in the form

$$E_v = \hbar\omega_h \left(v + \frac{1}{2}\right) \left[1 - x\left(v + \frac{1}{2}\right)\right], \tag{1.26}$$

and compare with Equation (1.21), we see that going from the harmonic to the anharmonic oscillator, the vibrational frequency ω is replaced by

$$\omega_v = \omega_h \left[1 - x\left(v + \frac{1}{2}\right)\right]. \tag{1.27}$$

From Equation (1.27) it is clear that with increasing vibrational quantum number v, the spacing, i.e. the transition frequency, between the energy levels, decreases, which is illustrated in Figure 1.1. The dissociation energy E_o is slightly less than the depth E_d of the potential well containing the bound states, because of the zero-point energy: $E_o = E_d - \hbar\omega_h/2$.

The occupation of the energy levels E_v is in thermal equilibrium proportional to the Boltzmann factor $e^{-E_v/kT}$. Since at room temperature, kT corresponds to about 200 cm^{-1},[‡] the stretch vibration of most diatomic molecules will be in the vibrational ground state, for example for HCl molecules, $E_{v=1} - E_{v=0} = 2886$ cm^{-1}.[178]

Molecules with more than two atoms have more vibrational degrees of freedom than a diatomic molecule and therefore have more vibrational modes than the single stretch mode of a diatomic molecule. The vibrations in a polyatomic molecule are often described in terms of normal modes. A normal mode is a synchronous motion of atoms or groups of

[‡]In spectroscopy, the unit cm^{-1} is formally the unit of the quantity $\bar{\nu}$, the *wave number*, the inverse of wavelength. The unit is however also often used for frequency (corresponding to light in vacuum with that wave number) and for energy (the energy of a photon with that wave number).

atoms in a polyatomic molecule that may be excited without leading to the excitation of any other normal mode. The normal-mode coordinates form a basis set for a description of the displacements of the centres of mass of the atoms in a molecule. The number of normal modes in an n-atomic molecule is equal to the number of its vibrational degrees of freedom which is $3n - 6$, or $3n - 5$ for a linear molecule. The symmetry of the normal mode is the same as the symmetry of the first vibrationally excited state of the molecule, which provides a way to determine whether a vibrational mode is active, i.e. whether the electric dipole transition associated with the excitation of that mode is allowed.

If the Hamiltonian of a molecule only contains terms of first and second order in the nuclear coordinates, the normal modes are decoupled from each other and can be described as independent harmonic oscillators. In reality, however, the Hamiltonian will also contain third- and higher-order terms. These anharmoncities cause the vibrational potential to more closely resemble a Morse potential than a harmonic potential (diagonal anharmonicity). Additionally, anharmonic couplings exist between the different normal modes in a molecule, giving rise to combined or combination vibrations (cross anharmonicity). For a comprehensive treatment of the vibrations of polyatomic molecules, see e.g. References 11, 12, 97, 108, and 115.

When excited vibrational states decay, energy is transferred from the vibrational mode which was originally excited to other modes, eventually leading to an equilibration over all degrees of freedom. Both the nature and the availability of these accepting modes strongly influence the lifetime T_1 of the excited state. The relaxation of an excited molecular vibration can be an *intra*molecular process, in which energy is transferred to other vibrations in the same molecule, through anharmonic couplings with the vibrational mode that was originally excited. The other type of mechanism is an *inter*molecular process, in which energy is transferred to vibrations of neighbouring (solvent) molecules or to low-frequency (solvent) modes. When the first step involves intramolecular energy transfer, one of the following steps involves intermolecular energy transfer, as eventually all energy is transferred to the heat bath formed by low-frequency modes, phonons in the case of solids and low-frequency liquid modes in the case of liquids.

If the frequency of the accepting mode is relatively high, which is usually the case with an intramolecular relaxation process, relaxation of an excited vibration is faster, i.e. the lifetime T_1 is shorter (in one step, energy transfer to e.g. two quanta of a molecular vibration is "easier" than to a much larger number of low-frequency modes[♯]). If there are no high-energy intramolecular vibrations to which the excited mode can couple, the lifetime will be long and will also be more strongly influenced by the solvent, as the relaxation mechanism will be an intermolecular process. Because the accepting modes are then formed by low-frequency solvent modes, there will also be a strong dependence on temperature. The strong influence of the availability of accepting modes is clearly illustrated in the lifetimes of different C–O stretch vibrations, described in Section 6.1. It is clear that by looking at the lifetimes and vibrational dynamics of excited vibrations a lot of information can be gathered on the couplings that exist within and between molecules in the condensed phase. For more details on the theory of vibrational dynamics and vibrational relaxation see e.g. References 15, 71, 128, 154, and 202 and references therein.

[♯] The energy gap law states that the vibrational relaxation rate is proportional to δ^{-N}, where N is the number of quanta dissipated in the accepting mode and $\delta \ll 1$, with δ a constant.[164]

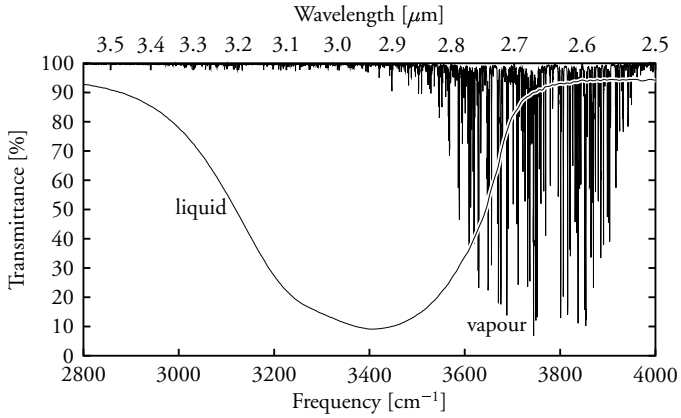

FIGURE 1.2. Transmittance spectrum of water (H_2O) vapour (∼20 cm air of normal humidity at room temperature) and transmittance spectrum of a water film with a thickness of ∼3 μm.[161]

1.4 ABSORPTION LINE BROADENING OF VIBRATIONAL TRANSITIONS

In the gas phase, the absorption spectrum of a molecular vibration has a characteristic substructure due to the coupling of vibration and rotation of these molecules. In the condensed phases, liquid and solid, the absorption spectrum often shows very broad bands, with very little structure, as is illustrated in Figure 1.2.

The broadening of absorption lines is caused by dephasing: a loss of coherence of the excited oscillators. The broadening can be caused by different mechanisms. There can be a static distribution of transition frequencies of the molecules. The dephasing can also be caused by the loss of coherence due to rapid changes in frequency of the oscillators around one central frequency, without the loss of excitation. And thirdly, decay of the excited state population with a time constant $1/T_1$ also contributes to dephasing.

If the dephasing is due to a static distribution of transition frequencies, which leads to a Gaussian line shape, an absorption line is *inhomogeneously broadened*. The two other dephasing mechanisms contribute to the *homogenous line broadening*, characterised by the homogeneous dephasing time T_2. The resulting absorption line will have the shape of a Lorentzian with a width $\Delta\nu$ given by

$$\Delta\nu = \frac{1}{\pi T_2}. \tag{1.28}$$

T_2 has two contributions:

$$\frac{1}{T_2} = \frac{1}{2T_1} + \frac{1}{T_2^*}, \tag{1.29}$$

where T_1 is the lifetime of the excited state and T_2^* is the pure dephasing time. Pure dephasing encompasses all dephasing not due to population relaxation.

In practice, the vibrational absorption bands in the condensed phase at room temperature are inhomogeneously broadened and are composed of an inhomogeneous distribution of homogenously broadened bands. For high-frequency molecular vibrations like the O–H

and C–H stretch vibrations, the homogeneous linewidths are mainly determined by pure dephasing, due to rapid fluctuations and only have a small contribution due to population relaxation. Measuring the linear absorption spectrum will therefore only give information on the width of the distribution of oscillator frequencies and not on the excited-state population relaxation. With non-linear spectroscopical techniques it is however possible to determine T_1 and T_2. The homogeneous dephasing time T_2 can be determined by photon-echo spectroscopy[100,175,197,201] and spectral hole burning.[32,33,34] When using these techniques it is usually assumed that the rapid fluctuations, giving rise to the homogeneous broadening, occur on a much faster timescale than the dynamics of the distribution of transition frequencies giving rise to the inhomogeneous linewidth, which are assumed to be very slow on the timescale of the experiment. It is however also possible that the distribution of transition frequencies homogenises during the measurement, a process that is referred to as spectral diffusion.[99,101,162,208] In this thesis, in Chapters 3, 4, 5, and 6, the vibrational lifetime T_1 of several vibrations is determined with vibrational pump-probe spectroscopy, which is introduced in Section 2.2.

1.5 Outline of this thesis

The largest part of this thesis is devoted to the investigation of the vibrational dynamics of small molecules and complexes in liquid solution and in the pure liquid. The experimental technique that was used is vibrational pump-probe spectroscopy. This form of time-resolved mid-infrared spectroscopy is described in detail in Chapter 2, together with the method of generation of short mid-infrared pulses. In Chapters 3 and 4, the focus is on hydrogen-bonded acid-base complexes in solution. In Chapter 3, a relatively weak form of hydrogen-bonding in complexes of hydrogen chloride with diethyl ether is encountered, whereas in Chapter 4, complexes in which hydrogen-bonding is exceptionally strong come under scrutiny, when complexes of hydrogen fluoride with pyridine are investigated.

The large influence of the nature and availability of accepting modes can be seen in Chapters 5 and 6. In Chapter 5, two-colour pump-probe experiments on the C–H stretch vibration of pure bromoform show that, compared to solutions of bromoform, the reduction in the number of accepting modes provided by the solvent for *inter*molecular energy transfer, greatly influences the mechanism and time scale of vibrational relaxation. The influence of the number of vibrational modes in a molecule on *intra*molecular vibrational relaxation, is manifested in Chapter 6. There, the vibrational dynamics are investigated after excitation of the C–O stretch vibration of the alcohols methanol and ethanol in solution.

In Chapter 7, the last chapter of this thesis, we focus on the non-linear optical process that is conveniently used to generate the mid-infrared pulses for the experiments featured in the other chapters. The focus is on the correlation properties of parametrically generated light. These properties arise from the fact that OPG is a very special type of conversion process, where one starts with an electromagnetic wave at one frequency and ends up with waves at three frequencies. This process can only be understood using a quantum mechanical description of the electromagnetic field. The correlation properties of the parametrically generated light reflect the macroscopic manifestation of the quantum fluctuations of the zero-photon electromagnetic field that seed the parametric generation process.

2 Time-resolved non-linear mid-infrared spectroscopy

The non-linear optical processes optical parametric generation and amplification and difference frequency generation are used in the generation of short mid-infrared pulses. A general overview of a laser system to generate femtosecond mid-infrared pulses illustrates the non-linear optical processes and components involved in generating these "ultrashort" pulses. These pulses can be used in time-resolved non-linear infrared spectroscopy. One such a technique, vibrational pump-probe spectroscopy, is discussed here.

2.1 Mid-infrared pulse generation

2.1.1 Parametric generation and amplification

To perform time-resolved mid-infrared experiments with (sub-)picosecond time resolution, one needs tunable, short, and intense mid-infrared laser pulses. There are few lasers that emit in the wavelength region 1–10 μm, therefore usually difference-frequency generation (DFG) and optical parametric generation and amplification (OPG/OPA) are used to generate mid-infrared pulses from the output of lasers that emit in the visible or near-infrared.

The description of parametric amplification can be done in a completely classical way using Maxwell's equations. It can be shown[190] that if no saturation effects or pump depletion occur, the amplitudes of idler (and signal) grow exponentially in the (collinear) propagation direction z:

$$\left|E_1(z)\right|^2 \propto \left|E_1(0)\right|^2 e^{gz}, \tag{2.1}$$

with

$$g = \sqrt{g_0^2 - (\Delta k)^2}, \tag{2.2}$$

where

$$g_0^2 = \frac{\omega_1 \omega_2}{n_1 n_2 c^2} \left(\chi_{\text{eff}}^{(2)}\right)^2 \left|E_3\right|^2 \tag{2.3}$$

and

$$\Delta k = k_3 - k_2 - k_1. \tag{2.4}$$

In Equation (2.3), c is the velocity of light, ω_1 the idler frequency, ω_2 the signal frequency, E_3 the electric field at the pump frequency ω_3, and $\chi_{\text{eff}}^{(2)}$ the effective second-order susceptibility.

At low pump intensities, such that $g_0^2 < (\Delta k)^2$, the gain g is purely imaginary. In that case, the parametric interaction does not lead to amplification of signal and idler but to a change of phase.[16] The gain is maximal when $\Delta k = 0$, i.e. when there is no phase-mismatch and $g = g_0$. It is also clear that the gain can still be appreciably high when Δk is nonzero and the intensity of the pump is sufficiently high. Hence, an increase of intensity of the

pump will lead to an increased spectral bandwidth of signal and idler. The bandwidth $\Delta\omega$ of the generated signal and idler pulses is given by

$$\Delta\omega = \frac{2}{a}\left(\frac{2g_0}{l}\ln 2\right)^{\frac{1}{2}}, \tag{2.5}$$

with

$$a = \left[\left(\frac{dk_1}{d\omega_1}\right)_{\omega_1^0} - \left(\frac{dk_2}{d\omega_2}\right)_{\omega_2^0}\right] \tag{2.6}$$

and l the length of the crystal. For a more comprehensive treatment of the case with $\Delta k \neq 0$ see Reference 9.

From Equation (2.3) one other aspect transpires; at degeneracy ($\omega_1 = \omega_2$) the gain factor g_0 is maximal, and decreases for signal and idler frequencies away from degeneracy, as the product $\omega_1\omega_2$ decreases. From Equation (2.5) it is also clear that the bandwidth decreases when signal and idler are tuned away from degeneracy, as the group-velocity mismatch in Equation (2.6) increases. Finally, it should be noted that at higher pump energies, the pump will get depleted and therefore Equations (2.1), (2.2), (2.3), and (2.5) will no longer be valid. Signal and idler will then no longer increase exponentially over the length of the crystal and even the opposite process of OPA, sum-frequency generation, can occur.

2.1.2 EXPERIMENTAL SET-UP

After continuous-wave mid-infrared generation using OPG/OPA had already been demonstrated,[83,151] Kaiser and co-workers were one of the first to report the generation of picosecond mid-infrared pulses with this technique and their use in pump-probe experiments, see References 73, 137, 138, 139, 140, and 188. They used picosecond pulses at 1058 nm from a neodymium:glass (Nd:glass) laser as pump pulses for OPG/OPA in lithium niobate ($LiNbO_3$) crystals. Later, neodymium:yttrium-aluminium-garnet (Nd:$Y_3Al_5O_{12}$ or Nd:YAG) lasers became more popular because of their higher pulse energies and repetition rates. A set-up based on this principle is used in Chapter 5 of this thesis, where the output of a Nd:YAG laser is used to generate picosecond pulses with a wavelength around 3 μm through OPG/OPA in $LiNbO_3$ crystals.

The development of titanium:sapphire (Ti:Al_2O_3) lasers with Kerr-lens mode locking[193] provided pump-lasers with femtosecond pulses which could be used to generate mid-infrared pulses of a few hundred fs. The experimental set-ups that are used in Chapters 3 and 4 are based on a laser system with titanium:sapphire as the active medium. In order to give an idea of the non-linear optical processes and components involved in generating these "ultrashort" mid-infrared pulses, a general overview of such a system is given here. The details on the different experimental set-ups used in the experiments in this thesis can be found in the relevant chapters.

The set-up consists of a commercial Ti:sapphire laser system, composed of an oscillator and an amplifier, which delivers pulses with a duration of around 100 fs, a wavelength around 800 nm, and an energy of 1–3 mJ. The repetition rate such the system often is 1 kHz. Part of the pulse energy is used to pump a commercial multi-pass OPG/OPA stage based on a β-barium borate (β-BaB_2O_4 or BBO) crystal. In this OPG/OPA stage, part of the energy is converted to tunable mid-infrared pulses (signal and idler). The wavelength of the idler pulses is tunable between 1600 and 2600 nm.

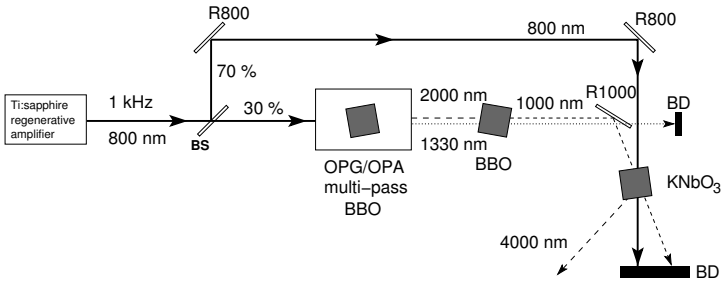

FIGURE 2.1. Generation of femtosecond pulses with a wavelength around 4000 nm for time-resolved non-linear spectroscopy. Legend: BBO, $KNbO_3$: crystals; R800, R1000: dielectric 800 nm, 1000 nm mirrors; BD: beam dump; OPG/OPA: three-pass optical parametric generation and amplification stage based on BBO.

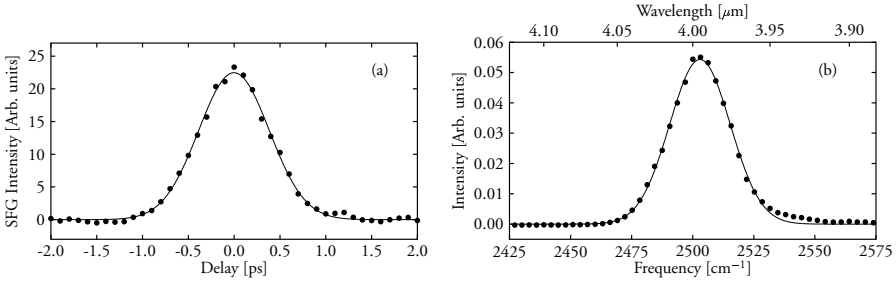

FIGURE 2.2. Typical cross correlation trace (a) and spectrum (b) of the laser pulses generated with the set-up that is described in §2.1.2. The solid lines are Gaussians with a FWHM of (a) 908 fs [corresponding to a pulse duration of 642 fs (FWHM)] and (b) 29 cm^{-1}, respectively.

In order to generate pulses with a wavelength around 3–4 μm, the idler pulses with a wavelength around 2 μm are first frequency-doubled in a second BBO crystal. Then, the resulting 1 μm light is combined with the remaining part of the 800 nm light in another crystal, usually potassium niobate ($KNbO_3$) or $LiNbO_3$, to generate the 3–4 μm pulses in a difference frequency generation (DFG) process. In this last conversion step, a non-collinear geometry can be used to spatially separate the 3–4 μm beam from the 800 nm and 1 μm beams. By tuning the wavelength of the seed pulse and by changing the phase-match angle of the DFG-crystal, the wavelength of the mid-infrared pulses can be tuned continuously. This final pulse has a typical energy of $\sim$20 μJ, a bandwidth of 60 nm (37 cm^{-1}), and a duration of $\sim$600 fs full width at half maximum (FWHM), see Figure 2.2. The pulse duration is determined by measuring the autocorrelation signal of the pulse via second harmonic generation (SHG).

2.2 VIBRATIONAL PUMP-PROBE SPECTROSCOPY

In a pump-probe experiment an excitation is created in a sample by one pulse (the pump) and probed by a second pulse (the probe). By varying the delay between the pump and probe pulses, the evolution of the excitation can be followed in time. This of course requires the pulses to be at least shorter than the decay of the excitation one wants to monitor. An example of an early pump-probe experiment is a Nuclear Magnetic Resonance (NMR) experiment by Bloembergen in 1948.[30] In this experiment, nuclear spins were excited by an electromagnetic pulse from a radio-transmitter with a duration of a few seconds. As the lifetimes were in the order of seconds, the decay could be monitored by eye on an oscilloscope. The lifetimes T_1 of excited vibrations in liquids lie in the (sub-)picosecond range. Therefore, the generation of mid-infrared pulses with a pulse duration of several picoseconds heralded the first vibrational pump-probe studies in the 1970s, measuring vibrational lifetimes in condensed phases.[137,139,140] Since then, pump-probe spectroscopy has been a widely used technique, and has helped to gain knowledge of the vibrational dynamics of vibrations of many different molecules. With the possibility of generating mid-infrared pulses of around 100 fs (= 0.1 ps) nowadays, even faster relaxation processes can be monitored. Many vibrational pump-probe studies have been published on e.g. the O–H stretch,[60,77,131,162,209,211] the O–D stretch,[132,145] the C–H stretch,[18,88,93,107,215] and the C–O stretch vibrations.[22,35,102,107,119,148]

Generally, in a vibrational pump-probe experiment, a pump pulse excites a vibration of a significant fraction of the molecules in a sample. This excitation causes a decrease in the absorbance of the sample, as there are now less molecules in the vibrational ground state that can absorb radiation at the $v = 0 \rightarrow v = 1$ transition frequency. In addition, there will be a contribution due to stimulated emission corresponding to the $v = 1 \rightarrow v = 0$ transition. The transmittance change is measured with a weaker probe pulse that passes through the sample after a variable delay t. The transmittance change is only observable if the anharmonicity constant x is non-zero, so that the $v = 1 \rightarrow v = 2$ transition frequency is shifted to a different frequency (see Section 1.3).†

A thin sample with a concentration of ρ absorbers per unit surface, each capable of absorbing one photon at the resonance frequency ω, has a transmittance

$$T_0 = e^{-\gamma_0 \rho \sigma}, \tag{2.7}$$

where σ is the absorption cross section of an individual absorber and γ_0 is a geometrical factor that takes into account that linearly polarised light preferably excites absorbers with their transition dipole moment aligned parallel to the axis of polarisation. The absorbers are diatomic molecules or the subunits of polyatomic molecules, involved in the considered vibration, e.g. the C–H group in the C–H stretch vibration of bromoform ($CHBr_3$). If the pump pulse at resonance frequency ω excites a fraction f_e absorbers per unit surface, the sample will temporarily have an altered transmittance T_ϵ depending on the polarisation ϵ of the probe pulse

$$T_\epsilon = e^{\rho \sigma (2 f_e \gamma_\epsilon - \gamma_0)}. \tag{2.8}$$

The factor 2 arises from the fact that the transmittance increase not only results from the ground state depletion but also from the stimulated emission out of the excited state. A

†For example, the C–H bend vibration in bromoform probably only has a very small anharmonicity, as in pump-probe experiments hardly any absorption change was observed.[40]

quantity used to express this pump-induced transmittance change is the absorbance change

$$\Delta\alpha_\epsilon \equiv -\ln\left(\frac{T_\epsilon}{T_0}\right). \tag{2.9}$$

When describing the evolution of Equation (2.9) in time, two processes have to be taken into account, population relaxation of the excited state and change in the anisotropy of the excited state population and of the ground state depletion due to reorientation of the molecules.[90] In the experiments described in this thesis, reorientation did not play a significant role. In Chapters 3 and 4, the angle between polarisations of pump and probe was the *magic angle* of $\arctan(\sqrt{2}) \approx 54.7°$, where (the decay of) the anisotropy does not influence the observed evolution in time of the transmittance change.[126,144,207] In Chapter 5, the reorientation time was fast enough on the timescale of the experiment that the excitation could be considered isotropic.[90] In Chapter 6, the reorientation time was slow enough on the timescale of the experiment, that the contribution of the anisotropy decay was very small. Hence, γ_ϵ can be considered time-independent in these experiments and the geometrical factors γ_ϵ and γ_0 can be included in a scaling factor when describing the data. Therefore, in the description below, the subscript ϵ is dropped. For a description that includes reorientation, see References 90 and 161. As the excited-state population decays to the ground state, described by a function $\xi(t)$, the absorbance change at a time t after the pump pulse will be

$$\Delta\alpha(t) = -2f_e\rho\sigma\xi(t). \tag{2.10}$$

If the studied vibration can be described as an exponentially decaying two-level system, $\xi(t) = \Theta(t)e^{-t/T_1}$, with $\Theta(t)$ the Heaviside function and T_1 the lifetime of the excited state, mentioned in Section 1.3.

In the description until now, any frequency dependence has been neglected. As was seen in Section 1.3, in reality there is a distribution of transition frequencies, especially in condensed phases. Let $f_e(\omega, t)$ describe the fraction of excited molecules as a function of ω and let $\sigma(\omega)$ be the cross section of an absorber at frequency ω. The fraction $f_e(\omega, t)$ will be frequency independent if the absorption line is homogeneously broadened and will have the form of the spectrum of the pump pulse if the absorption line is inhomogenously broadended. If there is spectral diffusion, $f_e(\omega, t)$ will be time dependent. The equivalents of Equations (2.7) and (2.10) can then be written as

$$\alpha_0(\omega) \equiv \ln(T_0(\omega)) = \rho\sigma(\omega), \tag{2.11}$$

$$\Delta\alpha(\omega, t) = -2f_e(\omega, t)\rho\sigma(\omega)\xi(t). \tag{2.12}$$

Equation (2.12) describes the *transient spectrum*. In this thesis and elsewhere, $\Delta\alpha(\omega, t)$ is often either shown as a function of delay t between pump and probe at fixed pump and probe frequencies, generally called a delay-scan; or as a function of pump and/or probe frequency at a certain delay t, which is generally called a transient spectrum. For a detailed description of pump-probe spectroscopy see References 71, 158, 198, and 205.

A typical pump-probe set-up is shown in Figure 2.3. Two mid-infrared pulses are used, an intense pump pulse that excites a significant fraction of the molecules and a weaker probe pulse that monitors the induced transmission change and thereby the decay of the excitation. The pump pulses can be delayed with respect to the probe pulses by varying the

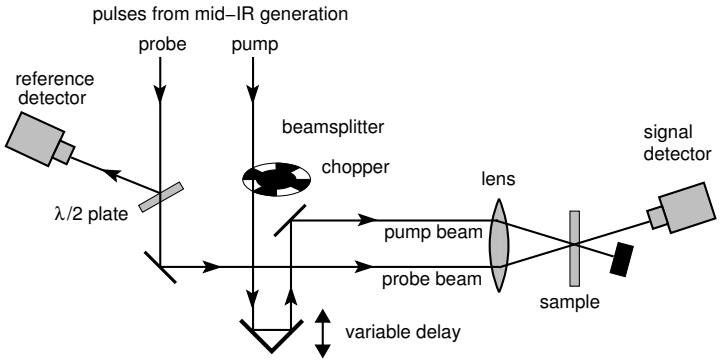

FIGURE 2.3. Typical set-up for pump-probe experiments

path length by means of a delay stage. The pump and probe beams are focused into a sample by a calcium fluoride (CaF_2) or barium fluoride (BaF_2) lens. To exclude reorientational effects of the molecules during the monitoring of the decay, the polarisation of the probe beam can be rotated over the magic angle (54.7°) with respect to the pump polarisation by means of a zero-order $\lambda/2$-plate. Part of the probe pulse is split off and measured as a reference to account for the pulse-to-pulse intensity fluctuations. The intensity of the transmitted probe pulses and of the reference pulses are measured by lead-selenide (PbSe) or mercury-cadmium-telluride (MCT) detectors. In the set-ups used in Chapters 3, 4, and 5, a chopper blocks every other pump pulse to enable a measurement of the intensities of the probe and reference pulses without the effect of the pump pulse on the sample.

The intensity of the probe pulse I_p is measured after the sample at a delay t after the pump pulse. The intensity I_r of the reference pulse is measured by a second detector. The intensities I_p° and I_r° of the probe and reference are also measured in absence of the pump pulse. Note that usually the intensities are measured with a single detector, i.e. not frequency-resolved, and thus one integrates over the spectrum of the pulses. The absorbance change

$$\Delta\alpha(\omega,t) = -\ln\left(\frac{T(\omega,t)}{T_\mathrm{o}(\omega)}\right) = -\ln\left(\frac{I_\mathrm{p}(t)}{I_\mathrm{r}}\cdot\frac{I_\mathrm{r}^\circ}{I_\mathrm{p}^\circ}\right) \tag{2.13}$$

is thus measured as a function of delay between pump and probe pulses. To correct for excessive noise in $\Delta\alpha$ for pulses with low intensity due to influences that do not scale with intensity, a special data acquisition procedure is used. In stead of mere averaging of the detector responses, $\Delta\alpha$ is calculated from T and T_o that result from a linear least-squares fit of $I_{\mathrm{p},j} = TI_{\mathrm{r},j}$ and $I_{\mathrm{p},j}^\circ = T_\mathrm{o}I_{\mathrm{r},j}^\circ$ to the data. The subscript j indicates the individual pulses. A more detailed description of this data acquisition procedure can be found in References 161 and 162.

3 Vibrational dynamics of hydrogen-bonded HCl-diethyl ether complexes

We studied the relaxation of the H–Cl stretch vibration of hydrogen-bonded HCl-diethyl ether [HCl–$(CH_3CH_2)_2O$] complexes at room temperature using femtosecond mid-infrared pump-probe spectroscopy. The lifetime of the H–Cl stretch vibration is determined to be 0.9 ± 0.2 ps. The relaxation is found to occur via an intermediate state which causes a transient blue shift of the H–Cl stretch frequency. This blue shift indicates that the low-frequency $(CH_3CH_2)_2O \cdots$H–Cl hydrogen bond is the main accepting mode of the vibrational energy. The excited population of this hydrogen-bond mode decays with a time constant of 3.1 ± 0.5 ps to the ground state.

3.1 Introduction

Hydrogen bonding is an important interaction, commonly appearing in nature, which determines the properties of a vast number of molecular systems ranging from water to complicated biomolecules. It is a relatively unspecific and weak interaction compared to covalent or ionic bonds with bond enthalpies between 12 and 40 kJ/mol (1000-3350 cm^{-1}).[125,146,189,194] The hydrogen bond between an acid HA and a base B often has a very strong influence on the dynamics of an acid-base reaction:

$$A\text{–}H \cdots B \rightarrow A^- \cdots H\text{–}B^+.$$

However, the microscopic mechanism behind this influence is poorly understood.

Extensive theoretical work has been done on the effect of solvation on the rate and mechanism of proton transfer in simple acid-base complexes for which the reaction coordinate is the position of the proton in the $A \cdots H \cdots B$ complex.[3,4,36,195] It was found that the potential energy as a function of this proton coordinate forms a double-well potential of which the precise shape is largely determined by the interactions with the surrounding molecules. It was also shown that the precise microscopic mechanism for the proton transfer strongly depends on the height of the potential-energy barrier that separates the two wells.[36]

For weakly hydrogen-bonded complexes of the molecules HA and B, the potential-energy barrier is high and the proton transfer results from a quantum-tunnelling process through this barrier. For strongly hydrogen-bonded complexes such as hydrogen chloride (HCl) and hydrogen fluoride (HF) in water,[3,4] the proton transfer from A to B proceeds via an adiabatic following by the proton of the solvent, with the proton remaining in its vibrational ground state. In the course of this reaction, the double-well potential for the proton strongly changes, which in turn causes a change of the energies of the proton

vibrational states. An interesting consequence of this mechanism is that the energy barrier for proton transfer can be much smaller for the first excited vibrational state, $v = 1$, than for the vibrational ground state, $v = 0$. Therefore, acid-base reactions may be induced by absorption of an infrared photon into the A–H stretch vibration in the hydrogen-bonded reactant complex and subsequent relaxation to the $v = 0$ state.

There have been a few experimental, time-resolved studies on the vibrational relaxation of hydrogen-bonded acid-base complexes in the gas phase, like HF-dimethyl ether with a $v = 1$ lifetime T_1 of 10 ns, after which dissociation of the complex occurs,[13] and in the liquid phase, like pyrrole-base and $(CH_3CH_2)_3SiOH$-base dissolved in carbon tetrachloride (CCl_4) with a T_1 between 1 and 70 ps depending on the base.[10,95,96] Here we report on a femtosecond mid-infrared pump-probe study of the H–Cl stretch vibration of hydrogen-bonded HCl–diethyl ether [HCl–$(CH_3CH_2)_2O$] complexes at room temperature. A study on the HF/FHF stretch combination vibration of more strongly hydrogen-bonded hydrogen fluoride-pyridine complexes can be found in Chapter 4.

In the seventies and eighties of the previous century the vibrational relaxation of pure hydrogen chloride has been studied in the gas phase,[52,53,130,143,196,216] in the liquid phase,[54,55,56,129,130] and in solid matrices at very low temperatures.[206] The time scale on which relaxation takes place strongly depends on the phase of the system and ranges from milliseconds to nanoseconds. From a comparison between HCl and DCl in the gas phase and in the liquid,[52,56] it was deduced that rotational degrees of freedom play an important role in the vibrational relaxation. If the HCl molecule forms an acid-base complex with diethyl ether, the vibrational relaxation might be strongly influenced by the hydrogen bond between the HCl and the diethyl ether molecules. This effect of hydrogen bonding on the vibrational relaxation of a strong, diatomic acid such as HCl has not been studied yet.

3.2 EXPERIMENT

We studied solutions of ~1 mol/l hydrogen chloride dissolved in diethyl ether. The sample thickness was 200 μm. It is chosen such that the transmittance at 2500 cm^{-1} (4000 nm) was approximately 10 %. As can be seen in Figure 3.1, the absorption band of the H–Cl stretch vibration in diethyl ether is very broad and structureless. It is shifted to the red by approximately 500 cm^{-1}, compared to the fundamental $v = 0 \rightarrow 1$ frequency of 2886 cm^{-1} in the gas phase.[178] This band shift predominantly results from the fact that the hydrogen chloride forms 1:1 complexes with diethyl ether.[171] The band is strongly inhomogeneously broadened due to the large distribution in hydrogen-bond lengths.

In order to investigate the vibrational dynamics of the H–Cl stretch vibration, one-colour pump-probe experiments are performed on the the $v = 0 \rightarrow 1$ transition at several frequencies in the absorption band with a wavelength around 4000 nm (2500 cm^{-1}) (see Figure 3.1). The technique of pump-probe spectroscopy is explained in Section 2.2. Because the relaxation is expected to occur on a sub-picosecond timescale, femtosecond pulses are required. For this purpose the a setup similar to the one described in §2.1.2 is used to generate the mid-infrared pulses.

The set-up consists of a commercial Ti:sapphire laser system (Spectra Physics Tsunami oscillator with a Quantronix 4800 amplifier) which delivers pulses with a duration of 120 fs full width at half maximum (FWHM), a wavelength of 800 nm, and an energy of 1 mJ (see

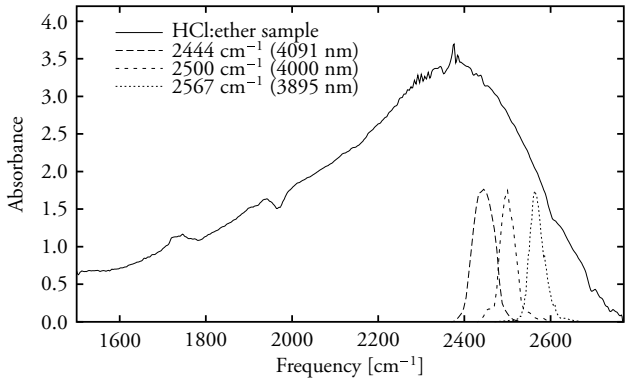

FIGURE 3.1. Absorption band of the H–Cl stretch vibration in diethyl ether corrected for the ether background (solid line). The absorbance A was calculated from the measured transmittance of the sample (T_{sample}) and the transmittance of air (T_{air}) by $A = -\ln(T_{\text{sample}}/T_{\text{air}})$. The dashed lines indicate the power spectra of the pulses used in the experiments.

Figure 3.2). The repetition rate of the system is 1 kHz.

Part of the pulse energy (0.3 mJ) is used to pump a commercial three-pass optical parametric generation and amplification stage (TOPAS, Light Conversion) based on a β-barium borate (β-BaB_2O_4 or BBO) crystal. In order to generate pulses with a wavelength around 4 μm in a difference frequency generation (DFG) process, one needs light with a wavelength of 1000 nm together with the 800 nm of the Ti:sapphire laser as input. Hence, the idler wavelength of the TOPAS is tuned to 2000 nm and frequency-doubled to 1000 nm in a second BBO crystal. Then the 1000 nm light is combined with the remaining part of the 800 nm light (0.7 mJ) in a 5-mm potassium niobate ($KNbO_3$) crystal to produce 4000 nm (2500 cm^{-1}) pulses. In this last conversion step, a non-collinear geometry is used to spatially separate the 4000 nm beam from the 800 and 1000 nm beams. By tuning the wavelength of the seed pulse and by changing the phase-match angle of the $KNbO_3$ crystal, the idler wavelength can be continuously tuned from 3700 to 4250 nm (2350-2700 cm^{-1}). This final pulse has a typical energy of 19 μJ, a bandwidth of 60 nm (37 cm^{-1}), and a duration of $\sim$ 600 fs (FWHM), see Figure 3.3. The pulse duration is determined by measuring the autocorrelation signal of the pulse via second harmonic generation (SHG) in a lithium iodate ($LiIO_3$) crystal.

The pump-probe set-up is very similar to the one shown in Figure 2.3. The pump and probe beams are focused into the sample by a calcium fluoride (CaF_2) lens (focal length 100 mm). The diameter of the focus is estimated to be 200 μm. The polarisation of the probe beam is rotated over the magic angle (54.7°) with respect to the pump polarisation by means of a zero-order $\lambda/2$-plate to exclude reorientational effects of the excited molecules during the decay, see Section 2.2. The intensity of the transmitted probe pulses and of the reference pulses are measured by lead-selenide (PbSe) photoconductive cells. The pump beam is chopped at 500 Hz to block every other pump pulse.

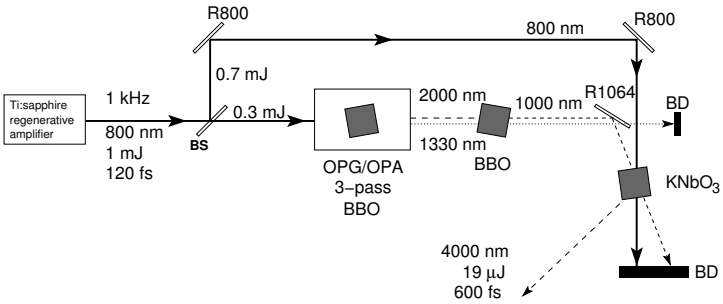

FIGURE 3.2. Generation of femtosecond pulses with a wavelength around 4000 nm for one-colour pump-probe experiments. Legend: BBO, $KNbO_3$: crystals; R800, R1064: dielectric 800 nm, 1064 nm mirrors; BD: beam dump; OPG/OPA: three-pass optical parametric generation and amplification stage based on BBO.

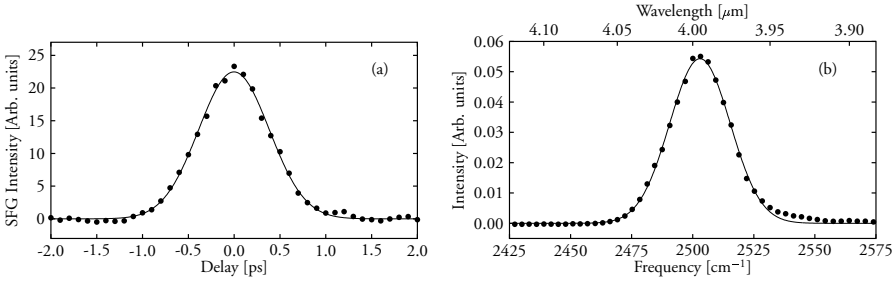

FIGURE 3.3. Typical cross correlation trace (a) and spectrum (b) of the laser pulses generated with the set-up that is described in Section 3.2. The solid lines are Gaussians with a FWHM of (a) 908 fs [corresponding to a pulse duration of 642 fs (FWHM)] and (b) 29 cm^{-1}, respectively.

3.3 RESULTS

One-colour pump-probe delay scans were carried out at several frequencies in the H–Cl stretch absorption band (see Figure 3.1). The results are shown in Figure 3.4. At the blue side (2567 cm^{-1}), the bleaching is observed to change into an induced absorption. This indicates that the relaxation of the excited H–Cl stretch vibration $|1\rangle$ takes place via an intermediate state ($|0^*\rangle$) rather than directly back to the ground state $|0\rangle$. The population of this intermediate state causes an induced absorption of the probe pulse at 2567 cm^{-1}. From this intermediate state the molecules decay to the ground state. The relaxation in two steps is also responsible for the non-single exponential decay observed at 2444 and 2500 cm^{-1}. In order to determine the decay-time constants of the two relaxation processes, we use a simple model to describe the relaxation.[163] The solid lines in Figure 3.4 are calculated with this model, which is illustrated in Figure 3.5 and described in the next section.

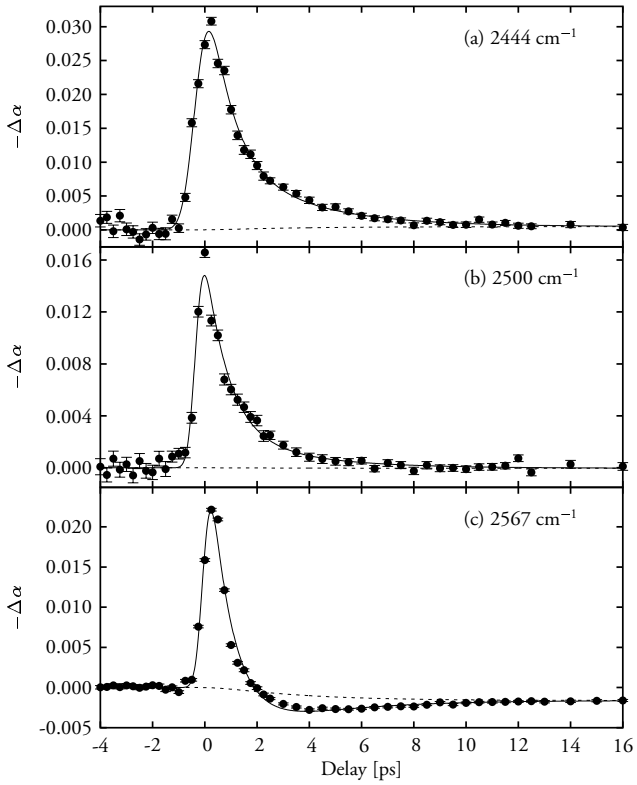

FIGURE 3.4. One-colour pump-probe delay scans of HCl:ether at three different wavelengths (see Figure 3.1). The solid lines are calculated using the model described in Section 3.4. The dashed line is the contribution of the change in temperature to the total fit.

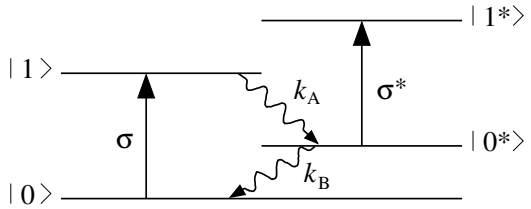

FIGURE 3.5. States and decay scheme used in the model of Section 3.4 to describe the relaxation of the H–Cl stretch vibration. The cross sections for a radiative transition are indicated by σ and σ^*. The rate of the $1 \rightarrow 0^*$ relaxation is given by k_A and the rate of the $0^* \rightarrow 0$ relaxation is given by k_B.

3.4 MODEL

The absorption for a transition $a \rightarrow b$ is proportional to $\sigma_{a\rightarrow b}(n_a - n_b)$, where $\sigma_{a\rightarrow b}$ is the cross section for a radiative transition and n_a, n_b are the occupation numbers of the two levels. Changes in the population difference $n_a - n_b$ due to excitation by the pump pulse and subsequent relaxation result in absorption changes, which affect the transmission of the probe pulse.

The centre frequency of the intermediate $0^* \rightarrow 1^*$ transition (see Figure 3.5) differs from that of the $0 \rightarrow 1$ transition. In our model this effect is described by a change in the cross section as it is monitored by the probe pulse: A shift of the absorption band towards the probe frequency results in an increase of $\sigma_{a\rightarrow b}$, a shift away from the probe frequency results in a decrease of $\sigma_{a\rightarrow b}$. The absorption α near the frequencies of the $0^* \rightarrow 1^*$ and $0 \rightarrow 1$ transitions is given by

$$\alpha \propto \sigma(n_0 - n_1) + \sigma^*(n_{0^*} - n_{1^*}), \tag{3.1}$$

where σ denotes the cross section for the $0 \rightarrow 1$ transition and σ^* the cross section for the $0^* \rightarrow 1^*$ transition at the probe frequency.

Assuming that the thermal population of $|0^*\rangle$ and excitation by the probe beam are negligible, we take $n_{1^*}(t) = 0$. Using $n_0 = N - n_1 - n_{0^*}$, where N is the total number of molecules, and subtracting the absorption in absence of the pump beam, $\alpha_0 \propto \sigma N$, we obtain the following expression for the absorption change $-\Delta\alpha_{01} = \alpha_0 - \alpha$,

$$-\Delta\alpha_{01}(t) \propto \sigma\left[2n_1(t) + \left(1 - \frac{\sigma^*}{\sigma}\right) n_{0^*}(t)\right]. \tag{3.2}$$

The rate of the $1 \rightarrow 0^*$ relaxation is given by $k_A = 1/T_1$ with T_1 the vibrational lifetime of the first excited state $|1\rangle$ and the rate of the $0^* \rightarrow 0$ relaxation is given by k_B (see Figure 3.5). If we assume a mono-exponential or first-order decay for both subsequent relaxations, the populations n_1, n_{0^*} and n_0 satisfy the following equations

$$\frac{dn_1}{dt} = -k_A n_1, \tag{3.3}$$

$$\frac{dn_{0^*}}{dt} = k_A n_1 - k_B n_{0^*}, \tag{3.4}$$

$$\frac{dn_0}{dt} = k_B n_{0^*}, \tag{3.5}$$

$$N = n_1 + n_{0^*} + n_0, \tag{3.6}$$

where, as before, N is the total number of molecules. The solutions are

$$n_1(t) = n_1(0)e^{-k_A t}, \tag{3.7}$$

$$n_{0^*}(t) = \frac{k_A}{k_B - k_A}(e^{-k_A t} - e^{-k_B t})n_1(0) + e^{-k_B t} n_{0^*}(0), \tag{3.8}$$

$$n_0(t) = N - n_1(t) - n_{0^*}(t). \tag{3.9}$$

Immediately after excitation, all excited molecules are in the $|1\rangle$ state and the $|0^*\rangle$ state is not populated, therefore $n_{0^*}(0) = 0$. As we are not interested in the absolute value of $\Delta\alpha_{01}$ we can set $n_1(0) = 1$ and use a scaling factor when fitting the model to our data.

In order to account for shifting changes in σ and σ^* due to temperature effects we add a term to Equation (3.2) which is proportional to

$$\int_{-\infty}^{t} k_B n_{0^*}(t')dt'. \tag{3.10}$$

In this way each molecule relaxing back to the ground state is assumed to contribute to a temperature increase. The integral (3.10) represents the total number of molecules that have decayed to the ground state at time t. In Figure 3.4 the contribution of this function to the total fit is shown as a dashed line. The unknown quantities k_A, k_B and the ratio σ^*/σ can be derived from our data. Before fitting the model to the data, we have to take into account that the pump and probe pulses have a finite duration. We therefore convolve the expressions (3.7) for $n_1(t)$ and (3.8) for $n_{0^*}(t)$ with the pump-probe cross-correlation signal $\mathcal{C}(t)$, which is assumed to have a Gaussian shape:

$$\mathcal{C}(t) = \frac{1}{d\sqrt{2\pi}} e^{-t^2/2d^2}, \tag{3.11}$$

where the constant d is a measure for the width of the signal.[†] After convolving we get for the expressions (3.7) and (3.8):

$$(\mathcal{C} * n_1) = \frac{2\sqrt{2}}{\pi} e^{-k_A t} e^{k_A^2 d^2/2} \left[1 + \mathrm{Erf}\left(\frac{t}{d\sqrt{2}} - \frac{k_A d}{\sqrt{2}}\right)\right] \tag{3.12}$$

and

$$\begin{aligned}(\mathcal{C} * n_{0^*}) = \frac{2\sqrt{2}}{\pi}\frac{k_A}{k_B - k_A} \Bigg\{ & e^{-k_A t} e^{k_A^2 d^2/2} \left[1 + \mathrm{Erf}\left(\frac{t}{d\sqrt{2}} - \frac{k_A d}{\sqrt{2}}\right)\right] \\ - \quad & e^{-k_B t} e^{k_B^2 d^2/2} \left[1 + \mathrm{Erf}\left(\frac{t}{d\sqrt{2}} - \frac{k_B d}{\sqrt{2}}\right)\right]\Bigg\},\end{aligned} \tag{3.13}$$

respectively. $\mathrm{Erf}(x)$ is the error-function, defined as

$$\mathrm{Erf}(x) \equiv \frac{2}{\sqrt{\pi}} \int_0^x e^{-\xi^2} d\xi. \tag{3.14}$$

All data can be fitted well with one set of k_A and k_B, as can be seen in Figure 3.4. The increase of the cross-section ratio σ^*/σ with increasing frequency from approximately 0.6 at 2444 cm^{-1} to 1.3 at 2567 cm^{-1} (see Table 3.1), implies that the $0^* \rightarrow 1^*$ transition is blue-shifted with respect to the $0 \rightarrow 1$ transition as is argued in Section 3.3.

The lifetime of the H–Cl stretch vibration ($T_1 = 1/k_A$) and of the intermediate level ($=1/k_B$) are 0.9 ± 0.2 ps and 3.1 ± 0.5 ps respectively. Because we did not take into account the effect of spectral diffusion, the lifetime of the H–Cl stretch vibration could be somewhat larger in reality than stated above. Due to spectral diffusion the excited molecules drift out of the spectral window of the probe pulse. The model treats these molecules as decaying from the first excited state while in reality only their resonance frequency is changing.

[†] In stead of the constant d, the full width at half maximum (FWHM) is more often used as a measure of the duration of the cross-correlation signal, as the FWHM is independent of any assumption about the shape. These two measures are related by FWHM (cross correlate) = $2d\sqrt{2\ln 2}$. If the individual pulses are each assumed to have a Gaussian shape, their pulse durations are given by FWHM (pulse) = $2d\sqrt{\ln 2}$.

$\nu(\mathrm{cm}^{-1})$	σ^*/σ
2444	0.63 ± 0.03
2500	0.79 ± 0.02
2567	1.3 ± 0.1

TABLE 3.1. Cross-section ratios σ^*/σ derived from the data using the model described in Section 3.4.

3.5 DISCUSSION

When energy is flowing to a hydrogen bond, this usually results in a blue shift of the absorption band. This is for example observed in the relaxation of the O–H stretch vibration of HDO dissolved in D_2O, see Reference 163, and of ethanol (CH_3CH_2OH) clusters dissolved in carbon tetrachloride (CCl_4).[92,135,211] For hydrogen chloride, vibrational energy transfer to the hydrogen bond stretch coordinate will even be enhanced due to the absence of other intramolecular vibrational modes. Thus, the blue shift that we observe can be explained well if the $|0^*\rangle$ state is an H–Cl stretch $v = 0$ state in combination with a highly excited or even dissociated hydrogen bond, since the amount of energy absorbed by the complex is close to the hydrogen-bond dissociation energy of $\sim$2500 cm^{-1}, see Reference 189. A qualitative picture of the energy levels involved is shown in Figure 3.6. The lifetime of the $|0^*\rangle$ state, $1/k_B$, is in our model the lifetime of the average excitation level of the hydrogen bond.

The relaxation of the hydrogen-bond mode with a time constant $1/k_B$ of 3 ps is fast compared to the relaxation time of 15 ps observed for ethanol dissolved in CCl_4, and slow compared to the relaxation time of 1 ps of liquid water. For ethanol dissolved in CCl_4, the apolar CCl_4 environment does not provide efficient accepting modes, and thus the excited population of the hydrogen-bond mode decays much more slowly. In contrast, in water there is a three-dimensional network of hydrogen bonds present through which the energy can be dispersed very quickly over the environment of the initially excited molecule.

In the experiments on ethanol clusters dissolved in CCl_4 and on HF-dimethyl ether complexes in the gas-phase[13] the respective excitation of the O–H stretch and the H–F stretch vibration, is observed to lead to the formation of dissociated species. Hence, in both cases the energy transfer to the hydrogen-bond mode causes the hydrogen bond to dissociate. However, if no dissociated species are observed, as is the case in liquid water,[77] one cannot conclude that the bulk of the vibrational energy is transferred to other degrees of freedom. When $1/k_B$ is on the order of or shorter than $T_1 = 1/k_A$, either the reassociation can be so fast that no significant accumulation of dissociated molecules is observed experimentally, or the excited population of the hydrogen-bond mode already decays before the bond breaks.

A study on pyrrole-base (C_4H_5N-base) complexes[96] has shown that the vibrational lifetime T_1 of the N–H stretch vibration decreases from 50 to 1 ps with increasing basicity of the bases used. The simultaneous increase of the redshift of the stretch vibration indicates that the hydrogen-bond becomes stronger with increasing basicity.[186] Apparently, stronger hydrogen bonding leads to faster relaxation of the stretch vibration. After relaxation of the N–H stretch vibration no significant dissociation is observed. However, the reassociation

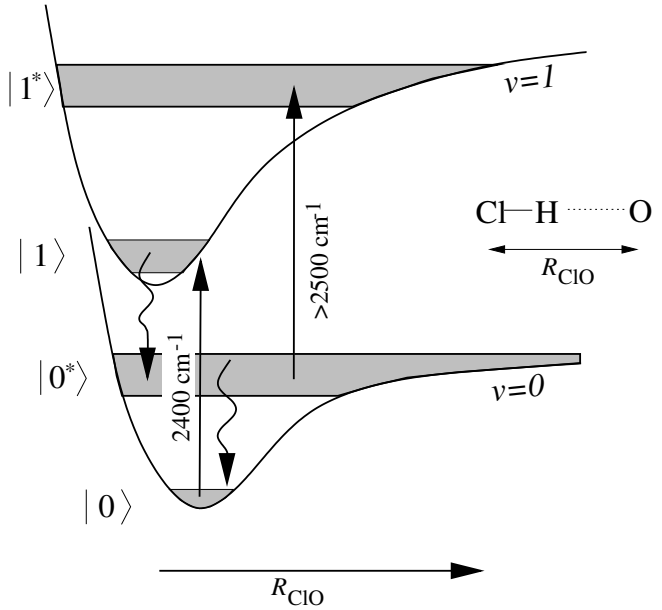

FIGURE 3.6. Schematic potentials for the $v = 0$ and the $v = 1$ H–Cl stretch modes. Within these potentials the proposed $|0\rangle$, $|1\rangle$, $|0^*\rangle$, $|1^*\rangle$ hydrogen-bond modes are indicated. The central excitation frequencies and the non-radiative decay paths are also shown.

of acid-base complexes, for which we observe a time constant of 3 ps, is on the order of or even faster than the lifetime of the excited N–H stretch vibration, as is measured by Grubbs *et al.*[96] Thus, even if most of the energy flows to the hydrogen-bond mode, this is not expected to result in the observation of dissociated species. Only if $k_B \ll k_A$ the dissociated species will accumulate sufficiently to be observed experimentally. Therefore, the fact that in the experiments of Reference 96 no dissociated species are observed does not exclude the possibility that the hydrogen bond accepts most of the vibrational energy. Hence, the conclusion of the authors that the hydrogen bond accepts only a minor part of the energy is not sufficiently substantiated.

In the present one-colour experiments on HCl-diethyl ether complexes, only a transient blue shift is observed. Hence, we cannot conclude whether real dissociation of the hydrogen-bonded HCl-diethyl ether complexes occurs or the excited population of the hydrogen-bond mode decays before that can happen. Two-colour experiments and transient spectra may give further insight.

Recently, it was observed that electronic excitation of a dye-solvent complex can also lead to a blue shift of the vibrational frequencies.[57,58] As in the present case, this blue shift results from a weakening of the hydrogen bond. However, in this case the weakening is not the result of an energy transfer to the hydrogen bond, but results from the change of the electronic structure of the excited dye-solvent complex. This change of the electronic structure affects the hydrogen-bond strength in two ways. In the first place, the electronic reorganisation within the dye molecule directly weakens the hydrogen bond. Second, the

dipole moment of the dye molecule strongly changes upon excitation, which is followed by a reorganisation of the solvent shell of the complex. This reorganisation of the solvent leads to a further weakening of the hydrogen bond. These effects do not play a role in the present case, because the change of the dipole moment upon excitation of the H-Cl stretch vibration is negligible.

Finally, we found that no acid-base reaction was induced between HCl and diethyl ether [$(CH_3CH_2)_2O$] by exciting the H–Cl stretch vibration. If a reaction was induced, we would expect to observe a redshift instead of a blue shift, because the transfer of the proton would lead to the formation of a vibration with a lower frequency than the H–Cl stretch vibration.[3,4,195]

3.6 Conclusions

We performed one-colour femtosecond mid-infrared pump-probe experiments to study the relaxation of the H–Cl stretch vibration of hydrogen-bonded HCl-diethyl ether complexes. The relaxation is found to occur in two steps. The first step is identified with the transfer of vibrational energy to the hydrogen-bond mode with a time constant T_1 of 0.9 ± 0.2 ps, which causes the absorption of the H–Cl stretch vibration to shift to the blue. The second step is the relaxation of the excited hydrogen bond with a time constant of 3.1 ± 0.5 ps. Furthermore, we found that excitation of the H–Cl stretch vibration does not lead to proton transfer from the strong acid HCl to the base $(CH_3CH_2)_2O$ because the energy is rapidly transferred to the hydrogen-bond mode.

4 Ultrafast pump-probe spectroscopy of strongly hydrogen-bonded hydrogen fluoride-pyridine complexes

We present a study on the vibrational dynamics of the HF/FHF stretch combination vibration of HF-pyridine complexes in diluted pyridine solution. The relaxation of the excited vibration was observed to occur in two steps. In the first step, energy is transferred from the excited combination vibration to the hydrogen bond F–H···F modes with a time constant of 0.51 ± 0.09 ps. In a second relaxation process these hydrogen bond modes decay with a time constant of 2.6 ± 0.3 ps.

4.1 Introduction

The diatomic acid hydrogen fluoride (HF) forms a model acid for studying acid-base reactions and a number of experimental studies on hydrogen-bonded complexes of HF with bases and other molecules were reported, see References 6, 7, 81, 105, 136, and 150. In these studies, a strong relation between the H–F stretch frequency and the proton affinity of the base was observed.[6] With increasing proton affinity of the "hydrogen acceptor", i.e. increasing base strength, the H–F stretch frequency decreases, because the hydrogen bond between the proton and the base becomes stronger, thereby weakening the H–F bond. The same behaviour is also seen in Chapter 3 for the H–Cl stretch frequency and is also observed for the O–H stretch frequency in hydrogen-bonded O—H···O systems. For example, the O–H stretch frequency of HDO shifts from its gas-phase value of 3700 cm^{-1} to 3400 cm^{-1} in the liquid.[163,191]

In hydrogen-bonded complexes of HF with amines, the red shift of the H–F stretch frequency is exceptionally large:[81,150] it is shifted to around 1800 cm^{-1} from its value of 3962 cm^{-1} in the gas-phase[178] or around 3400 cm^{-1} in liquid HF.[62] This large red shift indicates that hydrogen-bonding between the acid HF and the amine base is very strong. Compare, for example, with the blue shift from 2886 cm^{-1} to around 2500 cm^{-1} for the H–Cl stretch frequency in the more weakly hydrogen-bonded complexes in the previous chapter. A striking example of these HF-amine complexes are the ones formed by HF with the weak organic base pyridine. Pyridine forms remarkably stable solutions with HF up to a temperature of 55°C, which is much higher than the boiling point of 19.6°C of pure HF. The solution contains about 9 equivalents of HF to one equivalent of pyridine (70% (w/w) HF / 30% (w/w) pyridine). The high stability of this HF-pyridine solution at such high concentrations above the boiling point of HF can be attributed to the existence of large hydrogen-bonded networks, see References 166 and 167. ^{19}F and ^{1}H-NMR studies indicate the presence of a poly(hydrogen fluoride) species, in which each fluorine atom is surrounded by four hydrogen atoms. In liquid HF, "strands" of up to eight molecules

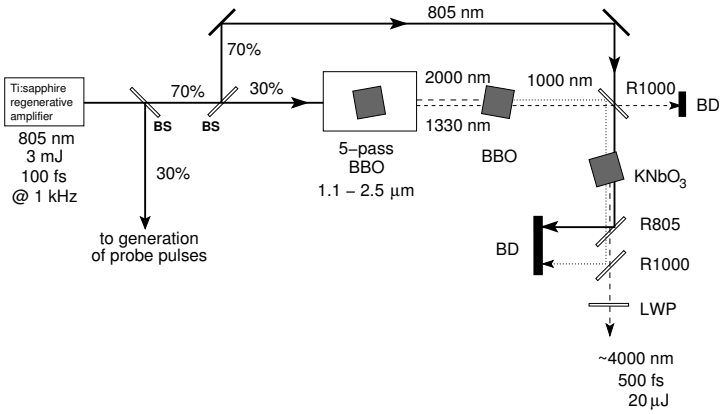

FIGURE 4.1. Generation of femtosecond pump pulses with a wavelength around 4 μm for two-colour pump-probe experiments. The probe pulses a generated in a similar set-up. Legend: BBO, $KNbO_3$: crystals; R805, R1000: dielectric 805 nm, 1000 nm mirrors; BD: beam dump; BS: beam splitter.

were shown to exist by neutron diffraction and infrared and Raman spectroscopy.[61,62,176] Apparently, the small amount of the base pyridine and its interaction with the acid HF is vital in forming a stronger and larger network of hydrogen bonds than the one that exists in liquid HF.†

In order to understand the very important interaction of hydrogen bonding, it should be studied in all its forms. Systems involving relatively weak hydrogen bonds have already been studied with time-resolved techniques, see e.g. Chapter 3 and References 82, 163, and 211. Exceptionally strong hydrogen bonds, like the ones found in the HF-pyridine complexes, have not yet been studied in detail with these techniques. Time-resolved experiments on the vibrational dynamics of these complexes can give direct insight into the nature of strong hydrogen bonds and into the mutual coupling of hydrogen-bond modes, as has already been shown in studies on hydrogen-bonded O—H $\cdots$ O systems.[163,211] Here we present the results of a femtosecond mid-infrared pump-probe study on an HF-pyridine solution.

4.2 EXPERIMENT

The experimental set-up used in these experiments is a two-colour pump-probe set-up which employs two independently tunable femtosecond mid-infrared pulses and which is similar in design to the experimental set-up described in §2.1.2 and Section 3.2. An explanation of pump-probe spectroscopy can be found in Section 2.2.

The mid-infrared pulses are generated using a commercial Ti:sapphire regenerative /

†The 70%/30% solution of HF with pyridine is also known as "Olah's reagent" and was proposed as a convenient fluorinating agent.[166,167] The poly(hydrogen fluoride) is reported to exist in equilibrium with small amounts of free HF, which renders it a convenient, less volatile source of HF. This solution has since then been reported as a very useful fluorinating agent in many areas of organic chemistry see e.g. References 43, 65, 98, 109, 160, 177, and 214.

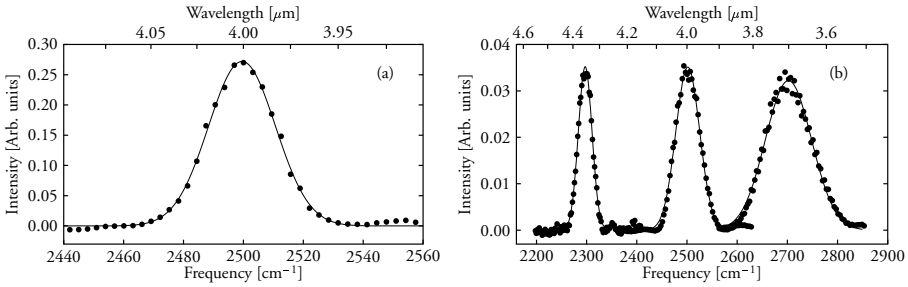

FIGURE 4.2. Typical spectra of the pulses generated with the set-up that is described in Section 4.2. (a) Spectrum of a pulse used as a probe pulse in the two-colour pump-probe experiments. The solid line is a Gaussian with a FWHM of 26 cm^{-1}. (b) Three spectra of pulses used as probe pulses. The solid lines are Gaussians with a FWHM of 31 cm^{-1} (spectrum centred at 2300 cm^{-1}), 56 cm^{-1} spectrum centred at 2500 cm^{-1}), and 108 cm^{-1} (spectrum centred at 2700 cm^{-1}), respectively.

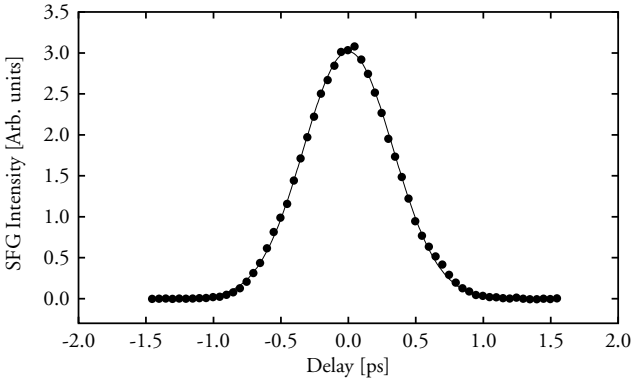

FIGURE 4.3. Cross correlation trace of the pump and probe pulses with frequencies of 2500 cm^{-1}. The solid line is a Gaussian with a FWHM of 783 fs, corresponding to pulse durations of 554 fs.

multi-pass amplifier (Spectra Physics Tsunami oscillator with a Quantronix TITAN amplifier) which delivers pulses with a duration of 100 fs and an energy of 3 mJ at a wavelength of 805 nm and a repetition rate of 1 kHz. To generate the mid-infrared pump pulses, part of this 805 nm laser light (0.9 mJ) is used to pump a commercial five-pass optical parametric generation and amplification stage (TOPAS, Light Conversion) based on BBO, which is tunable between 1100 and 2600 nm, see Figure 4.1. For the experiments described in this chapter, the signal and idler pulses are tuned to approximately 1330 nm and 2000 nm, respectively. The idler pulses are subsequently frequency-doubled to 1000 nm using an additional BBO crystal. The 1000 nm pulses are used as a seed in a second parametric amplification process, where they are combined with 1.4 mJ of 805 nm light in a 5 mm potassium niobate ($KNbO_3$) crystal to produce pulses with a wavelength around 4000 nm (2500 cm^{-1}). By tuning the seed pulses of this last OPA process, the generated mid-infrared pulses can be tuned between 3.7 μm and 4.4 μm (2700–2250 cm^{-1}), with a typical energy

of 20 μJ per pulse and a bandwidth of 40 nm (25 cm^{-1}) FWHM, see Figure 4.2.

The mid-infrared probe pulses are generated in a similar fashion. A three-pass TOPAS OPG/OPA stage based on BBO is pumped with 0.4 mJ of 805 nm pulses; its output of 2000 nm is also converted to 1000 nm with an additional BBO crystal. For the generation of the mid-infrared pulses, the 1000 nm pulses are combined with 0.1 mJ of 805 nm laser light in a lithium niobate ($LiNbO_3$) crystal. Here $LiNbO_3$ is used in stead of $KNbO_3$, because with the former, the spectral shape and energy of the generated pulses are more stable at lower energies. Cross-correlation traces of these mid-infrared pump and probe pulses typically have a FWHM of around 700 fs, corresponding to pulse durations of approximately 500 fs FWHM, see Figures 4.2 and 4.3.

The pump-probe set-up for the femtosecond two-colour experiments is very similar to the one for the one colour experiments described in Chapter 3, the main difference being the independent generation of pump and probe pulses. Again, the polarisation of the probe pulses is rotated by the magic angle (54.7°) with respect to the polarisation of the pump pulses to exclude reorientational effects of the excited molecules on the induced transmission changes.

The experiments were performed on a diluted solution of hydrogen fluoride in pyridine at room temperature in a sample cell with calcium fluoride (CaF_2) windows and a sample length of 0.2 mm. This diluted solution was prepared by adding 0.2 ml of a commercially available 70% (w/w) HF / 30% (w/w) pyridine solution to 16 ml pyridine. The chemicals were purchased from Sigma-Aldrich. Based on a density of 1.1 g/ml for the HF-pyridine solution, the diluted solution had a concentration of 0.04 mol HF/mol pyridine.

4.3 LINEAR ABSORPTION SPECTRUM: RESULTS AND DISCUSSION

The linear absorption spectrum of the 0.04 mol HF/mol pyridine solution is shown in Figure 4.4. In this figure the spectrum corrected for the pyridine absorptions is also shown. The band centred at 1850 cm^{-1} is identified with the H–F stretch absorption and the broad band centred at 2520 cm^{-1} is identified with absorption due to combinations of the H–F stretch and F–H$\cdots$F stretch hydrogen bond absorptions.[5,81,104,105,150]

Previous studies on HF-pyridine solutions propose structures with either two[46] or three[150] HF molecules per pyridine molecule at lower concentrations. Schematic structures for the pyridine$\cdot(HF)_2$ and pyridine$\cdot(HF)_3$ complexes are shown in Figure 4.5.

Low-temperature crystal structures of these complexes show that the hydrogen atom in the N$\cdots$H$\cdots$F bond is distinctly closer to the pyridine nitrogen atom than the fluorine atom.[31] The complexes can therefore be reformulated as pyridine-$H^+\cdot HF_2^-$ and pyridine-$H^+\cdot H_2F_3^-$. The hydrogen bond between pyridine-H^+ and $(H_{n-1}F_n)^-$ (n=2,3) is still very short and the cationic and anionic parts can be considered to form a nearly covalently bound complex.

The presence of the HF/FHF stretch combination absorption band in the diluted pyridine solution is quite surprising: it implies that even at this low concentration, complexes with at least two HF-molecules per pyridine molecule are present. From the present data one cannot conclude whether two or three HF-molecules are present in the complexes formed. The presence of a strongly absorbing combination mode implies that these F–H$\cdots$F stretch hydrogen bond modes and the H–F stretch modes in the $(H_{n-1}F_n)^-$ an-

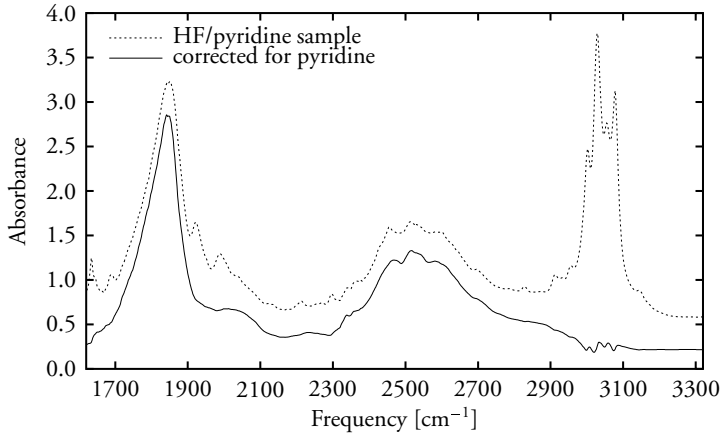

Figure 4.4. Linear absorption spectrum of a 0.04 mol HF/mol pyridine sample with a sample length of 0.2 mm (dashed line) and corrected for the absorption of pyridine (solid line). The absorbance A was calculated from the measured transmittance of the sample (T_{sample}) and the transmittance of air (T_{air}) by $A = -\ln(T_{\text{sample}}/T_{\text{air}})$.

ionic part are strongly coupled. This is in close analogy with hydrogen-bonded O—H $\cdots$ O systems, where the O–H stretch vibration is also strongly coupled to the O–O hydrogen bond mode.[163]

4.4 Femtosecond transient absorption experiments

4.4.1 Results

The pump-probe experiments were carried out at different pump and probe frequencies within and around the combination absorption band centred at 2520 cm^{-1}. Results of pump-probe measurements at different probe frequencies with a pump frequency tuned to 2500 cm^{-1} are shown in Figure 4.6. At the blue side of the absorption band, at a probe frequency of 2700 cm^{-1}, the bleaching signal quickly decays and changes into an induced absorption, which decays on a longer timescale. At the centre and the red side of the absorption band, only a bleaching signal is observed, which decays more slowly at lower probe frequencies. These observations suggest that the mechanism of vibrational relaxation involves at least two steps, in which the population of some intermediate state causes a transient blue shift of the absorption band. At longer delay times, there is a constant increased transmittance at the red side and the centre of the absorption band and a decreased transmittance at the blue side. This implies that after the second step in the relaxation, the system thermalises. This thermalisation of the deposited energy causes a blue shift of the absorption band.

Results of pump-probe measurements at a probe frequency of 2700 cm^{-1} at different pump frequencies are shown in Figure 4.7. Here one observes that the decay of the bleaching signal at a single probe frequency strongly depends on the frequency at which excitation occurs. When the pump frequency is tuned to the centre or the red side of the ab-

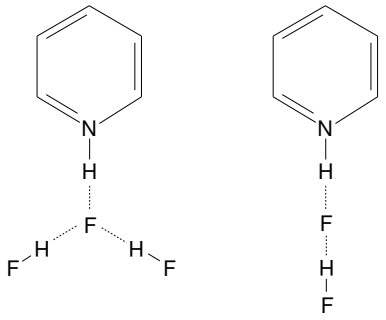

FIGURE 4.5. Schematic structures for the pyridine·$(HF)_2$ and pyridine·$(HF)_3$ complexes.

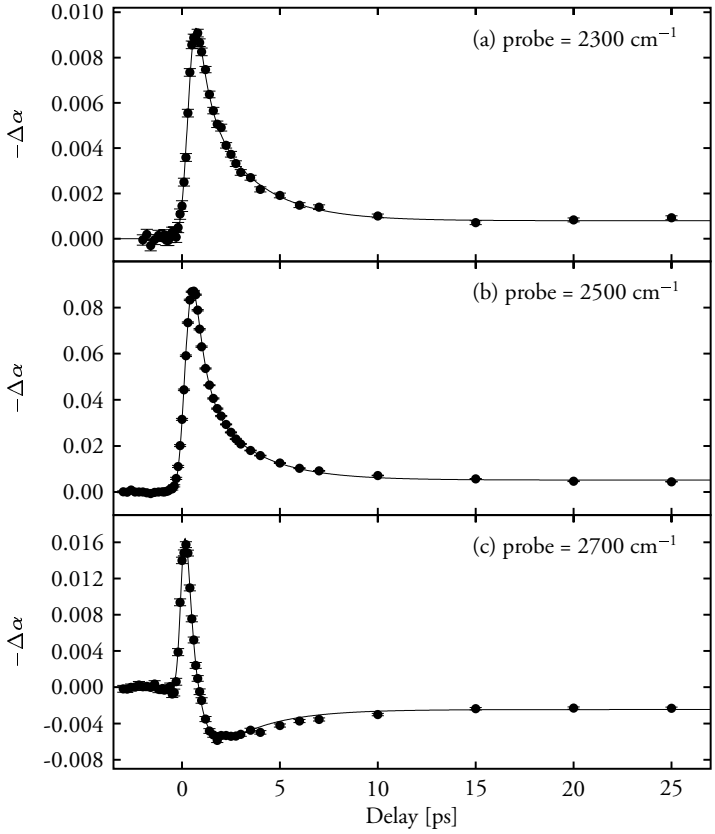

FIGURE 4.6. Pump-probe delay scans of a diluted solution of HF in pyridine at different probe frequencies with a pump frequency tuned to 2500 cm^{-1}. The solid line is calculated using a model which is described in §4.4.2.

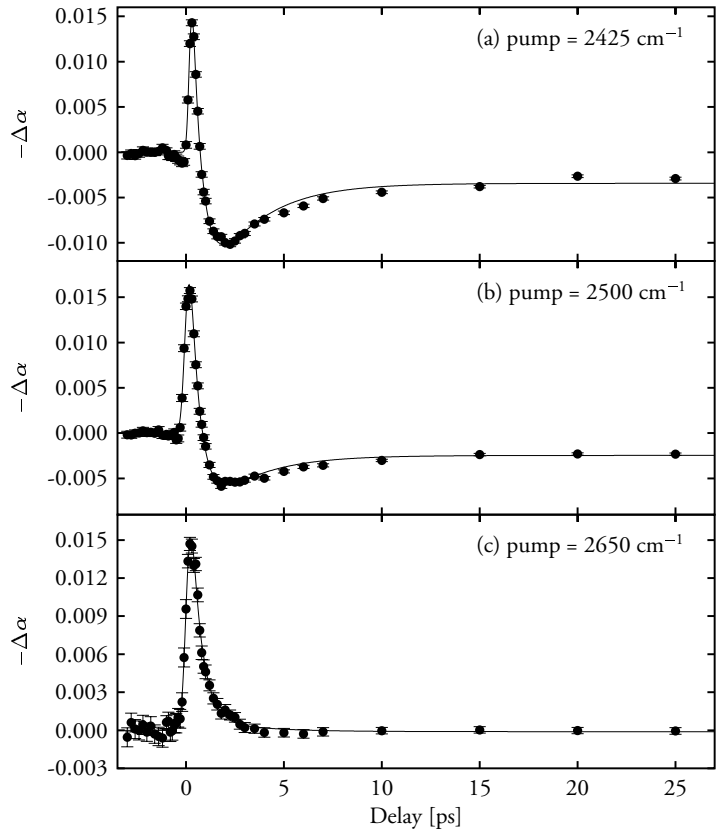

FIGURE 4.7. Pump-probe delay scans of a diluted solution of HF in pyridine at different pump frequencies with a probe frequency tuned to 2700 cm^{-1}. The solid line is calculated using a model which is described in §4.4.2.

sorption band, the initial bleaching signal at 2700 cm^{-1} decays into an induced absorption, which becomes stronger with decreasing excitation frequencies. When the pump frequency is tuned to the blue side, only a bleaching signal is observed. These observations indicate that the combination band centred at 2520 cm^{-1} is inhomogeneously broadened and that spectral diffusion is slow on the timescale of the experiments. Interestingly, the final level of transmission change depends on the pump frequency, which indicates that even after 25 ps, the system has not yet lost its memory for the pump frequency at which is was excited.

The measurements shown in Figure 4.6 and Figure 4.7 could include a contribution due to coherent effects. However, these effects appear to be negligible and we have not included them in our model that is described in §4.4.2.

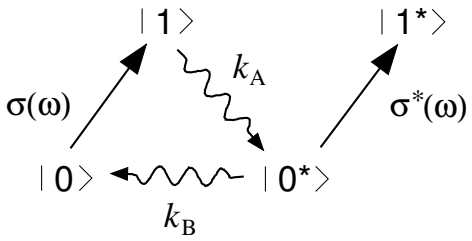

FIGURE 4.8. States and decay scheme used to describe the relaxation of vibration. The frequency dependent cross sections for a radiative transition are indicated by $\sigma(\omega)$ and $\sigma^*(\omega)$. The rate of the $1 \rightarrow 0^*$ relaxation is given by k_A and the rate of the $0^* \rightarrow 0$ relaxation is given by k_B.

4.4.2 MODEL

In order to determine the decay-time constants of the two relaxation processes, we use a simple kinetic model which is described in detail in Section 3.4 and elsewhere.[39,82] In this model, the relaxation of the excited vibration $|1\rangle$ occurs via an intermediate state $|0^*\rangle$, rather than directly back to the ground state $|0\rangle$. The rate of relaxation from the first excited state $|1\rangle$ to the intermediate state $|0^*\rangle$ is given by k_A and the relaxation rate of the second step in the relaxation $|0^*\rangle \rightarrow |0\rangle$ is given by k_B. The cross section of the $0 \rightarrow 1$ transition is denoted by $\sigma(\omega)$ and the cross section of the $0^* \rightarrow 1^*$ transition by $\sigma^*(\omega)$. A dependence of the cross section ratio $\sigma^*(\omega)/\sigma(\omega)$ on the probe frequency indicates a shift of the $0^* \rightarrow 1^*$ absorption spectrum relative to the $0 \rightarrow 1$ absorption spectrum. For example, an increase of the ratio $\sigma^*(\omega)/\sigma(\omega)$ with increasing frequency, indicates that a blue shift has occurred of the $0^* \rightarrow 1^*$ absorption spectrum relative to the $0 \rightarrow 1$ absorption spectrum. The solid lines in Figures 4.6 and 4.7 are calculated with this model, which is illustrated in Figure 4.8.

Using this model, the measurements at all pump and probe frequencies could be described with one set of k_A and k_B. The cross section ratios $\sigma^*(\omega)/\sigma(\omega)$ at the different pump and probe frequencies are shown in Table 4.1. The best fit of the model to the data was obtained by simultaneously fitting the values for $\sigma^*(\omega)/\sigma(\omega)$ for different pump and probe frequencies and one single set of values for k_A and k_B, equal for all sets. The lifetime of the excited HF/FHF stretch combination vibration in the HF-pyridine complex ($T_1 = 1/k_A$) was determined to be 0.51 ± 0.09 ps. The lifetime of the intermediate state $|0^*\rangle$ ($= 1/k_B$) was determined to be 2.6 ± 0.3 ps.

4.4.3 DISCUSSION

The increase in the ratio $\sigma^*(\omega)/\sigma(\omega)$ when tuning the probe frequency from the red side to the blue side of the absorption band shows that population of the intermediate state leads to a transient blue shift of the HF/FHF stretch combination frequency. This blue shift indicates that the first step in the relaxation of the excited combination vibration involves transfer of energy to the F···H···F hydrogen bond mode, thereby causing a shift of the H–F stretch frequency towards its frequency in the gas phase. In a second step, this

Table 4.1. Cross section ratios $\sigma^*(\omega)/\sigma(\omega)$ derived from the data using the model described in §4.4.2.

	ν_{pump} [cm^{-1}]		
ν_{probe}[cm^{-1}]	2425	2500	2650
2250	0.06 ± 0.03	–	–
2300	–	0.22 ± 0.03	–
2400	–	0.26 ± 0.02	0.04 ± 0.07
2425	0.51 ± 0.02	0.34 ± 0.02	–
2500	0.39 ± 0.02	0.47 ± 0.01	0.34 ± 0.02
2565	–	0.53 ± 0.01	–
2600	0.60 ± 0.02	–	–
2700	2.17 ± 0.02	1.57 ± 0.01	0.93 ± 0.02

relaxation is followed by equilibration of energy to all other degrees of freedom.

Transient blue shifts have been observed before, in the relaxation of the H–Cl stretch vibration in hydrogen-bonded HCl-diethyl ether complexes,[82] discussed in the previous chapter, and in the relaxation of the O–H stretch vibration of of HDO dissolved in D_2O, see Reference 163. In a study on the relaxation of the O–H stretch vibration of ethanol clusters in carbon tetrachloride (CCl_4), energy transfer to the hydrogen bond even causes the hydrogen bond to predissociate, leading to the transient observation of cluster fragments.[92,135,211] Breaking and subsequent reassociation of the $(H_{n-1}F_n)^-$ moieties instead of the proposed transient weakening of the hydrogen bonds does probably not occur, as this is likely to cause a much larger transient blue shift than we observed.

The observation that the level of transmission change at longer delay at a probe frequency of 2700 cm^{-1} depends on the pump frequency, indicates that after the second relaxation process, the energy is still located in the vicinity of the complex that was originally excited. Additionally, it indicates that there is a long-living inhomogeneity in the system. This inhomogeneity can be caused by the presence of a distribution of different HF-pyridine complexes, e.g. with two or three HF molecules per complex, or a uniform solute composition but very slow solvent dynamics of pyridine solvent molecules.

4.5 Conclusions

We studied the vibrational dynamics of the HF/FHF stretch combination absorption band of HF-pyridine complexes in diluted pyridine solution. The relaxation of the excited vibration was observed to occur in two steps. In the first step, energy is transferred from the excited combination vibration to the F–H$\cdots$F hydrogen bond modes with a time constant of 0.51 ± 0.09 ps, causing a transient blue-shift of the combination absorption frequency. In a second step, with a time constant of 2.6 ± 0.3 ps, energy is transferred from the F–F hydrogen bond modes to lower-frequency modes, leading to a local thermalisation of the energy.

5 Observation of a bottleneck in the vibrational relaxation of liquid bromoform

We present a study on the vibrational dynamics of the C–H stretch vibration of bromoform ($CHBr_3$) in the pure liquid using picosecond mid-infrared pump-probe spectroscopy. Delay scans and transient spectra confirmed earlier results that relaxation occurs via an intermediate level, which causes a transient redshift of the C–H stretch frequency. We determined this redshift to be 17 cm^{-1} and identified the intermediate level with the singly excited C–H bend mode. We observed that relaxation from the intermediate level is exceptionally slow and non-exponential. These observations suggest the presence of a "bottleneck" in the relaxation. The occupation of a long-living "bottleneck" level may also be responsible for the observation of a long-living absorption around 3022 cm^{-1}.

5.1 Introduction

In the past decades there have been many time-resolved studies on the vibrational dynamics of small molecules in the electronic ground state. These studies generally use intense infrared laser pulses to excite a molecular vibration and use either anti-Stokes Raman scattering[137] or induced infrared transmission changes[54] to monitor the decay of the excitation. In many time-resolved studies, the excitation of a high-frequency molecular vibration is observed to relax via two consecutive steps, see References 8, 15, 17, 18, 19, 85, 86, 87, 89, 90, 91, 93, 107, 111, 163, 202, 211, and 215. In a first step, energy is transferred from the excited vibration to a few selected other vibrational modes in the molecule. The excitation of these accepting modes often causes a shift of the absorption band of the vibration that was originally excited, because of anharmonic coupling. In a second step, the energy is equilibrated over all degrees of freedom, implying that the energy is redistributed over all other modes of the molecule, the modes of nearby molecules and intermolecular degrees of freedom.

The exact nature of the intermediate state is usually not well known, although likely candidates are often suggested in the form of (combinations of) low-frequency vibrations. There are only a few studies in which the intermediate state could be identified. For instance, in a recent study on the vibrational dynamics of liquid chloroform ($CHCl_3$),[93] it was found that the relaxation of the C–H stretch mode leads to a transient population of the C–H bend and C–Cl stretch modes.

Earlier studies on the vibrational dynamics of bromoform ($CHBr_3$), see References 15, 17, 85, 86, 87, and 90, also indicated the presence of an intermediate state in the relaxation of the C–H stretch mode. In these studies, a bi-exponential decay and a transient redshift of the C–H stretch absorption band were observed. However, the exact nature of the inter-

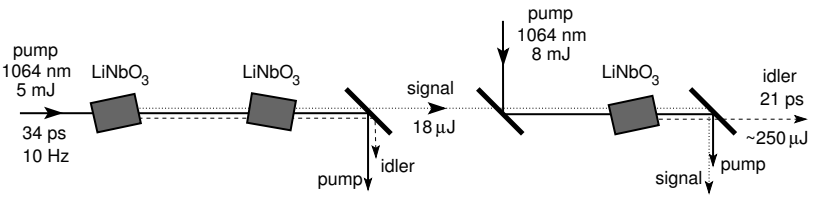

FIGURE 5.1. Schematic representation of one branch of the set-up used to generate picosecond pulses with a wavelength around 3 μm.

mediate state has remained unknown: One or more of the other vibrations of the $CHBr_3$ molecule are assumed to cause the redshift. Whether one mode or a combination of modes are excited with one or more vibrational quanta has not yet been determined. It is also unclear whether relaxation from the intermediate state involves one or more vibrational quanta.

Here we present a detailed investigation of the vibrational dynamics of $CHBr_3$ using two-colour mid-infrared pump-probe spectroscopy. We find strong evidence that the relaxation of the intermediate state does not lead to a full thermalisation, but encounters a vibrational "bottleneck".

5.2 EXPERIMENT

The experimental set-up to generate intense, tunable mid-infrared pulses is depicted schematically in Figure 5.1. The pump pulses for the parametric down-conversion process are provided by an actively and passively mode-locked Nd:YAG laser (Quantel YG502C). This laser delivers pulses of 34 ps (FWHM) with a wavelength of 1064.1 nm,[133] an energy up to 60 mJ and a repetition rate of 10 Hz. An autocorrelation trace of these pulses can be found in Section 7.2. These pulses are used to pump two identical OPG/OPA stages, based on three 5 cm long lithium niobate ($LiNbO_3$) crystals each (optical axis cut at 47.1°). In each branch, the first crystal is pumped with 5 mJ 1064.1 nm pulses. The parametrically generated signal and idler pulses are amplified in the second crystal with the remaining part of the pump energy. After the second crystal the idler and pump are reflected out of the beam. The signal pulses ($\sim$18 μJ), are used as a seed in a second OPA process in the third crystal, where they are combined collinearly with 8 mJ of 1064.1 nm light. After the third crystal, the signal and pump pulses are reflected out of the beam, yielding idler pulses continuously tunable from approximately 2.1–4.1 μm ($\sim$4580–2030 cm^{-1}) and a typical energy of 250 μJ. From a cross-correlation trace of idler pulses from each branch, generated through sum-frequency generation in a 5 mm lithium iodate ($LiIO_3$) crystal, the pulse duration was determined to be 21 ps, see Figure 5.2. Typical spectra of signal and idler pulses generated in this set-up can be found in Section 7.2.

The pump-probe set-up for picosecond two-colour experiments is shown in Figure 5.3. The idler beam of one OPG/OPA branch is used as a pump, the other is used as a probe. A low intensity probe pulse is split off the relatively intense beam by a broadband infrared beam splitter which reflects about 15 %. The transmitted high intensity part (85 %) of the

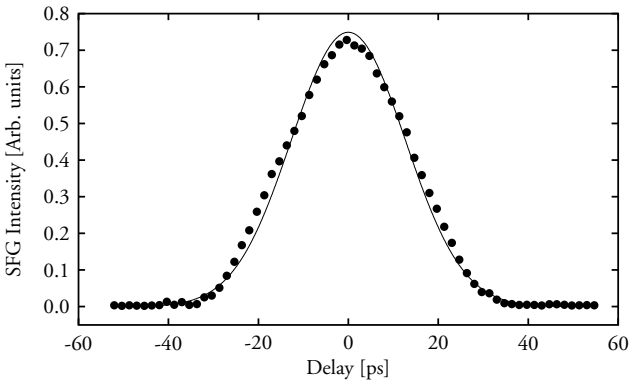

FIGURE 5.2. Cross-correlation trace of the idler pulses with a frequency of 3316 cm^{-1}. The solid line is a Gaussian with a FWHM of 29.9 ps, corresponding to a pulse duration of 21.1 ps (FWHM).

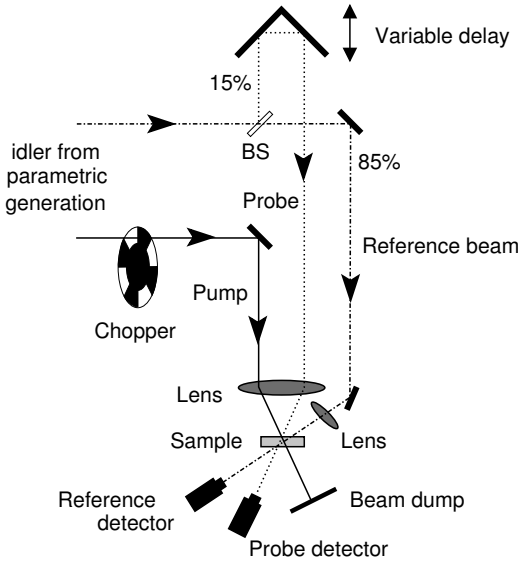

FIGURE 5.3. Two-colour pump-probe set-up used in the experiments described in this chapter. Legend: BS: beam splitter.

pulse is used as a reference beam. The pump and probe pulses are focused into the sample by a calcium fluoride (CaF_2) lens (focal length 100 mm) with an estimated diameter of the focus of approximately 300 μm. The probe pulses can be delayed with respect to the pump pulses by means of a variable delay (a gold-coated retro-reflector on a translation stage).

This set-up differs from the general description of a pump-probe set-up given in Section 2.2: The reference beam is slightly focused into the sample by a second CaF_2 lens and the intensity is measured by a reference detector to take into account not only the pulse-to-pulse intensity fluctuations, but also the spectral fluctuations of the probe pulses. Because the probe pulses in this picosecond set-up are far from bandwidth-limited, spectral fluctuations can be large. When the absorption band is relatively narrow, as is the case with the C–H stretch absorption of $CHBr_3$, or when the edge of the band is probed, these spectral fluctuations can have a large influence on the transmission. By sending the reference beam through the sample as well, the effect of the spectral fluctuations can be taken into account. The intensity of the transmitted probe pulses and of the reference pulses are measured by lead selenide (PbSe) photoconductive cells. The pump beam is chopped at 5 Hz to block every other pump pulse to monitor both the intensities of the probe pulse with and without the presence of a pump pulse. This set-up can be used for (quasi) one- or two-colour delay scans or to record transient spectra at a fixed delay between the pump and the probe pulses. The experiments are performed on pure $CHBr_3$, using a sample length of 50 μm.

5.3 Results and discussion

In all experiments the frequency of the pump pulses was tuned to the C–H stretch frequency of pure $CHBr_3$ at 3022 cm^{-1}. We measured transient spectra of pure $CHBr_3$ at various delay times. Three spectra at (relatively) short delay times are shown in Figure 5.4 and four spectra at longer delay times are shown in Figure 5.5. As can be seen in Figure 5.4, an induced absorption starts to appear around 2890 cm^{-1} during excitation. With increasing delay this absorption decreases, while another induced absorption, centred at 3005 cm^{-1}, increases. We identify the absorption around 2890 cm^{-1} with the $v = 1 \rightarrow v = 2$ transition of the C–H stretch vibration, which is at its maximum right after excitation and decays with a decay time constant of about 43 ps. The $1 \rightarrow 2$ transition of the C–H stretch vibration is red-shifted from the $0 \rightarrow 1$ transition, due to the anharmonicity of the C–H stretch mode. At 133 ps, the $1 \rightarrow 2$ absorption has almost completely disappeared, as has the bleaching signal at the position of the $0 \rightarrow 1$ transition. The maximum of the bleaching signal appears to shift to the blue, but this is because at 17 ps, there is almost no absorption around 3005 cm^{-1}, whereas at 40 ps, the absorption at 3005 cm^{-1} is strong and competes with the red side of the bleaching. The absorption centred at 3005 cm^{-1} is attributed to the absorption by molecules in an intermediate state $|0^*\rangle$, which is populated when relaxation from the $v = 1$ state occurs. This $|0^*\rangle$ state will most likely be a state in which one of the other vibrational modes is excited, thereby inducing an anharmonic shift of the C–H stretch frequency. Apparently the cross section of the C–H stretch vibration increases when relaxation to the intermediate state $|0^*\rangle$ occurs. From Figure 5.5 it is clear that the relaxation from the $|0^*\rangle$ state is very slow. At longer delay times the absorption starting from the $|0^*\rangle$ state starts to disappear, while another induced absorption simultaneously appears around 3022 cm^{-1}. This implies that the energy transfer to low-frequency modes of $CHBr_3$ leads

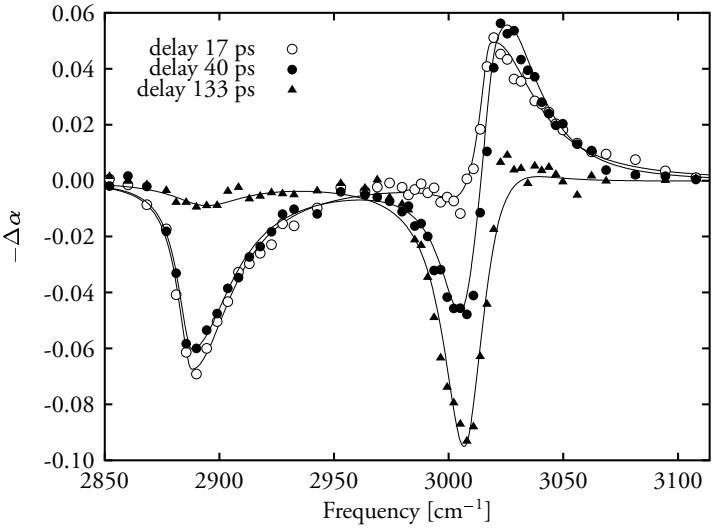

FIGURE 5.4. Transient spectra at short delay times. Pump frequency tuned to 3022 cm^{-1}. The solid lines are guides to the eye and are fitted to the data, assuming asymmetric Lorentzians for the different line shapes.

to an increased cross section of the C–H stretch vibration and to a negligible anharmonic shift.

From these transient spectra we can determine the anharmonic redshift of the frequency of the absorption starting from the $|0^*\rangle$ state, being 17 cm^{-1} with respect to the C–H stretch frequency. The transient spectra at large delays also give insight in the character of the $|0^*\rangle$ state. We note that the spectra in Figure 5.5 have an "isosbestic" point around 3019 cm^{-1}: at this frequency the induced absorption hardly changes when the second relaxation process takes place, which implies that the absorption of the $|0^*\rangle$ does not show a gradual shift during this relaxation. This suggests that the relaxation of the mode responsible for the anharmonic shift only involves one single quantum of vibrational energy. If the intermediate state $|0^*\rangle$ had been a highly excited vibrational state, a stepwise, more gradual decay of the redshift would have been expected. The C–H bend vibration is a very likely candidate, since a strong coupling is known to exist between the C–H stretch vibration and the first overtone of the C–H bend vibration, see References 63, 72, 79, 80, 94, 127, 137, and 179. Furthermore, in a recent study on the vibrational relaxation of liquid $CHCl_3$ by incoherent anti-Stokes Raman scattering, one relaxing C–H stretch quantum was found to produce one C–H bend quantum.[93] For the present data it can be concluded that the same relaxation mechanism applies to liquid bromoform. Another indication that the $|0^*\rangle$ state involves the C–H bend mode is given by estimates for the anharmonic redshifts of the $\nu_i \rightarrow \nu_1 + \nu_i$ transition, where ν_1 indicates one vibrational quantum in the C–H stretch mode and ν_i one of the other modes of the $CHBr_3$ molecule. These redshifts were reported to be:[78,85] 25 cm^{-1} for ν_4 (C–H bend), 4 cm^{-1} for ν_2 (C–Br_3 s-stretch), 3 cm^{-1} for ν_5 (C–Br_3 d-stretch) and about 1 cm^{-1} for ν_3 (C–Br_3 s-deform) or ν_6 (C–Br_3 d-deform). As

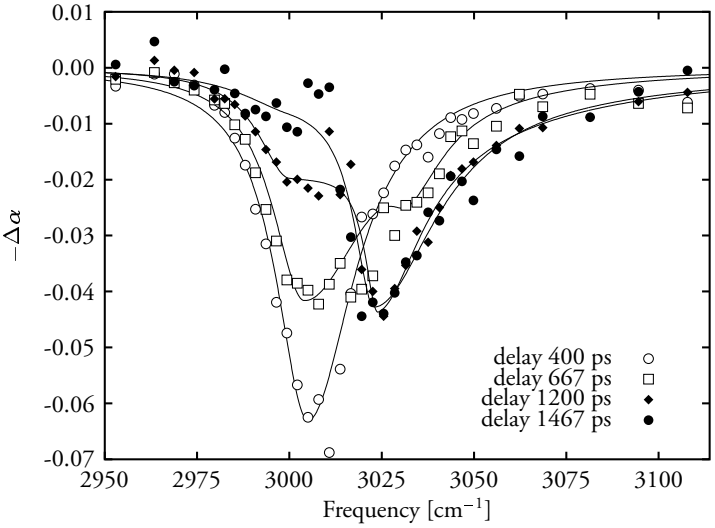

FIGURE 5.5. Transient spectra at long delay times. Pump frequency tuned to 3022 cm^{-1}. The solid lines are guides to the eye and are fitted to the data, assuming asymmetric Lorentzians for the different line shapes.

we concluded that the second relaxation involves one single vibrational quantum, the only candidate for the mode which causes the observed anharmonic shift is the ν_4, because for the other modes to produce the observed redshift, would require several quanta of these modes. It would still be possible for the other modes to be populated, but since the anharmonic shifts they cause are only a few cm^{-1}, they will not have an observable effect in our experiments. It is thus concluded that the relaxation of the induced absorption at 3005 cm^{-1} represents the relaxation of the C–H bend mode.

The observation of a two-step relaxation process agrees with the observations in earlier one-colour experiments on the pure liquid.[15] In order to determine the decay-time constants accurately, we also performed pump-probe delay scans, measured at four probe frequencies, as shown in Figure 5.6. With the pump frequency tuned to 3022 cm^{-1}, the probe frequency was tuned to 3023 cm^{-1} to perform a quasi one-colour experiment and to the red (3000 cm^{-1} and 3016 cm^{-1}) side of the $0 \rightarrow 1$ transition. Furthermore, the probe was tuned to the frequency of the $1 \rightarrow 2$ transition (2900 cm^{-1}). The solid curves in this figure are calculated with a kinetic model, which is illustrated in Figure 5.8 and has been described in detail in Section 3.4 and elsewhere.[82,163] In this model, the relaxation of the excited vibration $|1\rangle$ occurs via an intermediate state $|0^*\rangle$, rather than directly back to the ground state $|0\rangle$. The rate of relaxation from the first excited state $|1\rangle$ to the intermediate state $|0^*\rangle$ is given by k_A and the relaxation rate of the second step in the relaxation $|0^*\rangle \rightarrow |0\rangle$ is given by k_B. The cross section of the $0 \rightarrow 1$ transition is denoted by σ and the cross section of the $0^* \rightarrow 1^*$ transition by σ^*. As discussed above, the centre frequency of the $0^* \rightarrow 1^*$ transition is redshifted by 17 cm^{-1} with respect to the $0 \rightarrow 1$ transition, due to the anharmonic coupling between the C–H bend and C–H stretch modes. Therefore,

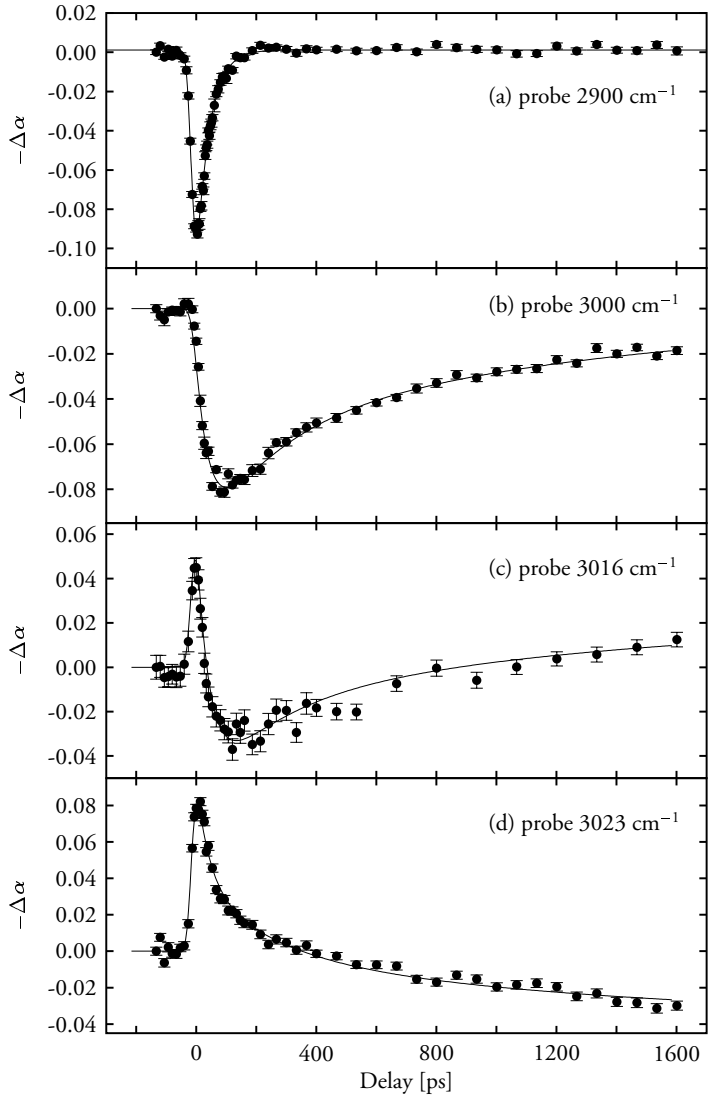

Figure 5.6. Two-colour pump-probe delay scans of pure $CHBr_3$. Pump frequency tuned to 3022 cm^{-1}. The solid lines are calculated using the model described in Section 5.3.

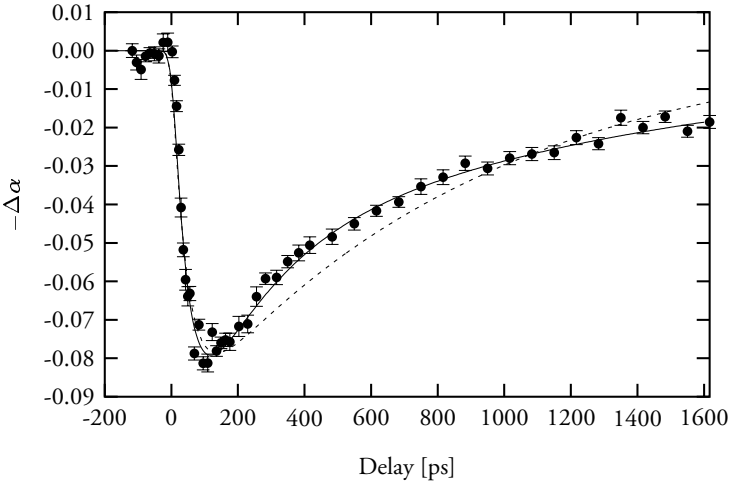

FIGURE 5.7. Comparison between a model, assuming an exponential decay (dashed line) and a model that includes a "bottleneck" (solid line) for the data at a probe frequency of 3000 cm^{-1}.

the cross section is different for each probe frequency.

If the frequency of the probe pulse is tuned to the $1 \rightarrow 2$ transition, the decay of the pump-induced absorption change $\Delta\alpha_{12}$ will only depend on the decay of n_1, since $n_2 = 0$:

$$\Delta\alpha_{12} \propto \sigma_{12} n_1(t) = \sigma_{12} n_1(0) e^{-k_A t} \tag{5.1}$$

and therefore k_A can be determined separately from k_B and the ratio σ^*/σ, contrary to, for example, the experiments described in Chapter 3, because in those one-colour experiments the frequency of the probe pulses could not be tuned separately from the frequency of the pump pulses.

From the data with the probe frequency tuned to the $1 \rightarrow 2$ transition we determined the lifetime $T_1 = 1/k_A$, to be 43 ± 1 ps. This value of the decay time for the first relaxation process ($1 \rightarrow 0^*$) agrees with the one determined by anti-Stokes Raman scattering:[87] 40 ± 4 ps. Using a value for k_A corresponding to $T_1 = 43 \pm 1$ ps, we tried to fit the data for the other probe frequencies. Especially at a probe frequency of 3000 cm^{-1}, the data could not be accurately fitted, when we described the second relaxation process by an exponential decay. As can be clearly seen in Figure 5.7, the decay from the $|0^*\rangle$ state is non-exponential. The decay from the intermediate level is faster than an exponential decay at first, but then slows down.

In addition, the relaxation from the $|0^*\rangle$ state is observed to be much slower for the pure liquid than for dilute solutions of $CHBr_3$. It is also observed that when the solvent fraction becomes smaller, the relaxation rate from the $|0^*\rangle$ state dramatically decreases.[15,17,90] These observations strongly suggest that molecules in the $|0^*\rangle$ state decay to another intermediate state, which acts as a "bottleneck": relaxation from this bottleneck state $|b\rangle$ is extremely slow and after some time becomes the so-called rate-limiting step in the relaxation mechanism. This implies that relaxation from the $|0^*\rangle$ state to the $|b\rangle$ state can initially be exponential, but after some time population accumulates in the bottleneck state and thus the relaxation

from the $|o^*\rangle$ state slows down. In view of the absence of an anharmonic shift, the bottleneck state is probably some low-energy mode of the $CHBr_3$ molecule, e.g. the C–Br_3 s- or d-stretch modes.

In ultrasonic dispersion measurements on pure $CHBr_3$ a relaxation time constant of 2 ns was observed.[200] In a previous study on concentrated solutions of $CHBr_3$ it was argued that the relaxation time constant for ultrasonic dispersion measurements should be related to the one found in pump-probe experiments by a Boltzmann factor.[85] However, this argument is not correct[116] and the lifetime of 2 ns is indeed the lifetime of a long-living vibrational mode in pure $CHBr_3$. Interestingly, similar ultrasonic dispersion measurements on $CHCl_3$ yielded a relaxation time which is nearly 8 times smaller.[200] Previous time-resolved studies on pure $CHCl_3$, see References 15 and 93, also showed that the relaxation in pure $CHCl_3$ is much faster than in pure $CHBr_3$.

Apparently, energy from this bottleneck level cannot be easily transferred to other (low-frequency) modes of the same or neighbouring $CHBr_3$ molecules. In solutions, there are more (solvent) modes available for the energy to be transferred to and therefore the bottleneck level can rapidly decay (and thus no longer forms a bottleneck) or decay via the bottleneck level will not be the only available decay channel; this will result in a faster vibrational decay.

We observed a persistent induced absorption around 3022 cm^{-1} at long delay times, which is even present at a delay of 4.7 ns. In order to investigate whether this absorption might be caused by heating effects, we have studied the temperature dependence of the linear absorption spectrum of the same sample. There we have found that with increasing temperature, there is a blue-shift of the central absorption frequency of about 0.05 cm^{-1} K^{-1} and a relative decrease of the absorbance of about 0.007 K^{-1} between room temperature and 363 K. This decrease of the absorbance includes the volume expansion effect. A typical value for the relative decrease by pure volume expansion is only 0.001 K^{-1} for organic liquids.[12] Hence, even if the volume would not expand at all after relaxation, an absorption decrease is expected, instead of the observed increase. This forms additional evidence that the relaxation of the intermediate state does not lead to a full thermalisation, but rather leads to the occupation of a specific, long-living bottleneck state. For $CHBr_3$ dissolved in carbon tetrachloride (CCl_4), we have found a persistent bleaching instead of an induced absorption, even at a very high concentration of 25 vol%. This same bleaching is also found in earlier studies on solutions of this concentration.[85] Apparently, in solution a rapid thermalisation occurs because the energy of the intermediate state can be transferred to modes of the solvent molecules.

Introduction of a bottleneck state in our model requires changes in the rate-equations, and therefore we replace Equation (3.4) with:

$$\frac{dn_{o^*}}{dt} = k_A n_1 - k_B(n_{o^*} - cn_b), \tag{5.2}$$

and we add an equation for population n_b of the bottleneck level:

$$\frac{dn_b}{dt} = -k_C n_b + k_B(n_{o^*} - cn_b), \tag{5.3}$$

where k_C is the relaxation rate from the bottleneck level and c a dimensionless constant.

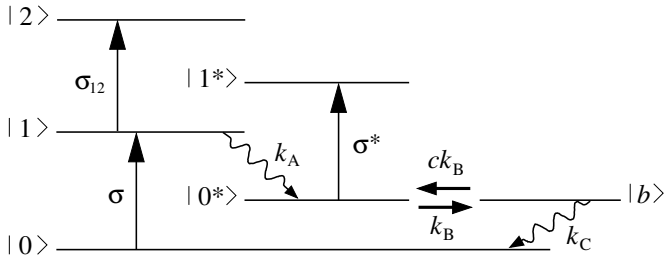

FIGURE 5.8. States and decay scheme used in the model for the relaxation of the C–H stretch of $CHBr_3$.

With this model (see Figure 5.8) we could describe the data obtained at a probe frequency of 3000 cm^{-1}, taking $\sigma^*/\sigma \gg 1$, $c = 0.55$, and values for k_B and k_C corresponding to decay times of $1/k_B = 425$ ps and $1/k_C = 833$ ps, respectively. With these values we could also describe the data at the probe frequencies of 3016 cm^{-1} and 3023 cm^{-1}. We obtained values for σ^*/σ of 1.4 and 0.45 at these respective probe frequencies.

In an earlier pump-probe experiment on pure liquid $CHBr_3$,[15] the time constant of the first relaxation process ($1 \rightarrow 0^*$) was determined to be 28 ± 2 ps, which is clearly too short. This value was determined by one-colour pump-probe experiments, which prohibited the independent determination of k_A, as was possible in the two-colour experiments described here. The large error in the previous determination of k_A is mainly due to the fact that the relaxation from the $|0^*\rangle$ state was assumed to be exponential, which is clearly not the case, as we have shown here.

5.4 CONCLUSIONS

Relaxation of the excited C–H stretch vibration of $CHBr_3$ in the pure liquid occurs in at least three consecutive steps. In the first step vibrational energy is transferred with a time constant of 43 ± 1 ps from the $v = 1$ state of the C–H stretch vibration to an intermediate state $|0^*\rangle$. From the transient spectra it is clear that the intermediate state is another molecular vibration of $CHBr_3$ which is singly excited and for which the C–H stretch frequency is anharmonically redshifted by 17 cm^{-1}. This suggests that the intermediate level $|0^*\rangle$ is formed by the singly excited C–H bend mode.

In the second step, relaxation from this intermediate level occurs. This relaxation from the $|0^*\rangle$ state is exceptionally slow and non-exponential. This suggests that the intermediate state mainly decays to another well-defined state, which slowly decays and acts as a bottleneck for the relaxation. This bottleneck state is probably some low-energy mode of the $CHBr_3$ molecule e.g. the C–Br_3 s- or d-stretch modes.

In contrast to solutions of $CHBr_3$ and pure $CHCl_3$, an induced absorption remains around 3022 cm^{-1} after the second relaxation. This absorption persists until at least a delay of 4.7 ns. The cause of this absorption is thought to be the long-living population of the bottleneck state, which frustrates thermalisation.

6 Vibrational dynamics of the C–O stretch vibration in alcohols

We present a study on the vibrational dynamics of the C–O stretch vibration of methanol and ethanol in carbon tetrachloride (CCl_4) solution. The relaxation of the excited C–O stretch vibration was observed to occur in two steps. In the first step energy is transferred from the $v = 1$ state of the C–O stretch vibration to an intermediate state with a time constant of 3.2 ± 0.2 ps for methanol and 3.2 ± 0.7 ps for ethanol. The intermediate state is most likely formed by the $n = 3$ or 4 state of the C–O–H bending mode, which is also known as the torsional mode. In the second step energy is transferred from this intermediate state to low-energy modes, leading to a full equilibration of the energy. In methanol this thermalisation occurs with a time constant of 28 ± 1 ps. In ethanol the second step is faster, with a time constant of 12 ± 2 ps.

6.1 Introduction

The lifetime of an excited molecular vibration strongly depends on the availability of modes to which energy can be transferred. These accepting modes can be lower-frequency vibrational modes within the excited molecule, but also low-frequency solvent modes. In the past decades, there has been a large number of studies on the dynamics of excited C–O stretch vibrations, see References 22, 23, 26, 35, 50, 51, 102, 106, 110, 111, 112, 113, 117, 118, 119, 122, 147, 170, 173, 201, and 202. Interestingly, a very broad range of lifetimes T_1 of the excited state of the different C–O stretch vibrations is reported, ranging from sub-picosecond to hundreds of picoseconds.

In studies on carbonyl (–CO) complexes of transition metals in liquid solution, exceptionally large values for T_1 of several hundreds of picoseconds have been found, see References 22, 110, 111, 113, 201, and 202. Apart from the central atom and other ligands of these complexes, the relaxation rate was observed to depend strongly on temperature and solvent. The long vibrational lifetime of the excited vibration can be explained by the absence of suitable accepting modes in the form of other intramolecular vibrations. The relaxation mechanism will therefore involve a transfer of energy directly to solvent modes or to vibrations of solvent molecules, which explains the strong solvent and temperature dependence of the relaxation rate. This is illustrated by the observation that for rhodium carbonyl complexes in chloroform ($CHCl_3$), T_1 varies between 600 and 750 ps for complexes with different numbers of rhodium atoms and CO-ligands, but for the complex $Rh(CO)_2(C_5H_7O_2)$, T_1 is found to be only 90 ps.[111] Apparently the more complex organic ligand acetyl acetonate ($C_5H_7O_2$) provides more accepting modes than the carbonyl ligands, resulting in a faster relaxation of the excited carbonyl C–O stretch vibration.

Another group of compounds with quite long lifetimes for C–O stretch vibrations is formed by complexes of carbon monoxide (CO) bound to haemoglobin, myoglobin and

model haem compounds (metalloporphyrin complexes).[117,118,119,147,170] For these systems, T_1 does not significantly depend on temperature[118] and solvent[119], and is mainly determined by the structure of the haem group and the central metal atom. For the different compounds, T_1 is found to lie between 10.7 and 44.5 ps. The predominant vibrational relaxation process was shown to be transfer of energy from CO to vibrations of the haem group by anharmonic coupling. As a result, there is hardly any solvent or temperature dependence, as energy transfer to solvent modes is not the dominant process.

When CO is chemisorbed to platinum or rhodium particles supported on SiO_2, the relaxation of the excited C–O stretch vibration is faster than that of the CO–haem complexes. For these systems T_1 is observed to be in the range 5–10 ps.[26,112] When CO is chemisorbed on metal surfaces the relaxation rate is even higher:[23,50,51,106] T_1 was found to be 2.2 ps for CO on a Pt(111) surface[23,50] and 3 ps for CO on a Cu(100) surface.[106] The relaxation mechanism is thought to be excitation of electron-hole pairs in the metal through dipole-dipole coupling, in agreement with the observation that T_1 does not depend on temperature or surface coverage.[23]

The fastest relaxation of the C–O stretch vibration is observed when the C–O group is part of an (organic) molecule. Then the mechanism probably involves intramolecular relaxation, where energy is transferred from the excited vibration to one or more other vibrations of the molecule by anharmonic coupling. The C–O stretch vibration of acetic acid in carbon tetrachloride (CCl_4) was observed to have a lifetime of 0.7 ps[35] and the amide I vibration in peptides† to have a lifetime around 1.2 ps.[102,173] The C–O stretch vibration of a coumarin dye was observed to have a lifetime of 2 ps.[122]

The relaxation mechanism of the C–O stretch vibration of systems where C–O acts as a ligand has been extensively studied and is quite well understood. In contrast, very little is known about the rate and mechanism of vibrational relaxation of excited C–O stretch vibrations when the C–O group is part of an (organic) molecule. Here we present a study on the vibrational dynamics of the C–O stretch vibration of methanol and ethanol in solution.

6.2 EXPERIMENT

In the one-colour pump-probe experiments described in this chapter, we made use of the output of a Free Electron Laser (FEL), that emits directly in the mid-infrared. A general background of pump-probe spectroscopy can be found in Section 2.2. In an FEL, a beam of relativistic electrons (i.e. moving at a velocity close to the velocity of light) passes through a transverse, periodic magnetic field, created by a periodic structure called the "undulator" to exchange energy with an electromagnetic radiation field through stimulated emission. Efficient energy transfer requires that the electrons experience nearly resonant forces from the radiation and undulator fields. This resonance is achieved when the radiation wavelength λ approximately satisfies $\lambda \approx \lambda_u/2\gamma^2$, where λ_u is the undulator period, $\gamma = (1 - v^2/c^2)^{-1/2}$ the Lorentz factor, c the velocity of light in vacuum, and v the velocity of the electrons. Two end-mirrors provide feedback for laser oscillation. Using bending magnets, the electron beam is first injected into the laser cavity and then deflected out of the cavity. The wavelength of the radiation is continously tunable as it is determined by the energy of the

†The amide I vibration of peptides mainly involves the C–O stretch modes of the amide backbone.

electron beam and the period of the undulator magnet, which can be varied. Depending on the design, an FEL can emit radiation with wavelengths from centimetres to nanometres. For a detailed and comprehensive treatment of the subject of FELs see e.g. References 59 and 199.

Unfortunately, the pulses from an FEL are not always ideally suited for vibrational pump-probe experiments in condensed phases, despite its apparent positive qualities. As the time structure of the laser reflects the time structure of the electron beam, the short light pulses are often not evenly spaced, but bunched in "macropulses", depending on the design of the FEL. Due to this bunching, the picosecond "micropulses" have a very short spacing in time and hence, the observation of transient absorption changes can often be hampered by artifacts due to heating, as a significant amount of energy is absorbed by the sample over the duration of the macropulse. Another disadvantage is that only one-colour experiments are possible when using an FEL as a source. It seems that these problems can be avoided by using a laser system, similar to the one described in §2.1.2, using DFG in crystals like silver gallium disulfide ($AgGaS_2$), silver gallium diselenide ($AgGaSe_2$), and gallium selenide (GaSe), which can produce femtosecond pulses in the wavelength range of 4–18 μm.[180]

The experiments described in this chapter were carried out at the free electron laser FELIX in The Netherlands, which has been described in detail elsewhere.[165] In short, this source for short infrared pulses is tunable from 5 μm to 110 μm (2000 cm^{-1} to 90 cm^{-1}) and delivers macropulses of 5–10 μs in duration, which consist of a train of micropulses. In our experiments, the micropulses were spaced by 40 ns, with a typical energy of 10 μJ. The micropulses had a typical length of 1.2 ps (FWHM). At a wavelength of 9.64 μm the micropulses had a bandwidth of 0.10 μm (=11 cm^{-1}) (FWHM), which means that the pulses are close to being transform-limited. The macropulses had a repetition rate of 10 Hz.

The pump-probe set-up used in our experiments is similar to the general set-up described in Section 2.2. The differences are discussed here. Before passing through the sample, the probe pulses are split in two parts of which one is delayed by an extra 20 ns. This part subsequently passes through the sample at a time when the sample is not affected by a pump pulse, contrary to the "undelayed" part of the probe. Since the bias of the mercury-cadmium-telluride (MCT) detector is actively reversed between the detection of the two probe pulses, the signal measured is $T - T_0$. This allows for a significant improvement of the signal-to-noise ratio, as in this way heating effects on the measured transmission changes are reduced, because both pulses are affected in the same way by heating. Separate measurement of T_0 allows the calculation of the relative transmission change T/T_0. The polarisation of the probe pulses was rotated 90°, with respect to the polarisation of the pump pulses, in order to eliminate coherent artefacts due to thermal gratings. The reflection of a zinc selenide (ZnSe) plate, placed in the probe beam, is used as a reference to correct for the macropulse to macropulse intensity fluctuations of the FEL. The beams are focused into the sample with two separate barium fluoride (BaF_2) lenses.

The experiments were performed on a 0.14 M solution of methanol in CCl_4 in a temperature controlled sample cell with BaF_2 windows and a sample length of 0.5 mm. Experiments were also performed on a 0.34 M solution of ethanol in CCl_4. The pump-probe experiments on the methanol solution were carried out at different temperatures, ranging from room temperature to 70°C, and at different wavelengths within the C–O stretch absorption band.

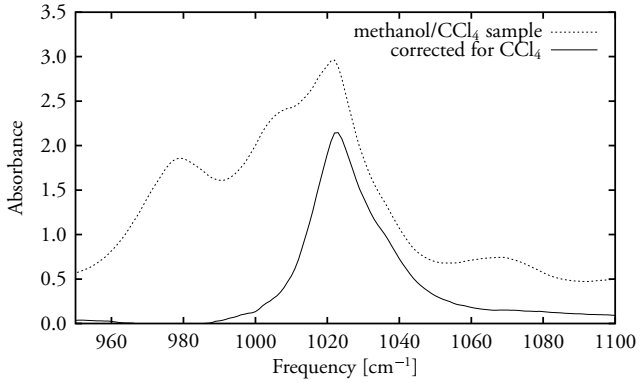

FIGURE 6.1. Linear absorption spectrum of a 0.14 M methanol in CCl_4 sample with a sample length of 0.5 mm (dashed line) and corrected for the absorption of CCl_4 (solid line).

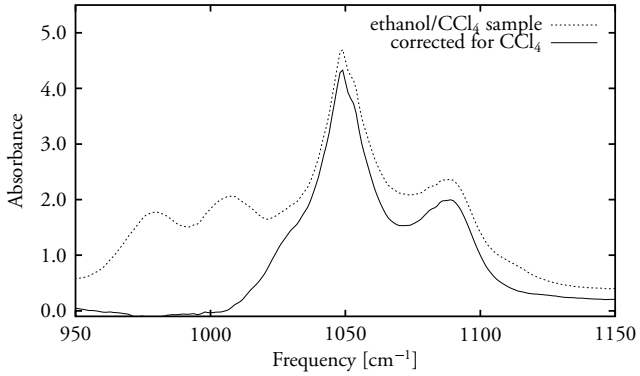

FIGURE 6.2. Linear absorption spectrum of a 0.34 M ethanol in CCl_4 sample with a sample length of 0.5 mm (dashed line) and corrected for the absorption of CCl_4 (solid line).

6.3 RESULTS

The linear absorption spectrum of the methanol solution is shown in Figure 6.1. The C–O stretch absorption band of methanol in CCl_4 is centred at 1023 cm^{-1}. The linear absorption spectrum of the ethanol solution is shown in Figure 6.2. The C–O stretch absorption band of ethanol in CCl_4 is centred at 1050 cm^{-1}. In these figures the spectra corrected for the absorption of CCl_4 are also shown. The absorbance A was calculated from the measured transmittance of the sample (T_{sample}) and the transmittance of air (T_{air}) by $A = -\ln(T_{sample}/T_{air})$.

For the methanol solution, pump-probe scans at different temperatures and at frequencies between 1020 cm^{-1} and 1045 cm^{-1} (λ=9.80 μm–9.57 μm) all showed bleaching signals similar to the measurement shown in Figure 6.3. The bleaching signal clearly exhibits a bi-exponential decay. The amplitude of the bleaching signal strongly decreases when the

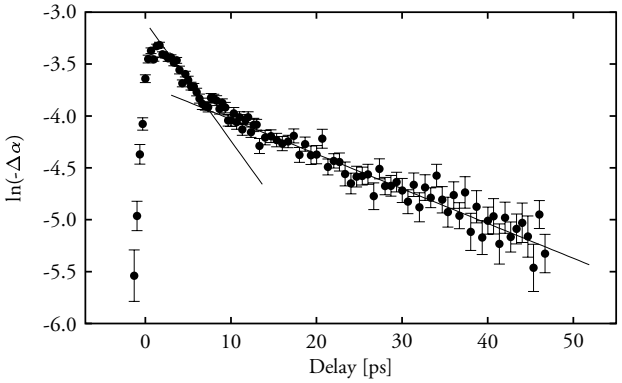

FIGURE 6.3. Pump-probe delay scan of methanol in CCl_4 at a frequency of 1037 cm^{-1} (λ=9.64 μm), T=43°C. The solid lines are guides to the eye and illustrate that the bleaching signal exhibits a bi-exponential decay.

laser frequency is tuned away from the centre of the absorption band.

At the red side of the C–O stretch absorption band of ethanol, at a frequency of 1045 cm^{-1}, an induced absorption was found, which decays at the same rate as the bleaching signal. This induced absorption is attributed to absorption of the $v = 1$ state of the C–O stretch vibration. The observed small red shift of the excited state absorption in ethanol indicates that the anharmonicity of this stretch vibration is quite small. This also explains the rapid decrease in bleaching signal amplitude, when the frequency of pump and probe is tuned away from the centre of the absorption band.

At the red side of the C–O stretch absorption band of methanol (1015 cm^{-1} and lower), no signal was observed, which can be explained by the fact that the red side of the C–O stretch absorption band of methanol overlaps with an absorption band of CCl_4.

6.4 DISCUSSION

Transfer of energy from an excited C–O stretch vibration to one or more other vibrations within the excited molecule is much faster and much less temperature dependent than transfer to low-energy solvent modes, see References 22, 110, 111, 113, 201, and 202. Indeed, the present observation that the vibrational relaxation of the C–O stretch vibration of methanol and ethanol in CCl_4 is fast and not temperature dependent, strongly suggests that the relaxation mechanism is an intramolecular process.

The CH_3-rock vibration is quite close in energy to the C–O stretch vibration, especially in ethanol. However, the coupling between these modes is very small[142] and it is therefore not very likely that the CH_3-rock mode is the accepting mode in the relaxation of the excited C–O stretch vibration. In addition, the energy difference between the C–O stretch mode and the CH_3-rock mode is quite different for methanol and ethanol. This difference in the "energy gap" would lead to different relaxation rates of the excited C–O stretch vibration of the two different alcohols if the CH_3-rock mode were the accepting mode. However, we observe identical lifetimes in both alcohols.

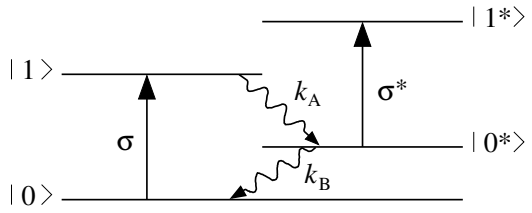

FIGURE 6.4. States and decay scheme used to describe the relaxation of the excited C–O stretch vibration. The cross sections for a radiative transition are indicated by σ and σ^*. The rate of the $1 \rightarrow 0^*$ relaxation is given by k_A and the rate of the $0^* \rightarrow 0$ relaxation is given by k_B.

In studies on gas-phase spectra of methanol, a strong coupling was found to exist between the $v = 1$ state of the C–O stretch vibration and the states with 3 or 4 quanta in the C–O–H bending mode (or torsional mode as it is also denoted).[141,181] This suggests that the C–O–H bending mode forms the accepting mode in the relaxation of the excited C–O stretch vibration in methanol and ethanol. This relaxation is followed by equilibration of the energy over all other degrees of freedom. In this way, the C–O–H bending mode would act as an intermediate state in the relaxation, thereby explaining the observed bi-exponential decay.

In order to determine the decay-time constants of the two relaxation processes, we use a simple model which is described in detail in Section 3.4 and elsewhere.[82,163] In this model, the relaxation of the excited vibration $|1\rangle$ occurs via an intermediate state $|0^*\rangle$, rather than directly back to the ground state $|0\rangle$. The rate of relaxation from the first excited state $|1\rangle$ to the intermediate state $|0^*\rangle$ is given by k_A and the relaxation rate of the second step in the relaxation $|0^*\rangle \rightarrow |0\rangle$ is given by k_B. The cross section of the $0 \rightarrow 1$ transition is denoted by σ and the cross section of the $0^* \rightarrow 1^*$ transition by σ^*. The solid line in Figure 6.5 is calculated with this model, which is illustrated in Figure 6.4.

Using this model, the measurements on the methanol solution at all the different frequencies and temperatures could be described with one set of k_A and k_B. The cross section ratios σ^*/σ at the different frequencies increase with increasing frequency from 0.10 ± 0.02 at 1025 cm^{-1} to 0.3 ± 0.1 at 1045 cm^{-1}. The lifetime of the excited C–O stretch vibration in methanol ($T_1 = 1/k_A$) was determined to be 3.2 ± 0.2 ps. The lifetime of the intermediate state $|0^*\rangle$ ($= 1/k_B$) was determined to be 28 ± 1 ps.

Using the same model we found for the excited C–O stretch vibration in ethanol a lifetime $T_1 = 1/k_A = 3.2 \pm 0.7$ ps. For ethanol, the lifetime of the intermediate state $1/k_B = 12 \pm 2$ ps, which is about twice as small as for methanol. The decay of the intermediate state is thus significantly faster in ethanol, probably because there are more low-frequency modes in the molecule to which this state can couple.

The increase in the ratio σ^*/σ when tuning the frequency from the red side to the blue side of the absorption band indicates that population of the intermediate state leads to a transient blue shift of the C–O stretch absorption band. Indeed, population of the C–O–H bending mode has been observed to cause a small blue shift of the C–O stretch frequency.[181] The frequency of the C–O stretch vibration could also be influenced by "local heating",

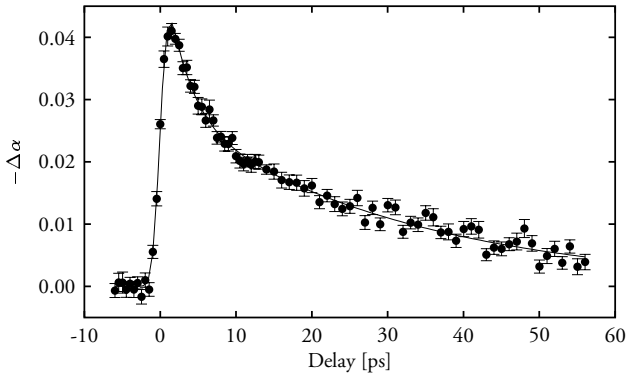

Figure 6.5. Pump-probe delay scan of methanol in CCl_4 at a frequency of 1025 cm^{-1} (λ=9.76 μm), T=31°C. The solid line is calculated using the model described in Section 6.4.

because a lot of energy is dumped into a small volume around the excited molecule right after the relaxation. This might cause the surroundings to resemble the gas-phase more closely and therefore cause the frequency of the C–O stretch vibration to shift towards its gas-phase value, i.e. to the blue. Whether the occupation of the C–O–H bending mode or the "local heating" is the main cause for the observed blue shift cannot be concluded from our experiments.

In a study on the relaxation of the O–H stretch vibration of ethanol clusters in CCl_4 also a transient blue shift of the initially excited vibration was observed. For this vibration, the relaxation mechanism is believed to involve energy transfer to the hydrogen bond, which even causes the hydrogen bond to predissiociate.[211] This in turn causes a blue shift of the O–H stretch vibration. However, in the case of the C–O stretch vibration, the blue shift cannot be caused by an energy transfer to the hydrogen bond, because a decrease in cluster size (and breaking of a hydrogen bond) causes a red shift of the C–O stretch frequency, instead of the observed blue shift.[44] In addition, judging by the relative intensities of the narrow O–H stretch absorption band due to monomers and the broad O–H stretch absorption band due to clusters in the linear spectrum, it is clear that at the concentration used in our experiments, there are mainly monomers present.

As the experiments were carried out with perpendicular polarisations for pump and probe to eliminate coherent artefacts due to thermal gratings, the transient signals due to population relaxation could be influenced by orientational relaxation.[90] From dielectric relaxation measurements, the Debye relaxation time τ_D was determined to lie in the ranges 47–56 ps for methanol and 138–170 ps for ethanol.[20,27,49,183] These relaxation times must be divided by a factor of 3 to get the rotational correlation time for a pump-probe experiment.[30] In a perpendicular configuration of the pump and probe polarisations, the reorientation could thus lead to a small and slow increase of the measured signal. This means that the lifetimes, especially those of the intermediate state, could in reality be slightly smaller than we found in our measurements.

6.5 CONCLUSIONS

We studied the vibrational dynamics of the C–O stretch vibration of methanol and ethanol in CCl_4. The relaxation of the excited C–O stretch vibration was observed to occur in two steps. In the first step energy is transferred from the $v = 1$ state of the C–O stretch vibration to an intermediate state with a time constant of 3.2 ± 0.2 ps for methanol and 3.2 ± 0.7 ps for ethanol. This intermediate state is most likely formed by the $n = 3$ or 4 state of the C–O–H bending mode. The presence of such a strongly coupled low-frequency mode in organic molecules provides a likely explanation why the lifetime of the excited C–O stretch vibration of these systems is much shorter than that of metal-carbonyl or CO-haem complexes.

In the second step energy is transferred from the intermediate state to low-energy modes. In methanol this thermalisation occurs with a time constant of 28 ± 1 ps. In ethanol the second step is faster, with a time constant of 12 ± 2 ps, because of the higher number of available accepting modes.

7 Correlation properties of parametrically generated light

The temporal coherence or correlation time τ_c of parametrically generated mid-infrared light is determined by measuring the twin-correlation peak in the sum-frequency spectrum as a function of delay between the signal and idler. The correlation time τ_c of the generated signal and idler fields was found to lie in the picosecond range and follows the frequency-dependence, predicted from the bandwidth by the relation $\tau_c = 1/\Delta\omega$.

7.1 Introduction

In parametric generation, a strong pump field is converted to signal and idler fields. In this process signal and idler start at the zero-photon level, which has as a consequence that the classical description using Maxwell's equations fails. If there are no photons present in a mode of the electric field, the expectation value of the field operator is zero. The expectation value of the square of the electric field operator, on the other hand, is non-zero due to the zero-point energy. The spread in the electric field given by

$$\Delta E = \sqrt{\langle E^2 \rangle - \langle E \rangle^2} \tag{7.1}$$

is thus also non-zero.[114] This means that there is quantum noise present at the signal and idler input fields. These zero-point or vacuum-fluctuations can act as a seed for the parametric generation and subsequent parametric amplification.[28] This means that parametric generation, like the Casimir effect,[47,48,157] is a macroscopic manifestation of microscopic quantum fluctuations.

The individual phases of the signal and idler fields in parametric generation can obtain any value, because these fields start from quantum noise. However, after being significantly amplified, the sum of their phases is related to the phase of the pump field, because parametric amplification is a phase-sensitive process. This means that the phases of the amplified signal and idler fields can be strongly modulated, leading to a bandwidth given by Equation (2.5), but these modulations will be complementary. As a result of the strong phase modulation, the (spectral) bandwidth of the parametrically generated signal and idler fields can be much larger than than the bandwidth of the pump field.

When the signal and idler fields are recombined in a sum-frequency generation process, generally a broad sum-frequency spectrum will result from the large-bandwidth signal and idler fields. However, when the signal and idler fields overlap within the coherence time of their phase-modulations, these modulations will cancel, resulting in a narrow peak in the sum-frequency spectrum. This narrow peak will have the same width as the pump spectrum. This narrow peak has been observed and is denoted as the *twin-correlation peak*.[1]

The term twin-correlation peak has been derived from a quantum-mechanical picture of the parametric generation process. In parametric generation, a pair of photons (*twins*) is generated simultaneously from one pump photon. The occurrence of a narrow peak in the sum-frequency spectrum is thought to signify the recombination of a photon with its twin brother. This picture is not entirely correct as each photon need not be recombined with its twin for the sum-frequency spectrum to display a narrow feature. Photons generated shortly after each other can still give rise to a twin-correlation peak, as the phases of signal and idler fields cannot change infinitely fast, since this would imply an infinitely high frequency.

Measuring the (relative) intensity of the twin-correlation peak as a function of delay between the signal and idler fields in the sum-frequency generation when they are recombined, will reveal the correlation time of the parametrically generated fields, which is a measure for the correlation time of the zero-point electric field, which acts as a seed for the parametric generation process. Generally, the coherence time of the phases of the signal and idler fields will be determined by the spectral bandwidth $\Delta\omega$ of the parametrically generated light. The coherence time or correlation time τ_c is related to the bandwidth by $\tau_c = 1/\Delta\omega$, according to the Wiener-Khintchine theorem.[68,120,153] This relation has been confirmed in an experiment, measuring the coincidence counts of signal and idler photons.[121,153]

The correlation properties of signal and idler fields have been used in a wide range of quantum optical experiments. A pair of twin-photons can be regarded as an *entangled state* and has been used to perform so-called Einstein-Podolsky-Rosen (EPR) experiments. This entangled or EPR-state was proposed to point out the apparent incompleteness of quantum mechanics.[70] These *gedanken* experiments were later extended by Bell to demonstrate the incompatibility of quantum mechanics with local descriptions by means of the Bell inequalities.[24,25] These inequalities are violated if the local realistic description fails, as was shown in different experiments, using parametric generation.[134,168,169] These entangled states, formed by parametrically generated photons, have also been proposed for and used in e.g. "quantum teleportation" [37,76] and "quantum cryptography". For a comprehensive treatment of the subject of quantum optics see References 14, 149, 153, 187, and 204.

The twin-correlation peak can also be used as an indicator for or a measure of correlation between parametrically generated fields. If signal and idler photons emanating from the same location in the generating medium are used, only information on the temporal correlation of the zero-point electric field will be obtained. If on the other hand signal and idler photons from two different regions are recombined in the sum-frequency generation, the relative intensity of the twin-correlation peak can be used as a measure for the spatio-temporal correlation of the zero-point electric field.

7.2 EXPERIMENTAL REMARKS

In these experiments we use experimental set-ups that are based on a set-up for the generation of picosecond mid-infrared pulses which is described in more detail in Section 5.2. These pulses have previously been used in time-resolved non-linear spectroscopy, see e.g. Chapter 5 and References 18, 34, 39, 42, and 210.

In all experiments, pulses from a Nd:YAG laser (Quantel YG502C) are used as pump

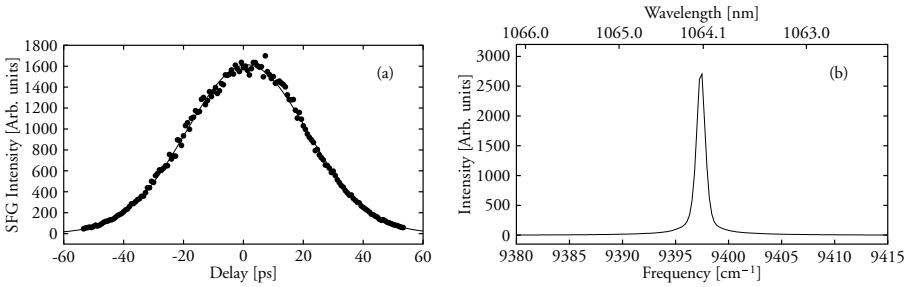

FIGURE 7.1. Autocorrelation trace (a) and spectrum (b) of pulses from the Nd:YAG laser used in the experiments described in this Chapter and in Chapter 5. The solid line in (a) is a Gaussian with a FWHM of 47.6 ps, corresponding to a pulse duration of 33.6 ps (FWHM).

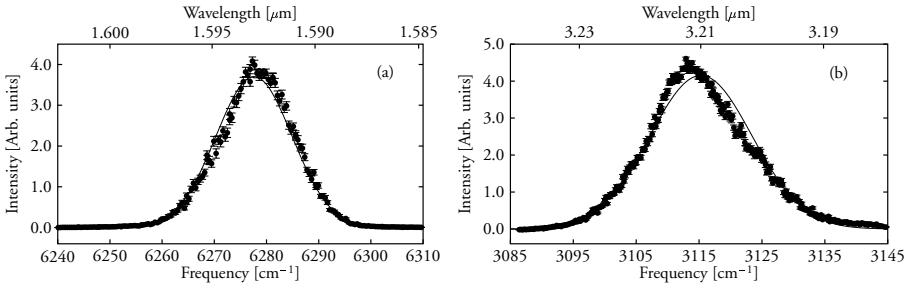

FIGURE 7.2. Typical spectra of signal (a) and idler (b) pulses used in the experiments in this Chapter and in Chapter 5. The solid lines are Gaussians with a FWHM of (a) 17 cm^{-1} and (b) 19 cm^{-1}, respectively.

pulses in the parametric generation and amplification processes in lithium niobate ($LiNbO_3$) crystals. This pump laser delivers pulses with a duration of 34 ps (FWHM) and an energy up to 60 mJ per pulse at a wavelength of 1064.1 nm[133] and a repetition rate of 10 Hz. An autocorrelation trace of these pulses, generated through sum-frequency generation in a 6.5 mm BBO crystal, is shown in Figure 7.1. Typical spectra of signal and idler pulses generated in this set-up are shown in Figure 7.2.

7.3 TEMPORAL CORRELATION

7.3.1 EXPERIMENT

The experimental set-up which is shown schematically in Figure 7.3 was used to measure the correlation time of the parametrically generated light as a function of the frequency of the signal and idler pulses. In a $LiNbO_3$ crystal (5 cm long, optical axis cut at 47.1°) signal and idler pulses are generated by 4 mJ pump pulses. The part of parametrically generated light which travels collinearly with the pump beam is amplified in a second $LiNbO_3$ crystal. After the second crystal, pump and idler wavelengths are filtered out, yielding signal pulses

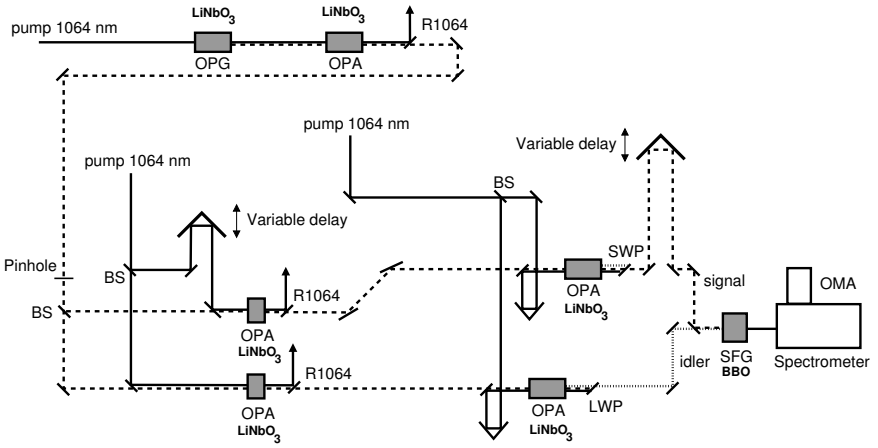

FIGURE 7.3. Experimental set-up for measuring the frequency dependence of the temporal correlation of the parametrically generated light. (Legend: OPG: Optical Parametric Generation. OPA: Optical Parametric Amplification. BS: beam splitter. SWP: Short-wave-pass filter and mirror for 1064 nm. LWP: Long-wave-pass filter and mirror for 1064 nm. SFG: Sum-frequency generation. OMA: Optical multichannel analyser. R1064: mirror for 1064 nm.).

with a typical energy of 18 μJ per pulse. These signal pulses are split in two equal parts and used as a seed for two separate amplification stages. The amplified seed pulses are then used in two further amplification stages, each yielding signal and idler pulses with typical energies of 500 μJ and 250 μJ per pulse, respectively. The signal pulses of one amplification stage and the idler pulses of the other are then collinearly combined in a β-barium borate (β-BaB_2O_4 or BBO) crystal. The light generated by the sum-frequency generation process in the BBO crystal is then analysed using a spectrometer with an Optical Multichannel Analyser (OMA). The signal and idler pulses can be delayed with respect to each other using a variable delay in the path of the signal pulse.

The frequency of the signal and idler pulses was varied by tuning the angles of the $LiNbO_3$ crystals. Sum-frequency spectra were recorded at different signal and idler frequencies and at different delay values between the signal and idler pulses.

7.3.2 RESULTS AND DISCUSSION

Several sum-frequency spectra recorded at different delay values between the signal beam of one amplification stage and the idler beam of the other are shown in Figure 7.4. These spectra were measured with the OPG/OPA stages tuned to a signal frequency ω_{signal}=5830 cm^{-1} (λ_{signal}=1715 nm). When the delay between signal and idler is larger than 2 ps, a broad sum-frequency spectrum, centred around 9398 cm^{-1} (1064.1 nm) is observed. At smaller delay values, a narrow peak appears on top of the broad spectrum. This narrow peak, which is the twin-correlation peak, is at its maximum at delay zero. It should be noted that the twin-correlation peak disappeared when the pinhole (diameter 200 μm) in front of the beam splitter, which splits the seed in two, was removed.

In Figure 7.5 the intensity of the maximum of the sum-frequency spectra at

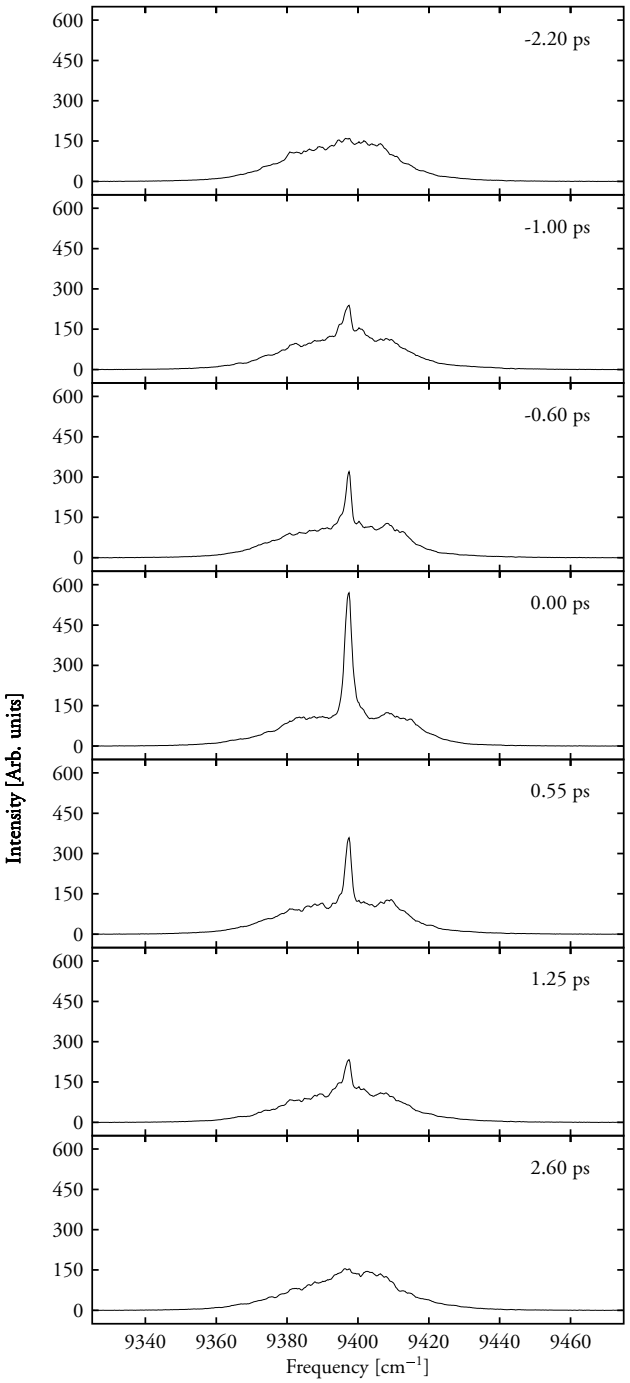

FIGURE 7.4. Sum-frequency spectra at different delays between signal and idler at ω_{signal}=5830 cm^{-1}.

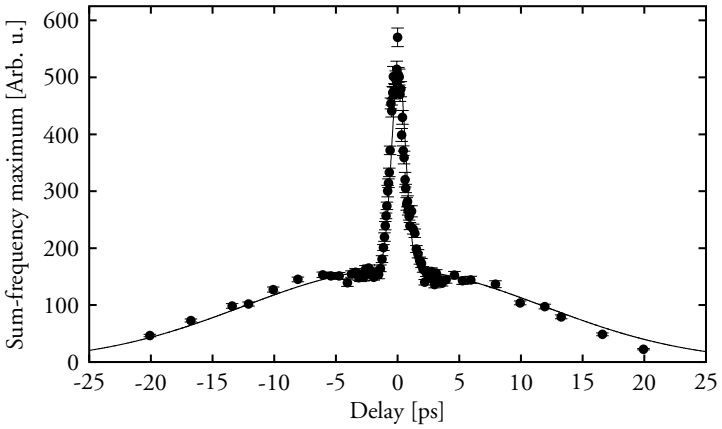

FIGURE 7.5. Maxima of the sum-frequency spectra at different delays between signal and idler at ω_{signal}=5830 cm^{-1}. The solid line is a fit to the data of a sum of two Gaussians with a full width at half-maximum of 1.3 ps and 29 ps respectively.

ω_{signal} =5830 cm^{-1} at different delay values is plotted as a function of delay between the signal and idler pulses. In order to obtain a good fit of the measured data of these "peak heights" as a function of delay, a Savitzky-Golay filtering procedure[174] was applied, as the data was quite noisy. This filtering algorithm was originally developed to extract peak widths and heights from noisy spectrometric data.[182] The characteristic feature of this filtering scheme is that the peak widths and heights of the original data are preserved. After the filtering procedure a good fit of a sum of two Gaussians (with a full width at half-maximum of 1.3 ps and 29 ps respectively at ω_{signal}=5830 cm^{-1}) to the data was obtained. In Figure 7.5 this fit is represented by the solid line. The long timescale is identified with the cross-correlation time of the intensity profile of the signal and idler pulses and the short timescale with the correlation time τ_c of the electric field.

The results of the experiments at different signal and idler frequencies are shown in Figure 7.6, where the correlation time of the parametrically generated light is plotted as a function of signal frequency. The solid line is calculated using Equation (2.5) for the bandwidth of the generated signal and idler pulses, the Sellmeier dispersion equations for $LiNbO_3$, see References 41 and 192, and assuming a gain factor g_o of 0.4 cm^{-1} over the length of the last amplification crystal.

Although these measurements do not yield accurate measurements of the correlation time τ_c of the parametrically generated light, the expected increase of τ_c when tuning away from degeneracy is clearly visible, when comparing the data to the calculated curve in Figure 7.6.

The measured values for τ_c also agree with the value of $\tau_c = 1.13 \pm 0.07$ ps at ω_{idler}=3450 cm^{-1} (ω_{signal}=5950 cm^{-1}), obtained from previous (incoherent) photon-echo experiments with a slightly modified set-up.[207,210] These incoherent photon-echo experiments make use of the fact that the time resolution is determined by the coherence time of the pulses, rather than the pulse duration.[155] This has lead to photon-echo experiments

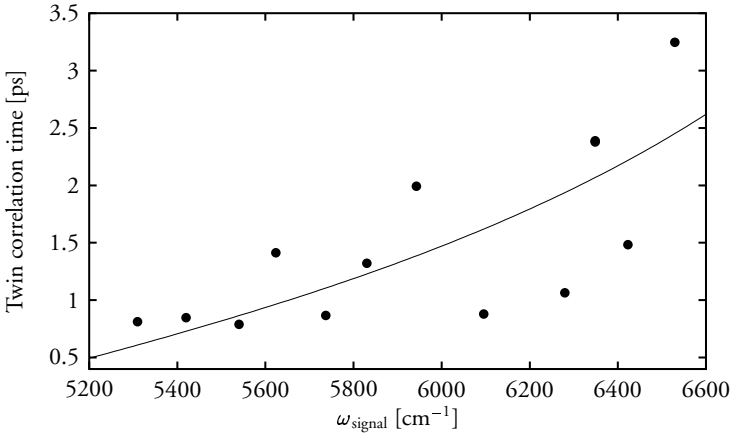

FIGURE 7.6. Correlation time of the signal and idler fields at different frequencies. The solid line is calculated using Equation (2.5).

with (sub)-picosecond time resolution with nanosecond laser pulses[21,156], but also using a synchrotron[124] and even a light bulb[75] as light sources.

7.4 SPATIO-TEMPORAL CORRELATION

7.4.1 EXPERIMENT

The experimental set-up shown in Figure 7.3 was modified in order to measure the spatio-temporal correlation of parametrically generated light. This set-up is shown schematically in Figure 7.7. Again, signal and idler pulses are generated in a $LiNbO_3$ crystal. After pump and idler are filtered out, the signal pulses are split into two equal parts and amplified in two separate amplification stages. In front of the beam splitter that divides the signal pulses in two, a lens is placed in such a way that the front face of the crystal is imaged in the planes of pinholes B1 and B2. Pinhole A is intended for alignment purposes. All pinholes had a diameter of 200 μm. Sum-frequency spectra were recorded at different delay values between the signal of one amplification stage and the idler of the other stage.

7.4.2 RESULTS AND DISCUSSION

When only pinhole A is in place in the set-up described Figure 7.7, a twin-correlation peak is observed in the sum-frequency spectra, similar to the results described in §7.3.2. This is not surprising, as the set-up, without the lens or pinholes B1 and B2 present, is in principle the same as the one in Figure 7.3. When pinhole A is subsequently removed, the twin-correlation peak disappears.

When pinholes B1 and B2 are placed with pinhole A present, the twin-correlation peak is present in the sum-frequency spectra, even when pinhole A is removed. When the position of pinhole B1 is varied in a lateral direction, the intensity of the twin-correlation peak

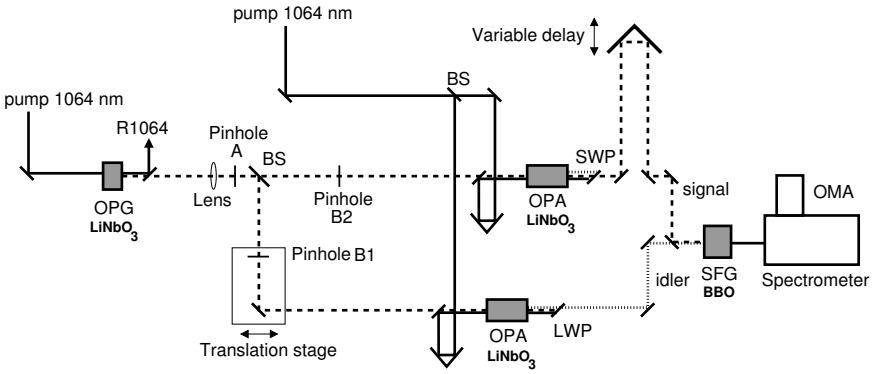

FIGURE 7.7. Experimental set-up for measuring the spatio-temporal correlation of the parametrically generated light. (Legend: OPG: Optical Parametric Generation. OPA: Optical Parametric Amplification. BS: beam splitter. SWP: Short-wave-pass filter and mirror for 1064 nm. LWP: Long-wave-pass filter and mirror for 1064 nm. SFG: Sum-frequency generation. OMA: Optical multichannel analyser. R1064: mirror for 1064 nm.).

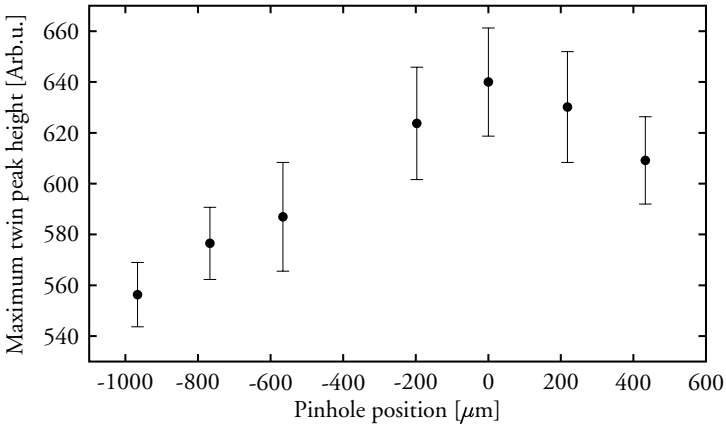

FIGURE 7.8. Intensity of the twin-correlation peak at different positions of pinhole B1 (see Figure 7.7, without the presence of a lens.).

Table 7.1. Presence of twin-correlation peak with different combinations of optical elements present in the set-up shown in Figure 7.7.

Elements in place	Twin-correlation peak present?
none	no
pinhole A	yes
pinholes B1,B2	yes
pinholes A,B1,B2	yes
lens	no
lens and pinholes B1,B2	no
lens and pinhole A	yes

with respect to the background at delay zero changes, as can be seen in Figure 7.8. However, these data do not provide information on the spatial correlation of the parametrically generated light or the zero-photon field in the generating crystal. As there is no imaging without the lens in place, the light going through pinhole B1 (and B2, for that matter) cannot be related to a certain position in the front face of the generating crystal. The measured pattern, is therefore only providing information on the correlation properties or "speckle" across the beam profile of the generated signal beam.

When the lens was placed with pinholes B1 and B2 in place, no correlation peak was observed. With the lens in place, the twin-correlation peak was only observed when pinhole A was in place as well. A summary of the presence or absence of the twin-correlation peak in combination with the different elements can be found in Table 7.1.

In order to get a good spatial resolution for the measurement of the spatio-temporal correlation, one needs to gather parametrically generated light with as many directions as possible. The signal and idler fields that are generated non-collinearly with the pump beam and that propagate in an off-axis direction contribute to the spatial resolution. However, these fields have a non-zero angle between signal and idler and will be phase-matched at different frequencies than the collinearly propagating signal and idler fields. Therefore, the off-axis genarated fields hold different "information" on frequency and phase than the collinearly generated beams. In the sum-frequency generation, only signal and idler with complementary frequencies will contribute to the twin-correlation peak, because then the phase modulations cancel. The fields that were generated with a different frequency will contribute to a broad background in the sum-frequency spectrum.

If only the collinearly generated signal and idler fields were amplified and subsequently used in the sum-frequency generation, only the twin-correlation peak would be observed, without a broad background. The more of the other off-axis fields are "mixed in", the more intense the broad sum-frequency spectrum will become. The necessity of the presence of the pinhole before the beam splitter in in set-ups in both Figure 7.3 and Figure 7.7 can be explained in this way. Without the pinhole to spatially select the parametrically generated light travelling collinearly with the pump, the eventual broad background will become so intense that the twin-correlation peak is completely "drowned". Indeed, the intensity of the mid-infrared pulses increases with the pinhole removed, as does the total intensity of the sum-frequency light.

An additional indication of the phase-sensitivity of the processes giving rise to the occurrence of the twin-correlation peak is provided by some observations concerning the sum-frequency generation. When the signal and idler beams are focused by a lens and/or overlapped in a non-collinear geometry, no twin-correlation peak is observed. Only when the signal and idler beam are combined collinearly without focusing in the BBO crystal, the twin-correlation peak is present around delay zero. It is very likely that in any other geometry than the collinear one, the parts of either beam that give rise to the twin-correlation peak are either smeared out or simply do not overlap in the crystal. This again will lead to a disappearance of the twin-correlation peak, because it is either drowned or absent.

The need for spatial resolution for the observation of the twin-correlation peak is in strong contradiction with the presence of an angular frequency dependence. The twin-correlation peak can therefore not be used as a measure for spatial correlation in these experiments. The solution to circumvent these promblems could be to use very thin crystals in the parametric generation process. However, in this case the intensity of the generated fields will the be very low.

7.5 DIRECTIONAL CORRELATION

The experiment described in this section was devised in order to test whether parametrically generated light with different directions, but with no phase-mismatch can give rise to a twin-correlation peak. If two pump beams are overlapped non-collinearly and are aligned in such a way that they make equal angles with the normal to the crystal face, the two collinearly generated signal fields are expected to have the same frequencies and phase-(mis)match and a twin-correlation peak is expected to be observed. In this way, the type of correlation that is sampled is not the spatial correlation but the directional correlation of the parametrically generated light.

7.5.1 EXPERIMENT

The set-up that was used in order to sample directional correlation of the parametrically generated light is shown in Figure 7.9. Here, two pump beams are overlapped non-collinearly in a $LiNbO_3$ crystal. These pump beams are aligned in such a way that they overlap on the front face of the crystal and that they make equal angles with the normal to the crystal face. The signal beams from the parametrically generated light in the first crystal are subsequently amplified. Again, sum-frequency spectra were recorded at different delay values between the signal of one amplification stage and idler pulses of the other stage.

7.5.2 RESULTS AND DISCUSSION

By overlapping the two pump beams in the front face of the generating crystal in the experimental set-up described in Figure 7.9, the same volume of the crystal can be "probed" by these two pump beams, without the need for imaging optics. This would in theory circumvent the problems encountered in the previously discussed imaging experiments. If the parametrically generated light, generated by the two pump beams were seeded by the same quantum fluctuation, a twin-correlation peak could be expected, and by varying the overlap of the two pump beams, measurement of the spatial correlation would be possible.

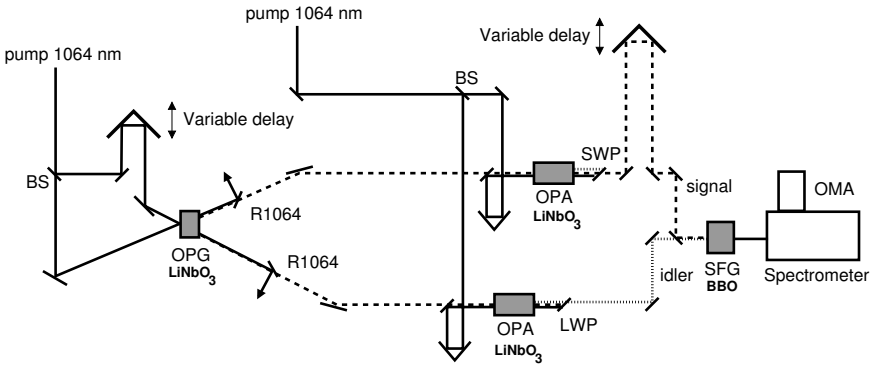

FIGURE 7.9. Experimental set-up for measuring the directional correlation of the parametrically generated light. (Legend: OPG: Optical Parametric Generation. OPA: Optical Parametric Amplification. BS: beam splitter. SWP: Short-wave-pass filter and mirror for 1064 nm. LWP: Long-wave-pass filter and mirror for 1064 nm. SFG: Sum-frequency generation. OMA: Optical multichannel analyser. R1064: mirror for 1064 nm.).

No twin-correlation peak was observed in this configuration, which suggests that there is no directional correlation of the quantum fluctuations in the $LiNbO_3$ crystal.

7.6 CONCLUSIONS

The temporal coherence of parametrically generated mid-infrared light was determined by measuring the twin-correlation peak in the sum-frequency spectrum as a function of delay between the signal and idler. Due to the phase-sensitive nature of the parametric generation and amplification processes, the determined coherence or correlation time τ_c can be directly related to the τ_c of the zero-point electromagnetic field, from which parametric generation starts. The correlation time τ_c of the generated signal and idler fields was found to lie in the picosecond range and was found to follow the frequency-dependence, predicted by the bandwidth from the relation $\tau_c = 1/\Delta\omega$.

The proposed method for the determination of the spatio-temporal correlation by using the twin-correlation peak as a measure of coherence was found to be unsuited. The need for a high spatial resolution and therefore a wide acceptance angle of the parametrically generated light was found to oppose the observation of a twin-correlation peak, as the frequency of the parametrically generated light shows a strong angular dependence.

Bibliography

1. I. Abram, R. K. Raj, J. L. Oudar, and G. Dolique. Direct observation of the second-order coherence of parametrically generated light. *Phys. Rev. Lett.* **57**(20), 2516–2519 (1996).

2. Abu Ali al-Hasan ibn al-Hasan ibn al-Haytham. *Opticae thesaurus: Alhazeni Arabis libri septem, nunc primum editi: eiusdem Liber de crepusculis et nubium ascensionibus: item Vitellonis Thuringopoloni libri X.* (Episcopios, Basel, 1572). Reprinted. Johnson Reprint, New York, 1972.

3. K. Ando and J. T. Hynes. Molecular mechanism of HCl acid ionization in water: Ab initio potential energy surfaces and Monte Carlo simulations. *J. Phys. Chem. B* **101**(49), 10464–10478 (1997).

4. K. Ando, A. Staib, and J.T. Hynes. Acid-base proton transfer in solution. In M. Chergui, editor, *Femtochemistry: Ultrafast chemical and physical processes in molecular systems*, pages 534–539. (World Scientific, Singapore, 1996).

5. L. Andrews, S. R. Davis, and G. L. Johnson. FTIR spectra of methyl-substituted amine-hydrogen fluoride complexes in solid argon and nitrogen. *J. Phys. Chem.* **90**(18), 4273–4282 (1986).

6. L. Andrews, G. L. Johnson, and R. Davis. FTIR spectra of the dimethyl ether-hydrogen fluoride complex and related complexes in solid argon. *J. Phys. Chem.* **89**(9), 1710–1715 (1985).

7. L. Andrews, G. L. Johnson, and R. Davis. Infrared spectrum of the benzene-hydrogen fluoride complex in solid argon. *J. Phys. Chem.* **89**(9), 1706–1709 (1985).

8. S. A. Angel, P. A. Hansen, E. J. Heilweil, and J. C. Stephenson. Application of ultrafast broadband infrared spectroscopy to measurement of metal-carbonyl dynamics. In C. B. Harris, E. P. Ippen, G. A. Mourou, and A. H. Zewail, editors, *Ultrafast Phenomena*, volume 7, pages 480–482. (Springer, Berlin, 1990).

9. J. A. Armstrong, N. Bloembergen, J. Ducuing, and P. S. Pershan. Interactions between light waves in a nonlinear dielectric. *Phys. Rev.* **127**(6), 1918–1939 (1962).

10. S. M. Arrivo and E. J. Heilweil. Conservation of vibrational excitation during hydrogen-bonding reactions. *J. Phys. Chem.* **100**(29), 11975–11983 (1996).

11. P. W. Atkins. *Molecular Quantum Mechanics*, 2nd edition. (Oxford University Press, Oxford, 1983).

12. P. W. Atkins. *Physical Chemistry*, 4th edition. (Oxford University Press, Oxford, 1990).

13. M. M. Audibert and E. Palange. Vibrational predissociation of the hydrogen-bonded $(CH_3)_2O\cdots HF$ complex. *Chem. Phys. Lett.* **101**(4–5), 407–411 (1983).

14. H.-A. Bachor. *A guide to experiments in quantum optics*. (Wiley-VCH, Weinheim, 1998).

15. H. J. Bakker. Effect of intermolecular interactions on vibrational-energy transfer in the liquid phase. *J. Chem. Phys.* **98**(11), 8496–8506 (1993).

16. H. J. Bakker, P. C. M. Planken, L. Kuipers, and A. Lagendijk. Phase modulation in second-order nonlinear-optical processes. *Phys. Rev. A* **42**(7), 4085–4101 (1990).

17. H. J. Bakker, P. C. M. Planken, L. Kuipers, and A. Lagendijk. Ultrafast infrared saturation spectroscopy of chloroform, bromoform and iodoform. *J. Chem. Phys.* **94**(5), 1730–1739 (1991).

18. H. J. Bakker, P. C. M. Planken, and A. Lagendijk. Role of solvent on vibrational energy transfer in solution. *Nature* **347**(6295), 745–747 (1990).

19. H. J. Bakker, P. C. M. Planken, and A. Lagendijk. Ultrafast vibrational dynamics of small organic molecules in solution. *J. Chem. Phys.* **94**(9), 6007–6013 (1991).

20. J. Barthel, K. Bachhuber, R. Buchner, and H. Hetzenauer. Dielectric spectra of some common solvents in the microwave region. Water and lower alcohols. *Chem. Phys. Lett.* **165**(4), 369–373 (1990).

21. R. Beach and S. R. Hartmann. Incoherent photon echoes. *Phys. Rev. Lett.* **53**(7), 663–666 (1984).

22. J. D. Beckerle, M. P. Casassa, R. R. Cavanagh, E. J. Heilweil, and J. C. Stephenson. Sub-picosecond time-resolved spectroscopy of the vibrational dynamics of $Rh(CO)_2(acac)$. *Chem. Phys.* **160**(3), 487–497 (1992).

23. J. D. Beckerle, R. R. Cavanagh, M. P. Casassa, E. J. Heilweil, and J.C. Stephenson. Subpicosecond transient infrared spectroscopy of adsorbates. Vibrational dynamics of CO/Pt(111). *J. Chem. Phys.* **95**(7), 5403–5418 (1991).

24. J. S. Bell. On the Einstein Podolsky Rosen paradox. *Physics* **1**(3), 195–200 (1964).

25. J. S. Bell. On the problem of hidden variables in quantum mechanics. *Rev. Mod. Phys.* **38**(3), 447–452 (1966).

26. J. D. Berkerle, M. P. Casassa, R. R. Cavanagh, E. J. Heilweil, and J. C. Stephenson. Time resolved studies of vibrational relaxation dynamics of $CO(v = 1)$ on metal particle surfaces. *J. Chem. Phys.* **90**(8), 4619–4620 (1989).

27. D. Bertolini, M. Cassettari, and G. Salvetti. The dielectric properties of alcohols-water solutions. I. The alcohol rich region. *J. Chem. Phys.* **78**(1), 365–372 (1983).

28. N. Bloembergen. *Nonlinear optics*. (W.A. Benjamin, New York, 1965).

29. N. Bloembergen. From nanosecond to femtosecond science. *Rev. Mod. Phys.* **71**(2), S283–S287 (1999).

30. N. Bloembergen, E. M. Purcell, and R. V. Pound. Relaxation effects in nuclear magnetic resonance absorption. *Phys. Rev.* **73**(7), 679–712 (1948).

31. D. Boenigk and D. Mootz. The system pyridine-hydrogen fluoride at low temperatures: formation and crystal structures of solid complexes with very strong NHF and FHF hydrogen bonding. *J. Am. Chem. Soc.* **110**(7), 2135–2139 (1988).

32. M. Bonn. *Picosecond non-linear infrared spectroscopy in zeolites and solution*. PhD thesis, Technische Universiteit Eindhoven, 1996.

33. M. Bonn, M. J. P. Brugmans, A. W. Kleyn, R. A. van Santen, and H. J. Bakker. Infrared picosecond transient hole-burning studies of the effect of hydrogen bonds on the vibrational line shape. *J. Chem. Phys.* **105**(9), 3431–3442 (1996).

34. M. Bonn, M. J. P. Brugmans, A. W. Kleyn, R. A. van Santen, and H. J. Bakker. Vibrational dephasing mechanisms in hydrogen-bonded systems. *Phys. Rev. Lett.* **76**(14), 2440–2443 (1996).

35. M. Bonn, S. Woutersen, and H. J. Bakker. Coherent vibron polaritons as probes of vibrational lifetimes. *Opt. Commun.* **147**(1–3), 138–142 (1998).

36. D. Borgis and J. T. Hynes. Curve crossing formulation for proton transfer reactions in solution. *J. Phys. Chem.* **100**(4), 1118–1128 (1996).

37. D. Bouwmeester, J.-W. Pan, K. Mattle, M. Eibl, H. Weinfurter, and A. Zeilinger. Experimental quantum teleportation. *Nature* **390**, 575–579 (1997).

38. R. W. Boyd. *Nonlinear optics*. (Academic Press, San Diego, 1992).

39. M. A. F. H. van den Broek and H. J. Bakker. Observation of a bottleneck in the vibrational relaxation of liquid bromoform. *Chem. Phys.* **253**(1), 157–164 (2000).

40. M. A. F. H. van den Broek and H.-K. Nienhuys. Private communication.

41. J.S. Browder, S.S. Ballard, and P. Klocek. Physical properties of crystalline infrared optical materials. In P. Klocek, editor, *Handbook of infrared optical materials*, volume 30 of *Optical Engineering*, pages 193–425. (Marcel Dekker, New York, 1991).

42. M. J. P. Brugmans, H. J. Bakker, and A. Lagendijk. Direct vibrational energy transfer in zeolites. *J. Chem. Phys.* **104**(1), 64–84 (1996).

43. S. Bruns and G. Haufe. Enantioselective introduction of fluoride into organic compounds. First asymmetric ring opening of epoxides by hydrofluorinating agents. *J. Fluorine Chem.* **104**(2), 247–254 (2000).

44. U. Buck, X. J. Gu, Ch. Lauenstein, and A. Rudolph. Infrared photodissociation of size-selected methanol clusters. *J. Chem. Phys.* **92**(10), 6017–6029 (1990).

45. R. L. Byer and R. L. Herbst. Parametric oscillation and mixing. In Y. R. Shen, editor, *Nonlinear infrared generation*, volume 16 of *Topics in Applied Physics*, pages 81–137. (Springer-Verlag, Berlin, 1977).

46. J. Carre and P. Barberi. Mesure des densités des solutions binaires HF-Pyridine. Exploitation des résultats obtenus. *J. Fluorine Chem.* **50**(1), 1–8 (1990).

47. H. B. G. Casimir. On the attraction between two perfectly conducting plates. *Proc. Kon. Ned. Akad. Wet.* **51**, 793–795 (1948).

48. H. B. G. Casimir and D. Polder. The influence of retardation on the London-van der Waals forces. *Phys. Rev.* **73**(4), 360–372 (1948).

49. E. W. Castner, Jr., M. Maroncelli, and G. R. Fleming. Subpicosecond resolution studies of solvation dynamics in polar aprotic and alcohol solvents. *J. Chem. Phys.* **86**(3), 1090–1097 (1987).

50. R. R. Cavanagh, J. D. Beckerle, M. P. Casassa, E. J. Heilweil, and J. C. Stephenson. Subpicosecond probing of vibrational energy transfer at surfaces. *Surf. Sci.* **269/270**, 113–119 (1992).

51. R. R. Cavanagh, E. J. Heilweil, and J. C. Stephenson. Time-resolved probes of surface dynamics. *Surf. Sci.* **283**(1–3), 226–232 (1993).

52. H.-L. Chen and C. B. Moore. Vibration $\rightarrow$ rotation energy transfer in hydrogen chloride. *J. Chem. Phys.* **54**(9), 4072–4080 (1971).

53. H.-L. Chen and C. B. Moore. Vibration $\rightarrow$ vibration energy transfer in hydrogen chloride mixtures. *J. Chem. Phys.* **54**(9), 4080–4084 (1971).

54. J. Chesnoy and D. Ricard. Experimental study of vibrational relaxation in liquid hydrogen chloride. *Chem. Phys. Lett.* **73**(3), 433–437 (1980).

55. J. Chesnoy and D. Ricard. Vibrational energy relaxation of high density HCl fluid in the 150–345 K range. *Chem. Phys.* **67**(3), 347–353 (1982).

56. J. Chesnoy and D. Ricard. Vibrational energy relaxation of liquid deuterium chloride. *Chem. Phys. Lett.* **91**(2), 130–134 (1982).

57. C. Chudoba, E. T. J. Nibbering, and T. Elsaesser. Site-specific excited-state solute-solvent interactions probed by femtosecond vibrational spectroscopy. *Phys. Rev. Lett.* **81**(14), 3010–3013 (1998).

58. C. Chudoba, E. T. J. Nibbering, and T. Elsaesser. Ultrafast structural response of hydrogen bonded complexes to electronic excitation in the liquid phase. *J. Phys. Chem. A* **103**(29), 5625–5628 (1999).

59. W. B. Colson, C. Pellegrini, and A. Renieri, editors. *Laser Handbook*, volume 6. (North-Holland, Amsterdam, 1990).

60. J. C. Deàk, S. T. Rhea, L. K. Iwaki, and D. D. Dlott. Vibrational energy relaxation and spectral diffusion in water and deuterated water. *J. Phys. Chem. A* **104**(21), 4866–4875 (2000).

61. M. Deraman, J. C. Dore, J. G. Powles, J. H. Holloway, and P. Chieux. Structural studies of liquid hydrogen fluoride by neutron diffraction. I. Liquid DF at 293 K. *Mol. Phys.* **55**(6), 1351–1367 (1985).

62. B. Desbat and P. V. Huong. Structure of liquid hydrogen fluoride studied by infrared and Raman spectroscopy. *J. Chem. Phys.* **78**(11), 6377–6383 (1983).

63. H.-R. Dübal and M. Quack. Tridiagonal Fermi resonance structure in the IR spectrum of the excited chromophore in CF_3H. *J. Chem. Phys.* **81**(9), 3779–3791 (1984).

64. M. H. Dunn and M. Ebrahimzadeh. Parametric generation of tunable light from continuous-wave to femtosecond pulses. *Science* **286**, 1513–1517 (1999).

65. S. Eddarir, H. Mestdagh, and C. Rolando. Synthesis of fluorinated enynes and dienes via 1-bromo-2-fluoro alkenes. *Tetrahedron Lett.* **32**(1), 69–72 (1991).

66. A. Einstein. Über einen die Erzeugung und Verwandlung des Lichtes betreffenden heuristischen Gesichtspunkt. *Ann. Phys.* **17**, 132–148 (1905).

67. A. Einstein. Zur Theorie der Lichterzeugung und Lichtabsorption. *Ann. Phys.* **20**, 199–208 (1906).

68. A. Einstein. Méthode pour la détermination de valeurs statistiques d'observations concernant des grandeurs soumises à des fluctuations irrégulières. *Archives des sciences physiques et naturelles* **37**, 254–256 (1914).

69. A. Einstein. Zur Quantentheorie der Strahlung. *Physikalische Zeitschrift* **18**, 121–128 (1917).

70. A. Einstein, B. Podolsky, and N. Rosen. Can quantum-mechanical description of physical reality be considered complete? *Phys. Rev.* **47**(10), 777–780 (1935).

71. M. D. Fayer, editor. *Ultrafast infrared and Raman spectroscopy*, volume 26 of *Practical spectroscopy*. (Marcel Dekker, New York, 2001).

72. A. Fendt, S. F. Fischer, and W. Kaiser. Vibrational lifetime and Fermi resonance in polyatomic molecules. *Chem. Phys.* **57**(1–2), 55–64 (1981).

73. A. Fendt, W. Kranitzky, A. Laubereau, and W. Kaiser. Efficient generation of tunable subpicosecond pulses in the infrared. *Opt. Commun.* **28**(1), 142–146 (1979).

74. P. A. Franken, A. E. Hill, C. W. Peters, and G. Weinreich. Generation of optical harmonics. *Phys. Rev. Lett.* **7**(4), 118–119 (1961).

75. T. Fuji, H. Fukuda, T. Hattori, and H. Nakatsuka. Femtosecond accumulated photon echoes excited by an incandescent lamp. *Opt. Commun.* **130**(1–3), 104–108 (1996).

76. A. Furusawa, J. L. Sørensen, S. L. Braunstein, C. A. Fuchs, H. J. Kimble, and E. S. Polzik. Unconditional quantum teleportation. *Science* **282**, 706–709 (1998).

77. G. M. Gale, G. Gallot, F. Hache, N. Lascoux, S. Bratos, and J-Cl. Leicknam. Femtosecond dynamics of hydrogen bonds in liquid water: A real time study. *Phys. Rev. Lett.* **82**(5), 1068–1071 (1999).

78. N. E. Gaponova, M. P. Lisitsa, and Yu. P. Tsyashchenko. Frequencies and intensities in the infrared spectrum of bromoform. *Opt. Spectrosc.* **8**, 245–249 (1960).

79. A. García-Allyón, J. Santamaría, and G.S. Ezra. Sensitivity of intramolecular vibrational energy relaxation to stretch-bend potential energy coupling and stability of periodic orbits. *J. Chem. Phys.* **89**(2), 801–811 (1988).

80. A. García-Ayllón and J. Santamaría. Stretch-bend coupling effect on the intramolecular vibrational relaxation in a two-mode model of CH overtone exited fluoroform. *Chem. Phys.* **141**(2–3), 197–209 (1990).

81. I. Gennick, K. M. Harmon, and M. M. Potvin. Hydrogen bonding. 8. Preparation, properties, and low-temperature infrared structural analysis of ammonium and alkylammonium trihydrogen tetrafluorides and tetramethylammonium dihydrogen trifluoride. *Inorg. Chem.* **16**(8), 2033–2040 (1977).

82. I. A. M. E. Giebels, M. A. F. H. van den Broek, M. F. Kropman, and H. J. Bakker. Vibrational dynamics of hydrogen-bonded HCl-diethyl ether complexes. *J. Chem. Phys.* **112**(11), 5127–5132 (2000).

83. J. A. Giordmaine and R. C. Miller. Tunable coherent parametric oscillation in $LiNbO_3$ at optical frequencies. *Phys. Rev. Lett.* **14**(24), 973–976 (1965).

84. J. P. Gordon, H. J. Zeiger, and C. H. Townes. Molecular microwave oscillator and new hyperfine structure in the microwave spectrum of NH_3. *Phys. Rev.* **95**(1), 282–284 (1954).

85. H. Graener. The equilibration of vibrational excess energy. *Chem. Phys. Lett.* **165**(1), 110–114 (1990).

86. H. Graener, R. Dohlus, and A. Laubereau. Infrared double-resonance spectroscopy of bromoform with picosecond pulses. *Chem. Phys. Lett.* **140**(3), 306–310 (1987).

87. H. Graener and A. Laubereau. Ultrafast overtone excitation for the study of vibrational population decay in liquids. *Chem. Phys. Lett.* **102**(1), 100–104 (1983).

88. H. Graener, T. Patzlaff, N. Kadarisman, and G. Seifert. Observation of intensity dependent, non-exponential vibrational relaxation in liquid bromoform. *Chem. Phys. Lett.* **348**(5–6), 403–410 (2001).

89. H. Graener and G. Seifert. Vibrational and orientational relaxation of monomeric water molecules in liquids. *J. Chem. Phys.* **98**(1), 36–45 (1993).

90. H. Graener, G. Seifert, and A. Laubereau. Direct observation of rotational relaxation times by time-resolved infrared spectroscopy. *Chem. Phys. Lett.* **172**(6), 435–439 (1990).

91. H. Graener, G. Seifert, and A. Laubereau. Vibrational and reorientational dynamics of water molecules in liquid matrices. *Chem. Phys.* **175**(1), 193–204 (1993).

92. H. Graener, T. Q. Ye, and A. Laubereau. Ultrafast dynamics of hydrogen bonds directly observed by time-resolved infrared spectroscopy. *J. Chem. Phys.* **90**(7), 3413–3416 (1989).

93. H. Graener, R. Zürl, and M. Hoffman. Vibrational relaxation of liquid chloroform. *J. Phys. Chem. B* **101**(10), 1745–1749 (1997).

94. W. H. Green, Jr., W. D. Lawrance, and C. B. Moore. Kinetic anharmonic coupling in the trihalomethanes: A mechanism for rapid intramolecular redistribution of CH stretch vibrational energy. *J. Chem. Phys.* **86**(11), 6000–6011 (1987).

95. W. T. Grubbs, T. P. Dougherty, and E. J. Heilweil. Bimolecular interactions in $(Et)_3SiOH$:Base:CCl_4 hydrogen-bonded solutions studied by deactivation of the 'free' OH-stretch vibration. *J. Am. Chem. Soc.* **117**(48), 11989–11992 (1995).

96. W. T. Grubbs, T. P. Dougherty, and E. J. Heilweil. Vibrational energy dynamics of hydrogen-bonded pyrrole complexes. *J. Phys. Chem.* **99**(27), 10716–10722 (1995).

97. H. Haken and H. C. Wolf. *Molecular physics and elements of quantum chemistry*. (Springer-Verlag, Berlin, 1995).

98. P. Halasyamani, M. J. Willis, C. L. Stern, and K. R. Poeppelmeier. Crystal growth in aqueous hydrofluoric acid and $(HF)_x$·pyridine solutions: syntheses and crystal structures of $[Ni(H_2O)_6]^{2+}[MF_6]^{2-}$ (M = Ti, Zr, Hf) and $Ni_3(py)_{12}F_6{\cdot}7H_2O$. *Inorg. Chim. Acta* **240**(1–2), 109–115 (1995).

99. P. Hamm and R. M. Hochstrasser. Structure and dynamics of proteins and peptides: femtosecond two-dimensional infrared spectroscopy. In M. D. Fayer, editor, *Ultrafast infrared and Raman spectroscopy*, volume 26 of *Practical spectroscopy*, pages 273–347. (Marcel Dekker, New York, 2001).

100. P. Hamm, M. Lim, W. F. DeGrado, and R. M. Hochstrasser. Stimulated photon echoes from amide I vibrations. *J. Phys. Chem. A* **103**(49), 10049–10053 (1999).

101. P. Hamm, M. Lim, and R. M. Hochstrasser. Non-Markovian dynamics of the vibrations of ions in water from femtosecond infrared three-pulse photon echoes. *Phys. Rev. Lett.* **81**(24), 5326–5329 (1998).

102. P. Hamm, M. Lim, and R. M. Hochstrasser. Structure of the amide I band of peptides measured by femtosecond nonlinear-infrared spectroscopy. *J. Phys. Chem. B* **102**(31), 6123–6138 (1998).

103. T. W. Hänsch and H. Walther. Laser spectroscopy and quantum optics. *Rev. Mod. Phys.* **71**(2), S242–S252 (1999).

104. K. M. Harmon and R. R. Lovelace. Hydrogen bonding. 13. Infrared study of the HF_2^- anion in *p*-toluidinium and tetraalkylammonium hydrogen difluorides. *J. Phys. Chem.* **86**(6), 900–903 (1982).

105. K. M. Harmon and A. C. Webb. Hydrogen bonding. Part 73. IR, NMR, and ab initio molecular orbital study of *N,N*-dimethyl-1-adamantamine-hydrogen fluoride, a crystalline, H_2O stable compound with a three-center N–H–F bond. *J. Mol. Struct.* **522**(1–3), 79–86 (2000).

106. A. L. Harris, N. J. Levinos, L. Rothberg, L. H. Dubois, L. Dhar, S. F. Shane, and M. Morin. Vibrational energy transfer to metal surfaces probed by sum generation: CO/Cu(100) and CH_3S/Ag(111). *J. Electron Sprectrosc. Relat. Phenom.* **54/55**, 5–16 (1990).

107. A. L. Harris, L. Rothberg, L. H. Dubois, N. J. Levinos, and L. Dhar. Molecular vibrational energy relaxation at a metal surface: methyl thiolate on Ag(111). *Phys. Rev. Lett.* **64**(17), 2086–2089 (1990).

108. D. C. Harris and M. D. Bertolucci. *Symmetry and spectroscopy: an introduction to vibrational and electronic spectroscopy*. (Dover Publications, New York, 1989).

109. A. E. A. Hassan, A. T. Shortnacy-Fowler, J. A. Montgomery, and J. A. Secrist III. A convenient synthesis of 2'-deoxy-2-fluoroadenosine; a potential prodrug for suicide gene therapy. *Nucleos. Nucleot.* **19**(3), 559–565 (2000).

110. E. J. Heilweil, R. R. Cavanagh, and J. C. Stephenson. Population relaxation of CO($v = 1$) vibrations in solution phase metal carbonyl complexes. *Chem. Phys. Lett.* **134**(2), 181–188 (1987).

111. E. J. Heilweil, R. R. Cavanagh, and J. C. Stephenson. CO($v = 1$) population lifetimes of metal-carbonyl compounds in dilute $CHCl_3$ solution. *J. Chem. Phys.* **89**(1), 230–239 (1988).

112. E. J Heilweil, R. R. Cavanagh, and J. C. Stephenson. Picosecond study of the population lifetime of CO($v = 1$) chemisorbed on SiO_2-supported rhodium particles. *J. Chem. Phys.* **89**(8), 5342–5343 (1988).

113. E. J. Heilweil, J. C. Stephenson, and R. R. Cavanagh. Measurements of CO($v = 1$) population lifetimes: Metal-carbonyl cluster compounds supported on SiO_2. *J. Phys. Chem.* **92**(21), 6099–6103 (1988).

114. W. Heisenberg. Über den anschaulichen Inhalt der quantentheoretischen Kinematik und Mechanik. *Z. Phys.* **43**, 172–198 (1927).

115. G. Herzberg. *Infrared and Raman spectra of polyatomic molecules*, volume 2 of *Molecular spectra and molecular structure*. (D. Van Nostrand Company, Princeton, 1945).

116. K. F. Herzfeld and Th. A. Litovitz. *Absorption and dispersion of ultrasonic waves*. (Academic Press, New York, 1959).

117. J. R. Hill, D. D. Dlott, M. D. Fayer, K. A. Peterson, C. W. Rella, M. M. Rosenblatt, K. S. Suslick, and C. J. Ziegler. Vibrational relaxation of carbon monoxide in model heme compounds. 6-coordinate metalloporphyrins (M = Fe, Ru, Os). *Chem. Phys. Lett.* **244**(3–4), 218-223 (1995).

118. J. R. Hill, A. Tokmakoff, K. A. Peterson, B. Sauter, D. Zimdars, D. D. Dlott, and M. D. Fayer. Vibrational dynamics of carbon monoxide at the active site of myoglobin: picosecond infrared free-electron laser pump-probe experiments. *J. Phys. Chem.* **98**(43), 11213–11219 (1994).

119. J. R. Hill, C. J. Ziegler, K. S. Suslick, D. D. Dlott, C. W. Rella, and M. D. Fayer. Tuning the vibrational relaxation of CO bound to heme and metalloporphyrin complexes. *J. Phys. Chem.* **100**(46), 18023–18032 (1996).

120. C. K. Hong and L. Mandel. Theory of parametric frequency down conversion of light. *Phys. Rev. A* **31**(4), 2409–2418 (1985).

121. C. K. Hong, Z. Y. Ou, and L. Mandel. Measurement of subpicosecond time intervals between two photons by interference. *Phys. Rev. Lett.* **59**(18), 2044–2046 (1987).

122. H.-J. Hübner, M. Wörner, W. Kaiser, and A. Seilmeier. Subpicosecond vibrational relaxation of skeletal modes in polyatomic molecules. *Chem. Phys. Lett.* **182**(3–4), 315–320 (1991).

123. Chr. Huygens. *Traité de la lumière, où sont expliquées les causes ce qui luy arrive dans la reflexion, et dans la refraction: et particulièrement dans l'étrange refraction du cristal d'Islande: avec un discours de la cause de la pesanteur*. (Van der Aa, Leiden, 1690). Reprinted, accompanied by a translation in Dutch. Epsilon Uitgaven, Utrecht, 1990.

124. H. Itoh, S. Nakanishi, M. Kawase, H. Fukuda, H. Nakatsuka, and M. Kamada. Accumulated photon echoes generated by synchrotron radiation. *Phys. Rev. A* **50**(4), 3312–3315 (1994).

125. G. A. Jeffrey and W. Saenger. *Hydrogen bonding in biological structures*. (Springer-Verlag, Berlin, 1991).

126. A. von Jena and H. E. Lessing. Coherent coupling effects in picosecond absorption experiments. *Appl. Phys.* **19**(2), 131-144 (1979).

127. E. Kauppi and L. Halonen. Fermi resonances between CH stretching and bending vibrations in CHF_3, $CHCl_3$ and $(CF_3)_3CH$. *J. Chem. Phys.* **90**(12), 6980–6992 (1989).

128. V. M. Kenkre, A. Tokmakoff, and M. D. Fayer. Theory of vibrational relaxation of polyatomic molecules in liquids. *J. Chem. Phys.* **101**(12), 10618–10629 (1994).

129. J. T. Knudtson and J. C. Stephenson. Vibrational relaxation of HCl in dilute CCl_4 and CCl_3F solutions. *Chem. Phys. Lett.* **107**(4–5), 385–388 (1984).

130. J. T. Knudtson and E. Weitz. Vibrational relaxation of HCl/liquid Xenon mixtures. *Chem. Phys. Lett.* **104**(1), 71–78 (1984).

131. M. F. Kropman and H. J. Bakker. Dynamics of water molecules in aqueous solvation shells. *Science* **291**, 2118–2120 (2001).

132. M. F. Kropman, H.-K. Nienhuys, S. Woutersen, and H. J. Bakker. Vibrational relaxation and hydrogen-bond dynamics of HDO:H_2O. *J. Phys. Chem. A* **105**(19), 4622–4626 (2001).

133. T. Kushida, H. M. Marcos, and J. E. Geusic. Laser transition cross section and fluorescence branching ratio for Nd^{3+} in yttrium aluminum garnet. *Phys. Rev.* **167**(2), 289–291 (1968).

134. A. Kuzmich, I. A. Walmsley, and L. Mandel. Violation of Bell's inequality by a generalized Einstein-Podolsky-Rosen state using homodyne detection. *Phys. Rev. Lett.* **85**(7), 1349–1353 (2000).

135. R. Laenen and C. Rauscher. Transient hole-burning spectroscopy of associated ethanol molecules in the infrared: Structural dynamics and evidence for energy migration. *J. Chem. Phys.* **106**(22), 8974–8980 (1997).

136. R. Lascola and L. Andrews. FTIR spectra of hydroxylamine-hydrogen fluoride complexes in solid argon. *J. Am. Chem. Soc.* **109**(16), 4765–4768 (1987).

137. A. Laubereau, S.F. Fischer, K. Spannner, and W. Kaiser. Vibrational population lifetimes of polyatomic molecules in liquids. *Chem. Phys.* **31**(3), 335–344 (1978).

138. A. Laubereau, L. Greiter, and W. Kaiser. Intense tunable picosecond pulses in the infrared. *Appl. Phys. Lett.* **25**(1), 87–89 (1974).

139. A. Laubereau and W. Kaiser. Vibrational dynamics of liquids and solids investigated by picosecond light pulses. *Rev. Mod. Phys.* **50**(3), 607–665 (1978).

140. A. Laubereau, D. von der Linde, and W. Kaiser. Direct measurement of the vibrational lifetimes of molecules in liquids. *Phys. Rev. Lett.* **28**(18), 1162–1165 (1972).

141. R. M. Lees and L.-H. Xu. On the assignment of optically pumped far-infrared laser emission from CH_3OH. *J. Mol. Spectrosc.* **196**(2), 220–234 (1999).

142. R. M. Lees and L.-H. Xu. Dark state illuminated: Infrared spectrum and inverted torsional structure of the ν_{11} out-of-plane CH_3-rocking mode of methanol. *Phys. Rev. Lett.* **84**(17), 3815–3818 (2000).

143. S. R. Leone and C. B. Moore. V $\rightarrow$ V energy transfer in HCl with tunable optical parametric oscillator excitation. *Chem. Phys. Lett.* **19**(3), 340–344 (1973).

144. H. E. Lessing and A. von Jena. Separation of rotational diffusion and level kinetics in transient absorption spectroscopy. *Chem. Phys. Lett.* **42**(2), 213–217 (1976).

145. N. E. Levinger, P. H. Davis, and M. D. Fayer. Vibrational relaxation of the free terminal hydroxyl stretch in methanol oligomers: Indirect pathway to hydrogen bond breaking. *J. Chem. Phys.* **115**(20), 9352–9360 (2001).

146. U. Liddel and E. D. Becker. Infra-red spectroscopic studies of hydrogen bonding in methanol, ethanol, and t-butanol. *Spectrochim. Acta* **10**, 70–84 (1957).

147. M. Lim, P. Hamm, and R. M. Hochstrasser. Protein fluctuations are sensed by stimulated infrared echoes of the vibrations of carbon monoxide and azide probes. *Proc. Natl. Acad. Sci.* **95**(26), 15315–15320 (1998).

148. M. Lim and R. M. Hochstrasser. Unusual vibrational dynamics of the acetic acid dimer. *J. Chem. Phys.* **115**(16), 7629–7643 (2001).

149. R. Loudon. *The quantum theory of light*, 2nd edition. (Oxford University Press, Oxford, 1983).

150. R. R. Lovelace and K. M. Harmon. Hydrogen bonding. Part 27. Amine/hydrogen fluoride molecular complexes. *J. Mol. Struct.* **193**, 247–262 (1989).

151. D. Magde and H. Mahr. Study in ammonium dihydrogen phosphate of spontaneous parametric interaction tunable from 4400 to 16000 Å. *Phys. Rev. Lett.* **18**(21), 905–907 (1967).

152. T. H. Maiman. Stimulated optical radiation in ruby. *Nature* **187**, 493–494 (1960).

153. L. Mandel and E. Wolf. *Optical coherence and quantum optics*. (Cambridge University Press, Cambridge, 1995).

154. P. Moore, A. Tokmakoff, T. Keyes, and M. D. Fayer. The low frequency density of states and vibrational population dynamics of polyatomic molecules in liquids. *J. Chem. Phys.* **103**(9), 3325–3334 (1995).

155. N. Morita and T. Yajima. Ultrahigh-time-resolution coherent transient spectroscopy with incoherent light. *Phys. Rev. A* **30**(5), 2525–2536 (1984).

156. F. Moshary, M. Arend, R. Friedberg, and S. R. Hartmann. Ultrafast relaxation and modulation in the oxazine dye nile blue. *Phys. Rev. A* **46**(1), R33-R36 (1992).

157. V. M. Mostepanenko and N. N. Trunov. *The Casimir effect and its applications*. (Clarendon Press, Oxford, 1997).

158. S. Mukamel. *Principles of nonlinear optical spectroscopy*. (Oxford University Press, Oxford, 1995).

159. I. Newton. *Opticks: or, a tretise of the reflections, refractions, inflections and colours of light*, 4th edition. (William Innys, London, 1730). Reprinted. Dover Publications, New York, 1952.

160. K. C. Nicolaou and H. J. Mitchell. Adventures in carbohydrate chemistry: New synthetic technologies, chemical synthesis, molecular design, and chemical biology. *Angew. Chem. Int. Ed.* **40**(9), 1576–1624 (2001).

161. H.-K. Nienhuys. *Femtosecond mid-infrared spectroscopy of water*. PhD thesis, Technische Universiteit Eindhoven, 2002.

162. H.-K. Nienhuys, R. A. van Santen, and H. J. Bakker. Orientational relaxation of liquid water molecules as an activated process. *J. Chem. Phys.* **112**(19), 8487–8494 (2000).

163. H.-K. Nienhuys, S. Woutersen, R. A. van Santen, and H. J. Bakker. Mechanism for vibrational relaxation in water investigated by femtosecond infrared spectroscopy. *J. Chem. Phys.* **111**(4), 1494–1500 (1999).

164. A. Nitzan, S. Mukamel, and J. Jortner. Energy gap law for vibrational relaxation of a molecule in a dense medium. *J. Chem. Phys.* **63**(1), 200–207 (1975).

165. D. Oepts, A. F. G. van der Meer, and P. W. van Amersfoort. The free-electron-laser user facility FELIX. *Infrared Phys. Technol.* **36**(1), 297–308 (1995).

166. G. A. Olah. Synthetic methods and reactions II. Hydrofluorination of alkenes, cyclopropane and alkynes with poly-hydrogen fluoride/pyridine (trialkylamine) reagents. *Synthesis* , 779–780 (1973).

167. G. A. Olah, J. T. Welch, Y. D. Vankar, M. Nojima, I. Kerekes, and J. A. Olah. Synthetic methods and reactions. 63. Pyridinium poly(hydrogen fluoride) (30% pyridine-70% hydrogen fluoride): A convenient reagent for organic fluorination reactions. *J. Org. Chem.* **44**(22), 3872–3881 (1979).

168. Z. Y. Ou and L. Mandel. Violation of Bell's inequality and classical probability in a two-photon correlation experiment. *Phys. Rev. Lett.* **61**(1), 50–53 (1988).

169. Z. Y. Ou, S. F. Pereira, H. J. Kimble, and K. C. Peng. Realization of the Einstein-Podolsky-Rosen paradox for continuous variables. *Phys. Rev. Lett.* **68**(25), 3663–3666 (1992).

170. J. C. Owrutsky, M. Li, B. Locke, and R. M. Hochstrasser. Vibrational relaxation of the CO stretch vibration in hemoglobin-CO, myoglobin-CO and protoheme-CO. *J. Phys. Chem.* **99**(13), 4842–4846 (1995).

171. A. A. Pankov, V. Yu. Borovkov, and V. B. Kazanskii. Study of complexes of hydrogen halides with diethyl ether in aprotic solvents by the method of IR spectroscopy. *J. Appl. Spectrosc.* **37**(2), 953–957 (1982).

172. P. M. Paul, E. S. Toma, P. Breger, G. Mullot, F. Augé, Ph. Balcou, H. G. Muller, and P. Agostini. Observation of a train of attosecond pulses from high harmonic generation. *Science* **292**, 1689–1692 (2001).

173. K. A. Peterson, C. W. Rella, J. R. Engholm, and H. A. Schwettman. Ultrafast vibrational dynamics of the myoglobin amide I band. *J. Phys. Chem. B* **103**(3), 557–561 (1999).

174. W. H. Press, S. A. Teukolsky, W. T. Vetterling, and B. P. Flannery. *Numerical recipes in C: the art of scientific computing*, 2nd edition. (Cambridge University Press, Cambridge, 1992).

175. C. W. Rella, A. Kwok, K. Rector, J. R. Hill, H. A. Schwettman, D. D. Dlott, and M. D. Fayer. Vibrational echo studies of protein dynamics. *Phys. Rev. Lett.* 77(8), 1648–1651 (1996).

176. J. W. Ring and P. A. Egelstaff. Hydrogen motions in liquid hydrogen fluoride. *J. Chem. Phys.* **51**(2), 762–770 (1969).

177. G. Rodriguez and P. Brant. Synthesis, structure and application of $[PhNMe_2H][B\{C_6F_4C(C_6F_5)_2F\}_4]$. *Organometallics* **20**(11), 2417–2420 (2001).

178. B. Rosen. *Données spectroscopiques relatives aux molécules diatomiques*, volume 17 of *Tables internationales de constantes sélectionnées*. (Pergamon Press, Oxford, 1970).

179. A. J. Ross, H. A. Hollenstein, R. R. Marquardt, and M. Quack. Fermi resonance in the overtone spectra of the CH chromophore in bromoform. *Chem. Phys. Lett.* **156**(5), 455–462 (1989).

180. F. Rotermund, V. Petrov, and F. Noack. Difference-frequency generation of intense femtosecond pulses in the mid-IR (4–12 μm) using $HgGa_2S_4$ and $AgGaS_2$. *Opt. Commun.* **185**(1–3), 177–183 (2000).

181. H. Rudolph, J. Avery, and J. O. Henningsen. Torsion-vibration interaction in CH_3OH. *J. Mol. Spectrosc.* **117**(1), 38–45 (1986).

182. A. Savitzky and M.J.E. Golay. Smoothing and differentiation of data by simplified least squares procedures. *Anal. Chem.* **36**(8), 1627–1639 (1964).

183. J. A. Saxton, R. A. Bond, G. T. Coats, and R. M. Dickinson. Dispersion at millimeter wavelenghts in methyl and ethyl alcohols. *J. Chem. Phys.* **37**(9), 2132–2138 (1962).

184. A. L. Schawlow and C. H. Townes. Infrared and optical masers. *Phys. Rev.* **112**(6), 1940–1949 (1958).

185. M. Schubert and B. Wilhelmi. *Nonlinear optics and quantum electronics*. (John Wiley & Sons, New York, 1986).

186. P. Schuster, G. Zundel, and C. Sandorfy, editors. *The Hydrogen Bond*. (Elsevier, Amsterdam, 1976).

187. M. O. Scully and M. S. Zubairy. *Quantum optics*. (Cambridge University Press, Cambridge, 1997).

188. A. Seilmeier, K. Spanner, A. Laubereau, and W. Kaiser. Narrow-band tunable infrared pulses with sub-picosecond time resolution. *Opt. Commun.* **24**(3), 237–242 (1978).

189. D. N. Shchepkin. The energy of the hydrogen bond in complexes of HBr, HCl and HF with organic bases. *Theor. Exp. Chem.* **2**(2), 276–279 (1966).

190. Y. R. Shen. *The principles of nonlinear optics*. (John Wiley & Sons, New York, 1984).

191. T. Shimanouchi. *Tables of Molecular Frequencies Consolidated Volume I*. (NSRDS, Washington, D.C., 1972).

192. D. S. Smith, H. D. Riccus, and R. P. Edwin. Refractive indices of lithium niobate. *Opt. Commun.* **17**(3), 332–335 (1976).

193. D. E. Spence, P. N. Kean, and W. Sibbett. 60-fsec pulse generation from a self-mode-locked Ti:sapphire laser. *Opt. Lett.* **16**(1), 42–44 (1991).

194. J. N. Spencer, C. L. Campanella, E. M. Harris, and W. S. Wolbach. Solvent effects on hydrogen-bond formation. 2. *J. Phys. Chem.* **89**(10), 1888–1891 (1985).

195. A. Staib, D. Borgis, and J. T. Hynes. Proton transfer in hydrogen-bonded acid-base complexes in polar solvents. *J. Chem. Phys.* **102**(6), 2487–2505 (1995).

196. R. V. Steele, Jr. and C. B. Moore. V $\rightarrow$ T,R energy transfer in HCl- and DCl-rare gas mixtures. *J. Chem. Phys.* **60**(7), 2794–2799 (1974).

197. J. Stenger, D. Madsen, P. Hamm, E. T. J. Nibbering, and T. Elsaesser. Ultrafast vibrational dephasing of liquid water. *Phys. Rev. Lett.* **87**(2), 027401 (2001).

198. G. Stock and W. Domcke. Detection of ultrafast molecular-excited-state dynamics with time- and frequency-resolved pump-probe spectroscopy. *Phys. Rev. A* **45**(5), 3032–3040 (1992).

199. O. Svelto. *Principles of lasers*, 4th edition. (Plenum Press, New York, 1998).

200. K. Takagi and H. Ozawa. Ultrasonic spectroscopy in liquid bromoform. *Jpn. J. Appl. Phys.* **21**, 83–85 (1982).

201. A. Tokmakoff and M. D. Fayer. Homogeneous vibrational dynamics and inhomogeneous broadening in glass-forming liquids: Infrared photon echo experiments from room temeperature to 10 K. *J. Chem. Phys.* **103**(8), 2810–2826 (1995).

202. A. Tokmakoff, B. Sauter, and M. D. Fayer. Temperature dependent vibrational relaxation in polyatomic liquids: picosecond infrared pump-probe experiments. *J. Chem. Phys.* **100**(12), 9035–9043 (1994).

203. C. H. Townes. The birth of the laser. *Opto & laser Europe* **69**, 20–30 (1999).

204. D.F. Walls and G. J. Milburn. *Quantum optics*. (Springer-Verlag, Berlin, 1994).

205. B. S. Wherrett, A. L. Smirl, and T. F. Boggess. Theory of degenerate four-wave mixing in picosecond excitation-probe experiments. *IEEE J. Quantum Elect.* **19**(4), 680–690 (1983).

206. J. M. Wiesenfeld and C. B. Moore. Vibrational relaxation of matrix-isolated HCl and DCl. *J. Chem. Phys.* **70**(2), 930–946 (1979).

207. S. Woutersen. *Femtosecond vibrational dynamics in hydrogen-bonded systems*. PhD thesis, Universiteit van Amsterdam, 1999.

208. S. Woutersen and H. J. Bakker. Hydrogen bond in liquid water as a Browninan oscillator. *Phys. Rev. Lett.* **83**(10), 2077–2080 (1999).

209. S. Woutersen and H. J. Bakker. Resonant intermolecular transfer of vibrational energy in liquid water. *Nature* **402**(507–509), (1999).

210. S. Woutersen, M. Bonn, M. J. P. Brugmans, U. Emmerichs, and H. J. Bakker. Generation of incoherent mid-infrared photon echoes with parametrically downconverted light. *Opt. Lett.* **21**(19), 1579–1581 (1996).

211. S. Woutersen, U. Emmerichs, and H. J. Bakker. A femtosecond midinfrared pump-probe study of hydrogen-bonding in ethanol. *J. Chem. Phys.* **107**(5), 1483–1490 (1997).

212. A. Yariv. *Optical Electronics*. (Holt-Saunders, New York, 1985).

213. A. Yariv. *Quantum Electronics*, 3rd edition. (John Wiley & Sons, New York, 1989).

214. N. Yoneda. The combination of hydrogen fluoride with organic bases as fluorination agents. *Tetrahedron* **47**(29), 5329–5365 (1991).

215. W. Zinth, C. Kolmeder, B. Benna, A. Irgens-Defregger, S. F. Fischer, and W. Kaiser. Fast and exceptionally slow vibrational energy transfer in acetylene and phenylacetylene in solution. *J. Chem. Phys.* **78**(6), 3916–3921 (1983).

216. P. F. Zittel and C. B. Moore. Vibrational relaxation of HBr and HCl from 144°K to 584°K. *J. Chem. Phys.* **59**(12), 6636–6640 (1973).

Summary

This thesis is devoted to the investigation of the dynamics of excited vibrations of small molecules and complexes in liquid solution and in the pure liquid. When excited vibrational states decay, energy is transferred to other modes, eventually leading to an equilibration over all degrees of freedom. The lifetime T_1 of the excited state, which is usually on the order of picoseconds in the condensed phase, depends on both the nature and the availability of the accepting modes. By looking at the lifetimes and vibrational dynamics of excited vibrations, a lot of information can be gathered on the couplings that exist within and between molecules.

The lifetimes and vibrational dynamics of several excited molecular vibrations are in this thesis investigated with vibrational pump-probe spectroscopy. In a pump-probe experiment, a pump pulse excites a vibration of a significant fraction of the molecules in a sample. This excitation causes a decrease in the absorbance of the sample, as there are less molecules in the vibrational ground state that can absorb radiation at the $v = 0 \rightarrow v = 1$ transition frequency. The transmittance change is measured with a weaker probe pulse that passes through the sample after a variable delay, so that the evolution of the excited vibration can be followed in time. This form of time-resolved spectroscopy requires the light pulses to be shorter than the typical time scale of the decay of the excitation.

The transition frequencies of the molecular vibrations that were studied lie in the mid-infrared, corresponding to wavelengths of 1–10 μm, so short mid-infrared (laser) pulses are needed. There are few lasers that emit in this wavelength region, therefore in most experiments non-linear optical processes like difference-frequency generation (DFG) and optical parametric generation and amplification (OPG/OPA) are used to generate "ultrashort" mid-infrared pulses from the output of lasers that emit in the visible or near-infrared.

Two different hydrogen-bonded acid-base complexes were investigated. A relatively weak hydrogen bond was encountered in complexes of hydrogen chloride (HCl) with diethyl ether [$(CH_3CH_2)_2O$]. The lifetime of the excited H–Cl stretch vibration was determined to be 0.9 ± 0.2 ps. The relaxation is found to occur via an intermediate state with the low-frequency $(CH_3CH_2)_2O \cdots$H–Cl hydrogen bond as the main accepting mode of the vibrational energy. The excited population of this hydrogen-bond mode decays in a second relaxation process with a time constant of 3.1 ± 0.5 ps. In hydrogen-bonded complexes of the acid hydrogen fluoride (HF) with amines, the hydrogen-bonding between the acid HF and the amine base is very strong. We studied the vibrational dynamics of the HF/FHF stretch combination absorption band of complexes of HF with the weak organic base pyridine in diluted pyridine solution. The relaxation of this excited vibration was also observed to occur in two steps. In the first step, energy is transferred from the excited combination vibration to the F–H$\cdots$F hydrogen bond modes with a time constant of 0.51 ± 0.09 ps. In a second step, with a time constant of 2.6 ± 0.3 ps, energy is transferred from the F–F hydrogen bond modes to lower-frequency modes, leading to a local thermalisation of the energy. Although the hydrogen-bond strengths are very different in both acid-base complexes, in

both cases a similar relaxation mechanism is seen, where the hydrogen-bond mode is the main accepting mode in the first step of the relaxation.

The relaxation of an excited molecular vibration can be an *intra*molecular process, in which energy is transferred to other vibrations in the same molecule, through anharmonic couplings with the vibrational mode that was originally excited, or an *inter*molecular process, in which energy is transferred to vibrations of neighbouring (solvent) molecules or to low-frequency (solvent) modes. Two-colour pump-probe experiments on the C–H stretch vibration of pure bromoform ($CHBr_3$) show that, compared to solutions of bromoform, the reduction in the number of accepting modes provided by the solvent for intermolecular energy transfer, greatly influences the mechanism and time scale of vibrational relaxation. The relaxation of the excited C–H stretch vibration in pure $CHBr_3$ occurs with a time constant of 43 ± 1 ps via an intermediate level, which causes a transient redshift of the C–H stretch frequency. We identified the intermediate level with the singly excited C–H bend mode. We observed that relaxation from this intermediate level is exceptionally slow and non-exponential, which suggests the presence of a "bottleneck" in the relaxation, in contrast to pure chloroform ($CHCl_3$) and solutions of bromoform. The population of this bottleneck state is very long-lived, which frustrates thermalisation.

The influence of the number of vibrational modes in a molecule on intramolecular vibrational relaxation, is manifested in the investigation of the vibrational dynamics after excitation of the C–O stretch vibration of the alcohols methanol and ethanol in carbon tetrachloride (CCl_4) solution. The relaxation of the excited C–O stretch vibration was observed to occur in two steps. In the first step energy is transferred from the $v = 1$ state of the C–O stretch vibration to an intermediate state with a time constant of 3.2 ± 0.2 ps for methanol and 3.2 ± 0.7 ps for ethanol. The intermediate state is most likely formed by the $n = 3$ or 4 state of the C–O–H bending mode, which is also known as the torsional mode. In the second step energy is transferred from this intermediate state to low-energy modes, leading to a full equilibration of the energy. In methanol this thermalisation occurs with a time constant of 28 ± 1 ps. In ethanol the second step is faster, with a time constant of 12 ± 2 ps, because of the higher number of available accepting modes.

In the last chapter of this thesis, we focus on the non-linear optical process that is conveniently used to generate the mid-infrared pulses for the experiments featured in the other chapters. The focus is on the correlation properties of parametrically generated light. These properties arise from the fact that OPG is a very special type of conversion process, where one starts with an electromagnetic wave at one frequency and ends up with waves at three frequencies. This process can only be understood using a quantum mechanical description of the electromagnetic field. The parametrically generated light is the macroscopic manifestation of the quantum fluctuations of the zero-photon electromagnetic field that seed the parametric generation process. The temporal coherence or correlation time τ_c of parametrically generated mid-infrared light is determined by measuring the twin-correlation peak in the sum-frequency spectrum as a function of delay between the signal and idler. The correlation time τ_c of the generated signal and idler fields was found to lie in the picosecond range and is related to the bandwidth $\Delta\omega$ by $\tau_c = 1/\Delta\omega$.

Samenvatting

Dit proefschrift is gewijd aan het onderzoek van de dynamica van geëxciteerde vibraties van kleine moleculen en complexen in oplossing en in de pure vloeistof. Bij het verval van een aangeslagen toestand wordt energie overgedragen naar andere toestanden, wat uiteindelijk leidt tot een equilibratie over alle vrijheidsgraden. De levensduur T_1 van een aangeslagen toestand, die normaal gesproken in de orde van picoseconden is, hangt af van zowel de aard als van de beschikbaarheid van de accepterende toestanden. Door te kijken naar de levensduur en dynamica van aangeslagen vibraties kan veel kennis worden vergaard over de koppelingen binnen en tussen moleculen.

In dit proefschrift worden de levensduur en vibratiedynamica van diverse aangeslagen moleculaire vibraties onderzocht door middel van vibrationele pomp-probe spectroscopie. In een pomp-probe experiment exciteert een pomp-puls een significant deel van de moleculen in een (vloeistof)monster. Deze excitatie veroorzaakt een toename van de transmissie van het monster, aangezien er zich minder moleculen in de vibrationele grondtoestand bevinden die straling kunnen absorberen bij de $v = 0 \rightarrow v = 1$ overgangsfrequentie. De verandering in de transmissie wordt gemeten door middel van een zwakkere probe-puls die het monster doorkruist na een variabele tijdsvertraging ten opzichte van de pomp-puls, zodat de ontwikkeling in de tijd van de aangelagen toestand gevolgd kan worden. Voor deze vorm van tijdsopgeloste spectroscopie zijn lichtpulsen nodig die korter zijn dan de karakteristieke tijdschaal waarop de excitatie vervalt.

De overgansfrequenties van de bestudeerde moleculaire vibraties liggen in het mid-infrarode deel van het spectrum, overeenkomend met golflengtes van 1 tot 10 μm en daarom zijn korte, mid-infrarode (laser) pulsen nodig voor het uitvoeren van de experimenten. Aangezien er weinig lasers zijn met een emissie in dit golflengtegebied, worden in de meeste beschreven experimenten niet-lineaire optische processen zoals verschilfrequentiegeneratie en optische parametrische generatie en versterking gebruikt om "ultrakorte" mid-infrarode pulsen te generen uit zichtbaar of nabij-infrarood laserlicht.

Er zijn twee verschillende waterstofgebrugde zuur-base complexen onderzocht. Een relatief zwakke waterstofbrug is te vinden in complexen van zoutzuur (HCl) met diethyl ether [$(CH_3CH_2)_2O$]. Voor de levensduur van de geëxciteerde H–Cl strekvibratie werd 0,9 $\pm$ 0,2 ps gevonden. Relaxatie vindt plaats via een tussentoestand, waarbij de laagfrequente $(CH_3CH_2)_2O \cdots$H–Cl waterstofbrug de voornaamste toestand is die de vibrationele energie opneemt. De populatie van deze aangeslagen waterstofbrugtoestand vervalt in een tweede vervalsproces met een tijdsconstante die 3,1 $\pm$ 0,5 ps bedraagt. In waterstofgebrugde complexen van waterstoffluoride (HF) met amines is de waterstofbrug tussen het zuur HF en de amine-base zeer sterk. Wij hebben de vibratiedynamica van de HF/FHF-strek combinatie-absorptieband bestudeerd van complexen van HF met de zwakke organische base pyridine, opgelost in pyridine. De relaxatie van deze aangeslagen vibratie blijkt ook in twee stappen te verlopen. In de eerste stap wordt er energie van de aangeslagen combinatievibratie overgedragen aan de F–H$\cdots$F waterstofbrugtoestanden met een tijds-

constante van 0,51 ± 0,09 ps. In een tweede stap, met een tijdsconstante van 2,6 ± 0,3 ps, wordt de energie overgedragen van de F–F waterstofbrugtoestanden naar lager-frequente trillingstoestanden, hetgeen leidt tot een locale thermalisatie van de energie. Hoewel de sterkte van de waterstofbrug in beide zuur-base complexen zeer verschillend is, is in beide gevallen een vergelijkbaar relaxatiemechanisme te zien, waarin de waterstofbrug de belangrijkste accepterende toestand is in de eerste stap van de relaxatie.

De relaxatie van een aangeslagen moleculaire vibratie kan een *intra*moleculair proces zijn, waarbij energie wordt overgedragen aan andere vibraties in hetzelfde molecule via anharmonische koppelingen met de vibratietoestand die oorspronkelijk werd geëxciteerd. De relaxatie kan ook een *inter*moleculair proces zijn, waarbij energie wordt overgedragen naar vibraties van naburige moleculen (al dan niet van het oplosmiddel) of naar laagfrequente (oplosmiddel)toestanden. Twee-kleuren pomp-probe experimenten aan de C–H strekvibratie van bromoform ($CHBr_3$) laten zien dat, vergeleken met oplossingen van bromoform, het mechanisme en de tijdschaal van de vibratierelaxatie sterk worden beïnvloed door de afname van het aantal accepterende toestanden van het oplosmiddel voor intermoleculaire overdracht van energie. Het verval van de aangeslagen C–H strekvibratie in puur $CHBr_3$ geschiedt met een tijdsconstante van 43 ± 1 ps via een tussentoestand, wat voor een roodverschuiving van de C–H strekfrequentie zorgt. Het tussenniveau werd door ons geïdentificeerd als de enkelvoudig aangeslagen C–H buigvibratie. De waarneming dat het verval van dit tussenniveau zeer langzaam en niet-exponentieel is, suggereert dat er zich een "flessenhals" in de relaxatie bevindt, in tegenstelling tot puur chloroform ($CHCl_3$) en oplossingen van bromoform, waar dit niet het geval is. De populatie van deze flessenhalstoestand leeft zeer lang, wat de thermalisatie frustreert.

De invloed van het aantal vibratietoestanden in een molecule op intramoleculaire vibratierelaxatie is te zien in de studie van de vibratiedynamica van de aangeslagen C–O strekvibratie van de alcoholen methanol en ethanol, opgelost in tetra (CCl_4). De relaxatie van de aangeslagen C–O strekvibratie vindt plaats in twee stappen. In de eerste stap wordt de energie overgedragen van de $v = 1$ toestand van de C–O strekvibratie naar een tussentoestand met een tijdsconstante die 3,2 ± 0,2 ps bedraagt voor methanol en 3,2 ± 0,7 ps voor ethanol. De tussentoestand wordt hoogstwaarschijnlijk gevormd door de C–O–H buigvibratie, die ook wel bekend staat als de torsie-toestand of torsie-vibratie. In de tweede stap wordt de energie van deze tussentoestand overgedragen naar laagfrequente toestanden, hetgeen leidt tot een volledige equilibratie van de energie. In methanol vindt deze thermalisatie plaats met een tijdsconstante van 28 ± 1 ps. In ethanol is de tweede stap sneller, met een tijdsconstante van 12 ± 2 ps, omdat in dat molecule een groter aantal accepterende toestanden beschikbaar is.

In het laatste hoofdstuk van dit proefschift wordt de aandacht gericht op het niet-lineaire optische proces dat dankbaar wordt toegepast om mid-infrarood licht te genereren voor de experimenten die worden beschreven in de andere hoofdstukken. De nadruk ligt op de correlatie-eigenschappen van parametrisch gegenereerd licht. Deze eigenschappen komen voort uit het feit dat optische parametrische generatie een zeer bijzondere omzetting is, waarbij uitgaande van een electromagnetische golf bij één frequentie, golven bij drie frequenties het resultaat zijn. Dit proces kan slechts worden begrepen door een quantummechanische beschrijving van het electromagnetisch veld te gebruiken. Het parametrisch gegenereerd licht is een macroscopische manifestatie van de quantumfluctuaties van het nul-foton electromagnetisch veld die de kiem vormen van de parametrische generatie. De

coherentie in de tijd of de correlatietijd τ_c van parametrisch gegenereerd licht is bepaald door de tweeling-correlatiepiek in het som-frequentiespectrum te meten als functie van de tijdsvertraging tussen signal en idler. Voor de correlatietijd τ_c van de gegenereerde signal- en idlervelden werd gevonden dat deze in de orde van enkele picoseconden ligt en van de bandbreedte $\Delta\omega$ afhangt als $\tau_c = 1/\Delta\omega$.

Samenvatting voor iedereen

Veel van de eigenschappen van een vloeistof worden bepaald door de manier waarop en de sterkte waarmee de moleculen (tijdelijk) aan elkaar gebonden zijn, terwijl ze doorelkaar bewegen. Een veelgebruikt en bekend voorbeeld is water. Watermoleculen zijn opgebouwd uit één zuurstofatoom (O) en twee waterstofatomen (H), zoals iedereen leert bij het opstellen van de chemische formule van dat molecule: H_2O. Eén van de bijzondere eigenschapen van water is dat het nog vloeibaar is bij kamertemperatuur, terwijl het uit zulke kleine en lichte moleculen is opgebouwd. Deze eigenschap is te danken aan de waterstofbruggen waarmee de watermoleculen aan elkaar vastzitten.

De atomen in een molecule zijn weliswaar stevig aan elkaar gebonden, maar ze kunnen toch een beetje ten opzichte van elkaar heen en weer trillen. Het beeld van bolletjes (de atomen) die met veertjes aan elkaar verbonden zijn (de bindingen tussen de atomen) geeft een goede indruk en wordt vaak als allereerste benadering gebruikt. De atomen waaruit het molecule bestaat kunnen op verschillende manieren ten opzichte van elkaar trillen. Deze verschillende trillingen worden meestal *vibraties* genoemd.

Een vibratie kan worden aangeslagen (*geëxciteerd*) door de opname (*absorptie*) van een lichtpuls van de juiste golflengte. Zichtbaar licht heeft een golflengte tussen de 400 en 700 nanometer (een nanometer is een miljoenste millimeter), maar bij het aanslaan van vibraties wordt mid-infrarood licht geabsorbeerd, met golflengtes in het gebied grofweg tussen 2.000 en 10.000 nanometer. Een aangeslagen vibratie draagt z'n energie binnen zeer korte tijd over, te weten binnen enkele picoseconden (1 picoseconde is 10^{-12} seconde, ofwel een miljoenste van een miljoenste van een seconde). Om deze processen te kunnen volgen is dus een "fototoestel" nodig met een "sluitertijd" van picoseconden of zelfs femtoseconden (1 femtoseconde is een duizendste picoseconde, dus 10^{-15} seconde). In de experimenten die in dit proefschrift zijn beschreven kan door gebruik van lasers met pulsen van enkele tientallen picoseconden tot enkele honderden femtoseconden gekeken worden naar de dynamica van aangeslagen vibraties. De gebruikte techniek is pomp-probe spectroscopie, een vorm van tijdsopgeloste mid-infrarood spectroscopie.

In een pomp-probe experiment wordt met een korte laserpuls (de pomp-puls) een vibratie aangeslagen. Zolang deze vibratie is geëxiteerd kan die vibratie geen tweede hoeveelheid licht opnemen van dezelfde golflengte. Hiervan wordt gebruik gemaakt door na een korte tijd een tweede laserpuls (de probe-puls) door het vloeistofmonster te sturen en te meten hoeveel van het licht er (minder) wordt geabsorbeerd. Door de tijdsvertraging tussen de twee pulsen te variëren kan steeds op een ander tijdstip na de pomp puls een meting worden gedaan ("een foto worden gemaakt") en door deze achter elkaar te zetten kan de dynamica van de aangeslagen vibratie in de tijd gevolgd worden.

Als een bepaalde vibratie in een molecule in gang wordt gezet, wordt de energie van die vibratie vervolgens zeer snel verspreid over andere vibraties van het molecule maar ook naar naburige moleculen. De oorspronkelijk aangeslagen trilling houdt dan op, terwijl de andere trillingen die de energie opnemen in gang worden gezet. Meestal hebben de energie-

accepterende vibraties een lagere energie en wordt die energie over meerdere trillingen verdeeld. Na een aantal van dit soort overdrachten wordt de energie verdeeld over de hele vloeistof. Door erachter te komen hoe snel en waarnaar de trillingsenergie wordt overgedragen is meer informatie te krijgen over hoe sterk de koppelingen zijn tussen en binnen de moleculen in een vloeistof.

In de hoofdstukken 3 en 4 is gekenen naar twee verschillende complexen van moleculen. Zo'n complex wordt gevormd door twee of drie moleculen die aan elkaar gebonden zijn door de eerder genoemde waterstofbruggen. In hoofdstuk 3 is de watersofbrug relatief zwak en in hoofdstuk 4 zeer sterk. Er bleek in beide gevallen dat als een vibratie in het complex wordt aangeslagen de energie wordt overgedragen aan die waterstofbrug die daardoor zwakker wordt, maar in beide gevallen niet lijkt te breken. Als even later de energie wegvloeit naar de omgeving van het complex keert de waterstofbrug weer terug naar z'n oude sterkte.

Hoe lang het duurt voordat de energie van de aangeslagen vibratie wordt overgedragen, ook wel de *levensduur* of T_1 van de vibratie genoemd, wordt heel sterk bepaald door het aantal mogelijkheden die er zijn om energie aan over te dragen. Dit is heel duidelijk te zien in de experimenten in hoofdstuk 5, waar de levensduur van een aangeslagen vibratie van bromoform ($CHBr_3$) veel langer is in de pure vloeistof dan wanneer de bromoform moleculen zijn opgelost in een oplosmiddel. Blijkbaar zijn er veel meer mogelijkheden om aan oplosmiddelmoleculen energie over te dragen dan aan soortgelijke moleculen bromoform. Een soortgelijk gedrag is ook te zien in hoofdstuk 6, waar naar de dynamica van een specifieke vibratie van methanol en ethanol ("gewone" alcohol) is gekeken.

De resultaten van de beschreven experimenten hebben voor een aantal uiteenlopende moleculen inzicht verschaft in de herverdeling van trillingsenergie in vloeistoffen. Hierdoor kan een nauwkeuriger beeld gevormd worden over de aard en de sterkte van de interacties tussen en binnen moleculen in een vloeistof.

Nawoord

Aan het einde van het promotie-onderzoek is dit de plaats om al degenen te bedanken die aan het proefschrift hebben bijgedragen. Allereerst Huib, mijn promotor, die mij wist te overtuigen dat het helemaal geen slecht idee was op een andere plek te promoveren dan waar je je afstudeeronderzoek hebt gedaan. Het is moeilijk je een betere begeleider en promotor in te denken. Zijn razendsnel fysisch inzicht en enthousiasme bij het zien van nieuwe resultaten zijn in de afgelopen jaren zeer stimulerend en inspirerend geweest. Daarnaast is hij zeker niet in de laatste plaats verantwoordelijk voor de goede en soms licht anarchistische sfeer in de groep Vibratiedynamica, tegenwoordig Ultrasnelle Spectroscopie geheten.

Mijn dank gaat ook uit naar alle andere (oud-)groepsgenoten: Han-Kwang Nienhuys, Michel Kropman, Arjan Lock, Sander Woutersen, Anne Willem Omta, Ingrid Giebels, Uli Emmerichs, Mingcheng Zong, Issa Abu-Shiekah en Mischa Bonn voor de fijne sfeer en samenwerking gedurende mijn promotietijd. Han-Kwang is de altijd onvermoeibare vraagbaak geweest voor natuurkundige problemen en vragen over Linux. Daarnaast heeft hij samen met mij menige al dan niet succesrijke meetsessie in Rijnhuizen doorgebracht, hetgeen uiteindelijk resulteerde in hoofdstuk 6. Het afstudeeronderzoek van Ingrid heeft tot hoofdstuk 3 geleid. Voor dat hoofdstuk en ook het daarop volgende hoofdstuk 4 zijn de experimentele kunsten van Michel onmisbaar geweest.

Het Amolf biedt een onderzoeksomgeving waar menig promovendus elders jaloers op kan zijn. Rob Kemper en Hinco Schoenmaker bedank ik voor hun onontbeerlijke technische ondersteuning en dat zij vaak bereid waren meteen dingen te maken of repareren die onmisbaar waren voor de experimenten. Op electronisch vlak hebben de mensen van de afdeling e&i hun bijdrage geleverd, met name Hans Alberda, Hans ter Horst en Idsart Attema. Verder wil ik alle andere amolfers bedanken die mijn promotietijd tot een zeer aangenaam verblijf in de Watergraafsmeer en daarbuiten hebben gemaakt. In het bijzonder wil ik de mensen van de afdeling qdams noemen.

De wetenschap dat er ook een leven buiten het onderzoek kan bestaan heb ik daarnaast te danken aan alle vrienden en bekenden, in het bijzonder de heeren van jaarclub "Summus". Tenslotte dank ik mijn ouders en zusje Liejet, die mij al deze jaren gesteund hebben.

Frederik van den Broek — Utrecht / Amsterdam, mei 2002